Dissociable control of motivation and reinforcement by distinct ventral striatal dopamine receptors

Juan Enriquez-Traba[1,2], Hector E Yarur-Castillo[1], Rodolfo J Flores[1], Tenley Weil[3], Snehashis Roy[4], Ted B Usdin[4], Christina T LaGamma[1], Miguel Arenivar[1], Huikun Wang[1], Valerie S Tsai[1], Amy E Moritz[5], David R Sibley[5], Rosario Moratalla[6], Zachary Z Freyberg[7,8#], Hugo A Tejeda[1*#]

[1]Unit on Neuromodulation and Synaptic Integration, National Institute of Mental Health, Bethesda, MD, 20894, USA.

[2]Department of Biochemistry, Universidad Autonoma de Madrid, Madrid, 28029, Spain.

[3]Section on Light and Circadian Rhythms, National Institute of Mental Health, Bethesda, MD 20892, USA.

[4]Systems Neuroscience Imaging Resource, National Institute of Mental Health, Bethesda, MD, 20894, USA.

[5]Molecular Neuropharmacology Section, National Institute of Neurological Disorders and Stroke, Bethesda, MD, 20892, USA.

[6]Department of Functional and Systems Neurobiology, Instituto Cajal-CSIC, Madrid, 28002, Spain.

[7]Department of Psychiatry, University of Pittsburgh, Pittsburgh, PA, 15213, USA.

[8]Department of Cell Biology, University of Pittsburgh, Pittsburgh, PA, 15213, USA.

[*]Lead contact (hugo.tejeda@nih.gov)

[#]Correspondence: hugo.tejeda@nih.gov, freyberg@pitt.edu

Dr. Hugo A. Tejeda

35 Convent Dr.

2D-913

Bethesda, MD 20892

Dr. Zachary Freyberg

3811 O'Hara Street

BST W1640

Pittsburgh, PA 15213

32 **Abstract**

33 Dopamine release in striatal circuits, including the nucleus accumbens (NAc), tracks

34 separable features of reward such as motivation and reinforcement. However, the cellular

35 and circuit mechanisms by which dopamine receptors transform dopamine release into

36 distinct constructs of reward remain unclear. Here, we show that dopamine D3 receptor

37 (D3R) signaling in the NAc drives motivated behavior by regulating local NAc

38 microcircuits. Furthermore, D3Rs co-express with dopamine D1 receptors (D1Rs), which

39 regulate reinforcement, but not motivation. Paralleling dissociable roles in reward

40 function, we report non-overlapping physiological actions of D3R and D1R signaling in

41 NAc neurons. Our results establish a novel cellular framework wherein dopamine

42 signaling within the same NAc cell type is physiologically compartmentalized via actions

43 on distinct dopamine receptors. This structural and functional organization provides

44 neurons in a limbic circuit with the unique ability to orchestrate dissociable aspects of

45 reward-related behaviors that are relevant to the etiology of neuropsychiatric disorders.

46

47

Main

Dopamine (DA) transmission is essential for reward function and its constituent features, including motivation and reinforcement. Motivation can be broadly defined as the internal process that activates and directs behavior, while reinforcement refers to the process in which the likelihood of a behavior is increased as a consequence of stimulus-response and action-outcome associations[1]. These separable constructs are coordinated to maximize reward outcomes[2-4], and alterations in these reward sub-features are implicated in neuropsychiatric disorders, such as substance use and mood disorders[5-7]. A major integrative hub mediating motivation and reward-driven reinforcement is the nucleus accumbens (NAc), which receives DAergic projections from the ventral tegmental area (VTA)[8,9]. Disparate models have been proposed to explain the various components of reward that DA regulates in the NAc[10-14]. For instance, tonic and phasic patterns of DA neuron activity, and axonal control of DAergic terminals, contribute to dynamic fluctuations in DA concentrations that are hypothesized to ultimately underlie reinforcement, motivation, and vigor[12,15-22]. However, the specific mechanisms by which DA release is translated into cellular changes via dopamine receptors to drive dissociable features of reward function, such as motivation and reinforcement, remain unknown.

As in the dorsal striatum, medium spiny neurons (MSNs) of the NAc express high levels of DA receptors, including D1Rs and DA D2 receptors (D2Rs). Expression of D1Rs and D2Rs is segregated into non-overlapping MSN cell types, D1-MSNs and D2-MSNs, respectively[23,24]. DA-mediated activation of NAc D1Rs and D2Rs has been shown to produce dichotomous effects on D1- and D2-MSN function, respectively[25-29]. However, unlike its dorsal counterpart, the NAc is specifically enriched with the D3R[30-33]. Importantly, this specialized expression of D3Rs within ventral striatal circuits coincides with the specialized control of motivation and reinforcement by the NAc[8]. Moreover, D3R is a high-affinity DA receptor with a ten-fold greater DA affinity than D2Rs[34, 35], suggesting that it may serve as an additional conduit for the detection of tonic changes or dips in DA concentrations besides the D2R. Although D3R expression in the ventral striatum has been suggested, its role in regulating reward-related behaviors remains poorly understood. Important clues come from pharmacological manipulations of D3R signaling. Indeed, NAc D3R pharmacological antagonism has been shown to inhibit drug-seeking

3

79 behavior[36,37]. However, an important limitation of these approaches is the relative inability

80 of antagonists to precisely distinguish D3R from D2Rs. Furthermore, studies using either

81 mice ectopically overexpressing D3R in all striatal MSNs or constitutive global knockout

82 of D3Rs reported disrupted motivation and increased cocaine-seeking behavior,

83 respectively[38,39]. However, striatum-wide D3R ectopic overexpression does not

84 determine how endogenous NAc D3Rs contribute to reward function. Further, global

85 knockout approaches do not distinguish contributions of NAc D3Rs versus D3Rs in other

86 regions implicated in reward-seeking behavior[40,41] or developmental compensation that

87 may perturb reward function. Thus, limited tools to selectively manipulate the function of

88 NAc D3Rs have hindered advances in our understanding of the specific contribution of

89 D3Rs to distinct features underlying reward function. Interestingly, NAc D1-MSNs have

90 been suggested to co-express D3R with D1R[42,41], and this could provide NAc D1-MSNs

91 with different modes by which DA may alter physiology and behavior. Because D1R and

92 D3Rs possess different affinities for DA and engage opposite signaling effectors, these

93 receptor-specific differences may translate into differential detection of DA concentrations

94 and downstream effects on MSN function. We therefore hypothesized that D1-MSNs in

95 the NAc may use distinct DA receptors for orchestrating dissociable reward-related

96 functions.

97   Here we sought to address this hypothesis using a combination of anatomical

98 tracing, slice electrophysiology and circuit-level manipulations of DA receptor function. In

99 this study, we overcame technical limitations to selectively study NAc D3R fucntion by

100 generating and characterizing a novel D3R conditional-knockout (cKO) mouse.

101 Leveraging this line, we found that NAc D3R activity is necessary for motivated behavior,

102 but not reinforcement, by acting presynaptically to inhibit NAc collateral transmission.

103 Conversely, NAc D1Rs, with which D3Rs are highly co-expressed, promote reward- and

104 aversion-driven reinforcement, but not motivation. Moreover, we demonstrated

105 dissociable roles for D3R and D1R in regulating MSN synaptic physiology, which

106 explained the dissociable roles in behavior. Our findings describe a novel framework by

107 which DA signaling via D3R and D1R provides NAc D1-MSNs with the unique ability to

108 regulate dissociable constructs underlying reward-related behaviors.

109 **Results**

110 **Conditional knockout of NAc D3Rs results in motivational deficits**

111   We first investigated whether NAc D3Rs regulate specific sub-features of reward-

112 related behaviors. To overcome limitations associated with pharmacological antagonism

113 and constitutive knockouts of D3Rs, we generated *Drd3* cKO mice (*Drd3*^{fl/fl}) mice

114 (Extended Data Fig. 1a) to selectively knockout D3R expression in the NAc. We achieved

115 this aim by injecting Cre-expressing virus (AAV8-hSyn-GFP-Cre) into the NAc of *Drd3*^{fl/fl}

116 mice (NAc-D3RcKO; Fig. 1a). Indeed, NAc-D3RcKO mice had decreased expression of

117 *Drd3* mRNA as shown by fluorescent *in-situ* hybridization (Fig. 1b). Furthermore, we

118 observed decreased *Drd3* mRNA expression as assessed by qPCR obtained from micro-

119 dissected NAc. Importantly, no changes in *Drd1a* or *Drd2* expression were observed with

120 NAc *Drd3* cKO, suggesting that this manipulation is specific to the D3R (Fig. 1c). We then

121 assessed the impact of NAc D3R cKO in mediating reward function by first determining

122 its role in motivation for exercise using wheel-running (Extended Data Fig. 1b), a

123 rewarding stimulus for laboratory and feral rodents[43-45]. In this context, WT and *Drd3*^{fl/fl}

124 control mice injected with Cre-expressing and GFP-expressing virus, respectively,

125 displayed robust wheel running activity when exposed to a novel wheel during their

126 inactive cycle (lights on), when animals should be at rest and locomotor activity is typically

127 low (Fig. 1d). In contrast, NAc-D3RcKO mice had reduced wheel-running activity during

128 this exposure to the novel running wheel in the inactive cycle (Fig. 1d), which dissipated

129 prior to the onset of the active cycle (Extended Data Fig. 1c). However, running behavior

130 triggered by the onset of the active cycle when lights turned off and did not differ between

131 controls and NAc-D3RcKO mice (Extended Data Fig. 1c). Moreover, locomotor activity

132 during the animals' active cycle (lights off) in an open field was not impacted (Extended

133 Data Fig. 1f). Intact locomotor activity during exploratory behavior in the open field and in

134 response to diurnal shifts after the initial exposure to the running wheel, suggest that D3R

135 cKO in the NAc is impacting the motivational value of running, not locomotor activity or

136 running performance. Indeed, running behavior triggered by novel wheel exposure during

137 the subjective daytime in rodents contains a strong motivational component[46-48]. Further,

138 interference of running behavior is more sensitive during the acquisition of wheel running

139   before habituation and experience[49]. With habituation to voluntary running, running

140   behavior can be decoupled from enhancements in motivational state and driven by other

141   factors, including but not limited to, habitual / stereotyped behavior, diurnal shifts, internal

142   states, arousal-driven locomotor activity, and/or non-photic circadian entrainment[47,48]. In

143   agreement with this notion, in rats habituated with running wheels, inactivation of the NAc

144   does not impair running, unless motivation to run is increased by wheel deprivation[50].

145   Together, our results suggest that the initial motivation to engage in wheel running, but

146   not locomotor activity or running performance, is decreased in NAc-D3RcKO mice.

147   To further investigate whether cKO of NAc D3R expression impacted acquisition

148   of motivation to run, we designed a choice task wherein mice were allowed to choose to

149   spend time on either a fixed or a freely-moving disk, a distinct running apparatus, in an

150   open field arena during the animal's active cycle (Fig. 1e). WT-Cre and *Drd3*^{fl/fl}-GFP

151   control mice spent significantly more time on the freely-moving disk than on the fixed disk,

152   in addition to showing robust running behavior (Fig. 1e-f). Conversely, NAc-D3RcKO mice

153   did not significantly prefer the freely moving disk over the fixed disk and displayed minimal

154   running (Fig. 1e-f). Running disks are angled relative to the ground (~ 30° angle). As such,

155   persistence is required for optimal running to develop since early attempts are marked by

156   mice consistently falling off the disk. In control mice, preference for and running on the

157   freely-moving disk did not begin immediately upon exposure but rather developed across

158   the session as mice learned to run on the disk (Extended Data Fig. 1d). Consistent with

159   increased persistence, control mice displayed increased entries into the freely-moving

160   disk relative to NAc-D3RcKO mice (Extended Data Fig. 1e). These data provide support

161   for NAc D3R in driving motivated running behavior, independent of diurnal cycle. We

162   subsequently determined whether NAc D3R cKO would impact approach to other

163   rewarding stimuli. We observed that NAc-D3RcKO mice displayed a non-significant

164   decrease in sucrose preference relative to controls (Extended Data Fig. 1g). Further, this

165   manipulation did not affect social approach (Extended Data Fig. 1h), suggesting that

166   pursuit of low-effort palatable and social rewards is not affected by NAc D3R cKO.

167   Anxiety-like behavior in the open-field and light-dark box (Extended Data Fig. 1f, i), as

168   well novel object recognition (Extended Data Fig. 1j) was not different between controls

169   and NAc-D3RcKO mice, demonstrating that exploratory behavior or interaction with novel

170   stimuli are not impacted by NAc D3R cKO. These results collectively suggest that cKO of

171   D3Rs in the NAc strongly disrupts running behavior associated with a motivated state.

172   We subsequently determined the role of NAc D3Rs in effort-related instrumental

173   motivation, we used an operant conditioning paradigm in which animals had to lever press

174   to acquire a chocolate pellet reward (Fig. 1g). Importantly, *Drd3* cKO in the NAc did not

175   alter the body weight of NAc-D3RcKO mice relative to WT controls throughout the course

176   of the experiment (Extended Data Fig. 2a). Animals first underwent an initial acquisition

177   phase consisting of fixed-ratio (FR) 1 and 5 schedules to determine whether loss of NAc

178   D3R signaling impacted reinforcement of food-seeking behavior. NAc-D3RcKO and WT

179   groups displayed similar levels of active lever pressing and accuracy during FR1 sessions

180   (Fig. 1h, Extended Data Fig. 2b-c), indicating that NAc D3R signaling is not essential for

181   reinforcement. Interestingly, NAc-D3RcKO mice transiently displayed lower levels of

182   responding when the effort required to obtain reward was increased from a FR1 to a FR5

183   schedule (Fig. 1i). To directly assess whether NAc D3Rs regulate motivation, mice

184   subsequently underwent testing in an effort-based choice task in which they had the

185   choice of consuming freely available standard chow or working for a higher-palatable

186   chocolate reward[51,52] (Fig. 1j, left). In this context, WT mice preferred to work for more

187   palatable rewards over freely available lab chow (Fig. 1j). This pattern was absent in NAc-

188   D3RcKO mice, which consumed higher quantities of regular chow than WT controls and

189   did not show a preference towards working for a higher-palatable chocolate reward (Fig.

190   1j). Importantly, the overall amount of food consumed was similar across groups

191   (Extended Data Fig. 2d), suggesting that there was a decrease in effort-based motivation

192   but not homeostatic drive to eat in a hunger state. The same effect was observed when

193   mice were given a choice between operant-obtained chocolate pellets and freely available

194   chocolate pellets (Extended Data Fig. 2e-f). This indicates that control mice prefer to exert

195   effort versus obtaining freely-available reward and that loss of NAc D3Rs biases choice

196   towards reward-seeking behaviors that require less effort. Importantly, this is consistent

197   with previous reports demonstrating that decreasing NAc DA signaling increases intake

198   of low-effort food rewards and decrease effort or activity-based reward seeking behavior,

199   without impacting overall food intake[51-56]. Subsequently, mice were subjected to

200   progressive ratio (PR) schedules to further dissect the role of NAc D3R in regulating

201   motivation. NAc-D3RcKO mice had decreased break points relative to WT controls in

202   both PR3 (Fig. 1k) and PR7 schedules (Fig. 1l), as well as decreased PR session lengths

203   (Extended Data Fig. 2g-h). These results indicate there is decreased motivation to exert

204   effort to obtain food rewards with NAc D3R knockout. These data collectively indicate that

205   motivated behavior necessary to obtain both appetitive food and running reward relies on

206   NAc D3R function.

207   **NAc D3Rs are primarily expressed in D1-MSNs**

208   The NAc is primarily composed of dichotomous cell types defined by DA receptor

209   subtype (*i.e.*, D1R- and D2R-expressing MSNs), in addition to other molecular markers

210   such as prodynorphin and proenkephalin[23]. To examine the NAc cell types in which D3R

211   signaling occurs, we performed fluorescent *in-situ* hybridization experiments to detect the

212   co-expression of *Drd1*a, *Drd2* and *Drd3* mRNA. *Drd3* mRNA, together with *Drd1a* and

213   *Drd2*, was widely expressed in the NAc (Fig. 2a). Moreover, using *Drd3*-Cre mice crossed

214   with tdTomato reporter mice, we observed robust tdTomato labeling in the NAc, in

215   addition to the islands of Calleja (IC) (Extended Data Fig. 3a), but not the dorsal striatum.

216   We found that in the NAc, a large majority (75.46% ± 0.89%) of *Drd3*-positive cells co-

217   expressed *Drd1a*, with 20.51% ± 0.91% co-expressing *Drd2* (Fig. 2b-c). We also found

218   that 81.79% ± 1.35% and 17.72% ± 1.32 of NAc *Drd1a*- and *Drd2*-positive neurons

219   express *Drd3*, respectively (Fig. 2d), corroborating the finding that *Drd3*-expressing MSNs

220   constitute a large subpopulation of D1-MSNs. Furthermore, the relative expression level

221   of *Drd3* mRNA within the D1-MSN population was 20% higher than the level of *Drd3*

222   expression in D2-MSNs (Fig. 2e). In addition, we obtained evidence of preferential

223   expression of *Drd3* in NAc D1-MSNs when we recorded ChR2-mediated photocurrents

224   in slices obtained from *Drd1a*-tdtomato/*Drd3*-Cre mice injected with AAV-DIO-ChR2-

225   eYFP (Fig. 2f). Consistent with *in situ* hybridization results above, 77% of ChR2-positive

226   neurons were positive for *Drd1a*-tdTomato (Fig. 2f). *Drd3* is therefore widely co-

227   expressed in NAc D1-MSNs and less robustly in a subset of NAc D2-MSNs, suggesting

228   that within the same neuronal population DA may serve different functions by acting on

229   distinct receptor subtypes.

230   NAc MSNs play a role in the selection of appropriate goal-directed behaviors
231   through connectivity with downstream brain regions. D1-MSNs project to the ventral
232   pallidum (VP), lateral hypothalamus (LH) and ventral tegmental area (VTA), while NAc
233   D2-MSNs projections are largely restricted to the VP[57-67]. To dissect the circuit-level
234   mechanisms through which NAc D3R signaling- regulates motivated behavior, we
235   determined the anatomical projections of *Drd3*-expressing MSNs using viral-assisted
236   anterograde tracing in adult mice. Injection of AAV-FLEX-tdTomato-T2A-Synaptophysin-
237   eGFP in the NAc of *Drd3*-Cre mice (Fig. 2g, left) allowed for the visualization of both fibers
238   of passage and terminals of *Drd3*-expressing MSNs. We indeed observed putative
239   presynaptic terminals labeled with Synaptophysin-eGFP puncta that were distinct from
240   bundles of tdTomato-positive fibers, lacking eGFP (Supplementary Video 1). Consistent
241   with the expression of D3Rs in D1-MSNs, GFP fluorescence revealed dense innervation
242   within the NAc and of the VP, LH and VTA (Fig. 2g, right). Quantification of tdTomato
243   fluorescence showed that fibers of passage were most prominent in more anterior regions
244   (*i.e.*, VP), whereas putative terminals in the VP, LH or VTA (Extended Data Fig. 3b). Thus,
245   D3-MSNs project downstream to the VP, LH and VTA and form discrete synaptic contacts
246   in each of these regions.

247   We next used ChR2-assisted mapping to test the functional connectivity between
248   NAc *Drd3*-expressing MSNs and their output regions. Patch clamp recordings in brain
249   slices from *Drd3*-Cre mice injected with Cre-dependent ChR2 demonstrated
250   optogenetically-evoked inhibitory post-synaptic currents (oIPSCs) recorded in the
251   majority of VP, LH and VTA neurons (Fig. 2h-k). Light-evoked IPSCs were blocked by
252   application of the GABA$_A$-receptor antagonist picrotoxin (PTX) indicating that currents
253   were mediated by GABA$_A$-receptors (Fig. 2h-j). These findings indicate NAc D3-MSNs
254   may regulate information processing in limbic circuits by sending inhibitory outputs to the
255   VP, LH and VTA.

256   Distinct D1-MSNs have been shown to project to the VP, LH, and VTA[58, 61-63].
257   Importantly these different MSN outputs do not collateralize, play distinct roles in
258   behavior, and exhibit differential plasticity in response to behavioral experiences. To
259   determine the proportion of D3R-expressing MSNs projecting to each of these three

9

260 output regions, we performed retrograde tracing experiments in combination with *in-situ*

261 hybridization (Fig. 2l). We found that, as reported, NAc MSN neurons projecting to these

262 structures were anatomically segregated. VP-projecting MSNs were present in both NAc

263 core and shell subregions (Fig. 2l, left). LH-projecting MSNs were primarily localized in

264 the NAc shell (Fig. 2l, middle) whereas VTA-projecting MSNs were mainly located in the

265 NAc core (Fig. 2l, right). In addition, quantification of cells positive for retrobeads and *Drd3*

266 labeling showed that the proportion of D3R-expressing MSNs projecting to LH and VTA

267 was higher than those projecting to VP (Fig. 2m). Further, *Drd3* mRNA expression was

268 lower in VP-projecting MSNs, consistent with reduced expression in subsets of NAc D2-

269 MSNs (Fig. 2n), which exclusively project to the VP. These results reveal the anatomical

270 architecture by which *Drd3*-expressing MSNs connect within the NAc and to the VP, LH

271 and VTA. These results led us to determine whether the role of NAc D3Rs in regulating

272 motivation differed based on where the D3R expressing MSNs project.

273 **NAc D3R is essential for motivated behavior independent of projection neuron**

274   NAc MSN projections to VP, LH and VTA have been previously shown to control

275 reward-related behavior since distinct NAc projection neurons do not collateralize across

276 these regions[58, 59, 62-68], we hypothesized that D3R signaling in different MSN projections

277 would differentially modulate motivated behavior. We tested this hypothesis by selective

278 cKO of NAc *Drd3* expression in MSNs targeting either the VP, LH or VTA using

279 intersectional viral and genetic approaches. To this end, we injected CAV-Flp-GFP in VP,

280 LH or VTA of *Drd3*^{fl/fl} mice or WT control mice. This enabled expression of Flp

281 recombinase in NAc MSNs targeting each of these distinct outputs (Fig. 3a). We then

282 injected AAV-fDIO-Cre in the NAc to express Cre recombinase in retrogradely-infected

283 NAc neurons expressing Flp and to effectively knockout D3Rs based on NAc outputs to

284 either VP, LH, or VTA. In addition, we included AAV-FLEX-tdTomato into the NAc for

285 histological confirmation of injection site (Fig. 3b, Extended Data Fig. 4). Three weeks

286 after viral injection, mice were tested for motivation in running and operant tasks.

287 Selective deletion of D3Rs from neurons projecting to either the VP, LH, or VTA in *Drd3*^{fl/fl}

288 mice resulted in decreased motivation to run compared to WT controls, as reported in

289 wheel running activity (Fig. 3c-e) and less preference for and running in the freely-moving

10

290   disk in the disk choice task (Fig. 3f-h). Mice with cKO of D3Rs in either VP-, LH-, or VTA-

291   projecting MSNs displayed diminished wheel running activity upon first exposure during

292   the subjective day period (Fig. 3c-e), but not in response to diurnal shift to the animals'

293   inactive cycle (Extended Data Fig. 5a). The only exception were mice lacking D3R

294   expression from VTA-projecting NAc MSNs, which displayed a decrease in dark cycle-

295   initiated running (Extended Data Fig. 5a). Collectively, our findings indicate that D3R is

296   essential for promoting motivated running behavior irrespective of their projections to

297   downstream targets.

298   We then assessed the effect of pathway-specific D3R cKO from either VP-, LH-,

299   or VTA-projecting NAc MSNs in operant conditioning procedures. *Drd3*^fl/fl mice did not

300   show changes in body weights (Extended Data Fig. 5b) or acquisition of responding on a

301   FR1 schedule (Fig. 3i, Extended Data Fig 5c-d) relative to WT controls in all pathways.

302   Interestingly, mice with selective cKO of *Drd3* from VTA-projecting NAc neurons had

303   increased lever pressing under FR5 schedules. During choice tests, where animals could

304   select between freely-available chow versus operant-derived chocolate pellets, selective

305   cKO of D3Rs from either the VP-, LH-, or VTA-projecting MSNs increased intake of freely-

306   available chow (Fig. 3j, Extended Data Fig. 5e-f). This was also observed when mice

307   could choose between operant-derived and freely-available chocolate pellets (Extended

308   Data Fig. 5g-i). These data indicate that *Drd3* cKO from either pathway biased

309   consummatory behavior towards low effort rewards and away from higher effort rewards.

310   NAc D3R cKO from VP- and LH-projecting MSNs resulted in deficits in motivation as

311   shown by decreased breaking points in PR7 (Fig. 3k), but not PR3 (Extended Data Fig.

312   5j), consistent with decreased effort-based motivation. This effect did not reach statistical

313   significance for mice lacking D3Rs in VTA-projecting MSNs. Our data collectively show

314   that pathway-specific cKO D3Rs suppresses motivated behavior, but not reinforcement,

315   independently of output region.

316   **D3R regulates GABAergic transmission from NAc collaterals and to the VP via a**

317   **presynaptic site of action**

318         $G_{i/o}$-coupled GPCRs, such as D3Rs, regulate circuit function by inhibiting

319   neurotransmitter release from axon terminals[69,70]. Local collaterals arising from NAc

11

320   MSNs constitute a large proportion of inhibitory synapses onto MSNs, which are regulated

321   by $G_{i/o}$-coupled GPCRs and have been implicated in controlling striatal circuit recruitment

322   during reward-related behavior[71-75]. To determine the functional role of D3R in shaping

323   MSN function, we first examined the effect of D3R signaling on inhibitory synaptic

324   transmission from MSN collaterals to neighboring MSNs. *Drd1a*-tdTomato/*Drd3*-Cre mice

325   were injected with a virus expressing ChR2-eYFP in Cre-expressing neurons (Cre-ON;

326   AAV-DIO-ChR2-eYFP) or Cre-negative neurons (Cre-OFF; AAV-DO-ChR2-eYFP),

327   respectively, to selectively evoke GABA release from *Drd3*-positive or *Drd3*-negative NAc

328   MSNs, respectively (Fig. 4a-b). Consistent with a higher proportion of *Drd3*-negative NAc

329   neurons than *Drd3* positive, baseline oIPSC amplitudes were larger in the Cre-OFF

330   condition (Extended Data Fig. 6a). Furthermore, in NAc MSNs recorded from mice

331   expressing ChR2-eYFP in D3R-positive MSNs (Cre-ON), D3R activation with the D3R-

332   selective agonist PD-128907 (1 µM) decreased oIPSC amplitude (Fig. 4c). Conversely,

333   oIPSCs evoked from D3R-negative NAc cells (Cre-OFF) were insensitive to PD-128907

334   (Fig. 4c). These results suggest a presynaptic site of action for depression of D3-MSN

335   collateral transmission by D3Rs. These results also validate the selectivity of PD-128907

336   for the D3R and selective viral-mediated transgene expression in D3R-expressing NAc

337   MSNs in the *Drd3*-Cre mouse line. For confirmation, we also used the novel, highly

338   selective D3R agonist ML417[76], which also decreased oIPSC amplitude from NAc MSN

339   collaterals (Extended Data Fig. 6b-d). In line with a role for presynaptic D3R in the

340   regulation of NAc collaterals, the paired pulse ratio (PPR) increased (Fig. 4D), and the

341   coefficient of variation ($1/CV^2$) decreased (Fig. 4e) with PD-128907 in the Cre-ON

342   condition. This reduction in GABA release probability was confirmed in experiments

343   where the frequency of spontaneous inhibitory postsynaptic currents (sIPSCs), but not

344   amplitude or kinetics, was decreased with PD-128907 application (Extended Data 6f-g),

345   consistent with widespread D3R expression in D1-MSNs and a small subset of D2-MSNs.

346   We next determined whether presynaptic D3R signaling differentially inhibited

347   presynaptic D3-MSN collaterals onto D1- and D2-MSNs. First, D1-MSNs were identified

348   by tdTomato fluorescence in *Drd1a*-tdTomato mice, while putative D2-MSNs were

349   identified by lack of tdTomato fluorescence (Fig. 4b). Application of PD-128907 similarly

350   inhibited oIPSCs evoked by optogenetic stimulation of D3-MSN collaterals in D1- and D2-

351   MSNs (Extended Data Fig. 6h-i). Collectively, these results demonstrate that presynaptic

352   D3R inhibits GABAergic outputs from MSN collaterals onto D1- and D2-MSNs.

353   Though NAc *Drd3*-expressing MSNs project to the VP, LH and VTA, it is unclear

354   whether presynaptic D3Rs regulate GABAergic synaptic transmission from the NAc to

355   each of these downstream targets. We therefore used ChR2-assisted functional mapping

356   to examine the potential D3R modulation of synaptic connectivity between NAc D3-MSNs

357   and VP, LH and VTA neurons. D3R activation using PD-128907 decreased GABA release

358   onto VP neurons that was optogenetically evoked from *Drd3*-positive MSNs (Fig. 4f-g).

359   This D3R-mediated decrease in GABA release was associated with an increase in PPR

360   and decreased $1/CV^2$ (Fig. 4h-i). Conversely, GABA release from D3-negative MSNs

361   targeted with Cre-OFF ChR2 onto VP neurons was not inhibited by PD-128907 (Fig. 4g).

362   These findings demonstrate that D3Rs inhibit GABA release from MSNs onto VP neurons

363   via a presynaptic site of action. Interestingly, D3R activation failed to decrease oIPSC

364   amplitude in both LH and VTA neurons (Fig. 4j-q), suggesting that MSN connections onto

365   LH and VTA neurons lack functional D3R. Taken together, our results reveal that

366   presynaptic D3R on NAc MSNs selectively inhibits local collaterals and GABAergic

367   transmission to the VP, but not in the outputs to the LH and VTA.

368   **Motivated behavior requires local D3R signaling within the NAc**

369   Our electrophysiology results demonstrated that NAc collaterals and outputs to the

370   VP, but not LH and VTA, are regulated by NAc D3Rs expressed in MSNs. However, cKO

371   of D3Rs from NAc neurons projecting to VP, LH or VTA generally produced motivational

372   deficits. Therefore, given that neurons projecting to VP, LH and VTA represent different

373   populations, we hypothesized that D3R signaling is acting locally within the NAc to

374   influence motivated behavior. We first tested whether microinfusion of the D3R antagonist

375   [77, 78] (1.8 ng per infusion site) into the NAc resulted in decreased running behavior (Fig.

376   5a). NAc D3R antagonism decreased preference for, and running on the freely-moving

377   disk in the disk choice task (Fig. 5b), a result consistent with the hypothesis that D3R

378   signaling within the NAc is essential for motivated running behavior. However, D3R

379   antagonism within the NAc blocks D3R signaling in MSNs as well as any putative afferent

380   inputs that may potentially express D3Rs at their terminals, such as the VTA, PVT or

13

381   mPFC[79-81].   Thus, non-MSN D3Rs on afferent inputs might be contributing to D3R

382   regulation of motivation. To specifically assess whether D3R acting on MSNs locally

383   within the NAc microcircuitry is driving motivation, we implemented novel functional

384   disconnection procedures involving pharmacological antagonism and cKO of NAc D3Rs

385   (Fig. 5c). In these experiments, control $Drd3^{fl/fl}$ mice received direct microinfusion of SB-

386   277011A and ipsilateral injection of AAV-hSyn-GFP-Cre into the NAc (Fig. 5d). In this

387   group, the unmanipulated hemisphere still has intact D3R signaling, hence supporting

388   motivated behavior (Fig. 5e-f). Our experimental group (contralateral $Drd3^{fl/fl}$ mice)

389   underwent functional disconnections wherein unilateral NAc microinjections of SB-

390   277011A and AAV-hSyn-GFP-Cre were made in contralateral hemispheres. Under these

391   conditions, only D3R signaling in MSNs within the NAc underwent bilateral disruption (Fig.

392   5d). We posited that if motivated running behavior does not rely on local D3R signaling,

393   then independently manipulating D3R activity in each of these hemispheres should not

394   disrupt NAc D3R-mediated motivation. On the other hand, if motivation is mediated by

395   local D3R signaling, then contralateral disconnection should disrupt motivation. Indeed,

396   contralateral $Drd3^{fl/fl}$ mice showed motivational deficits as shown by decreased running

397   behavior and preference towards the freely-moving disk, (Fig. 5e-f) relative to their

398   ipsilateral counterparts. As additional controls, we also quantified running disk

399   performance in $Drd3^{fl/fl}$ mice unilaterally injected with Cre-expressing virus or WT mice

400   that had unilateral infusions of SB-277011A (Extended Data Fig. 7a-b). Consistent with

401   the necessity of bilateral dysfunction in D3R signaling to observe changes in running

402   choice behavior, unilateral disruption of D3R signaling by either cKO or pharmacological

403   antagonism failed to modify preference for the freely-moving disk (Extended Data Fig. 7a-

404   b). Taken together, these results suggest that D3Rs acting on MSNs locally within NAc

405   microcircuitry is necessary for motivated behavior in mice.

406   Specific effects of D3R signaling on MSN physiology, such as inhibition of local

407   collaterals and outputs to the VP, but not LH and VTA, may underlie regulation of

408   motivation. We therefore determined the effects of non-selectively activating $G_{i/o}$-coupled

409   GPCRs using chemogenetics throughout the cell to determine how this differed from

410   endogenous D3Rs which have location- specific effects on MSNs and drive running. To

411   this end, we bilaterally injected AAV-hSyn-DIO-hM4D(G_i)-mCherry or AAV-hSyn-DIO-

412 mCherry in the NAc of *Drd3*-Cre mice and subjected the mice to the running disks choice

413 task (Extended Data Fig. 7c). Chemogenetic inhibition with clozapine N-oxide (CNO) 30

414 min prior to the start of testing significantly reduced preference for the freely moving disk

415 and decreased running behavior in mice expressing hM4Di relative to mCherry controls

416 (Extended Data Fig. 7d). hM4D-mediated suppression of NAc D3-MSN activity did not

417 affect, however, general locomotor activity or open field anxiety (Extended Data Fig. 7e).

418 Of note, this approach causes DREADD overexpression in all compartments of D3-MSNs

419 [82], including dendrites and outputs to LH and VTA, where we showed NAc D3R do not

420 regulate synaptic transmission. This further emphasizes that the specific presynaptic

421 distribution of D3Rs in NAc MSNs is essential to drive motivational running. Thus, taken

422 together, our results suggest that D3R-induced decrease in GABAergic output drives

423 motivation to run via presynaptic inhibition of NAc MSN collaterals.

424 **NAc D1Rs mediate reinforcement, but not motivation**

425 Since *Drd3* is largely co-expressed with *Drd1a* D1Rs and the vast majority of D1-

426 MSNs express *Drd3* (Fig 1)*,* we determined if these DA receptor subtypes differ in

427 controlling reward function. As low-affinity receptors, NAc D1Rs modulate reward-related

428 behaviors presumably by detecting phasic changes in DA and modifying synaptic

429 transmission onto MSNs[25-27] However, the precise role of NAc D1Rs, as compared to

430 D3Rs, in regulating motivation and reinforcement remains unclear. *Drd1a*fl/fl mice injected

431 with AAV-Cre (NAc-D1RcKO) into the NAc were run concomitantly with the NAc-D3RcKO

432 experiments described above (Fig. 6a). We found that cKO of *Drd1a* in the NAc resulted

433 in impaired FR1 acquisition, suggesting that D1R signaling in the NAc is necessary for

434 reward-driven reinforcement (Fig. 6b). The decrease in lever pressing in NAc-D1RcKO

435 mice persisted under FR5 schedules of reinforcement and dissipated with training (Fig.

436 6c). Similar to WT controls and opposite NAc-D3RcKO mice, NAc-D1RcKO mice

437 preferred to work for a higher palatable reward in the effort-based choice task (Fig. 6d).

438 Furthermore, break points during progressive ratio schedules did not differ between WT

439 and NAc-D1RcKO mice (Fig. 6e), indicating that the motivation to seek a palatable reward

440 remained intact. Similar to the lack of effect in instrumental motivation, NAc *Drd1a* cKO

441 did not strongly impact motivated running behavior in the running wheel and disk choice

15

442 behaviors (Fig. 6f-g, Extended Data Fig. 8a). Furthermore, NAc *Drd1a* cKO did not have

443 alter sucrose preference (Extended Data Fig. 8b), sociability (Extended Data Fig. 8c),

444 light-dark box (Extended Data Fig. 8d) or novel object recognition (Extended Data Fig.

445 8e) tests, indicating that NAc D1R function is not essential for hedonic processing,

446 anxiety-like and novelty-seeking behaviors, respectively. Taken together, our results

447 suggest that D1Rs, but not D3Rs, play a role in reinforcement.

448 The role of NAc D1Rs may not be limited to positive reinforcement, but may also

449 play a role in reinforcement of threat avoidance (negative reinforcement) in addition to

450 positive reinforcement. We determined whether reinforcement of avoidance of a

451 footshock requires NAc D1Rs using a modified platform-mediated avoidance

452 paradigm[83,84]. Here, mice were presented with an auditory cue (CS, tone) that co-

453 terminated with a footshock (Fig. 6h), and mice could avoid the footshock by mounting a

454 platform located in one of the corners of the chamber. NAc-D1RcKO had avoidance

455 deficits and received more shocks and spent significantly less time on the platform than

456 WT mice (Fig 6i). In contrast, NAc-D3RcKO mice did not display deficits in shock

457 avoidance. Deficits in avoidance behavior in NAc-D1RcKO mice were also observed

458 upon re-exposure to the platform-mediated avoidance task 24 hours later (Extended Data

459 Fig. 8f), supporting a sustained deficit in threat avoidance. These results further

460 demonstrate that NAc D1R, but not D3R, activity is essential for negative reinforcement,

461 suggesting that D1Rs regulate both positive and negative reinforcement. Collectively,

462 these results show that D3Rs and D1Rs play dissociable roles in regulating motivation

463 and reinforcement, respectively.

464 **D3R and D1R regulate separable features of NAc D1-MSN physiology**

465 We hypothesized that the dissociable roles of D1Rs and D3Rs in motivation and

466 reinforcement may be a consequence of divergent physiological effects in NAc D1-MSNs.

467 Previous studies have proposed that D1R regulation of N-methyl-D-aspartate receptor

468 (NMDAR)-dependent plasticity is a fundamental mechanism driving reward learning[26, 27,

469 85]. Using glutamate uncaging to evoke isolated postsynaptic NMDAR currents (Fig. 7a),

470 we found that activation of NAc D1Rs with the D1-like receptor agonist SKF-81297

471 potentiated AP-5-sensitive NMDAR currents in D1R-positive neurons, an effect that was

16

472 blocked with bath-application of the D1R-selective antagonist SCH39166 (Fig. 7b-d).

473 Interestingly, D3R activation failed to modify NMDAR currents (Fig. 7b-d). Furthermore,

474 SKF-81297 failed to potentiate NMDAR currents in D1R-positive projection neurons with

475 D1R cKO, demonstrating the specificity of our pharmacological and genetic manipulations

476 (Fig. 7e-h). Thus, D1Rs, but not D3Rs, potentiate NAc NMDAR currents, which provide a

477 potential substrate for reward learning and reinforcement. We subsequently

478 demonstrated that D1R activation using SKF-81297 did not modify GABA release from

479 D3R MSNs NAc collaterals (Fig. 7i-l), consistent with separable control of inputs and

480 outputs of NAc MSNs by D1Rs and D3Rs, respectively. Altogether, these results

481 demonstrate that dissociable control of motivated and reinforced behaviors by D1Rs and

482 D3Rs likely stems from dissociable physiological effects in D1-MSNs.

483   Lastly, to determine whether D1R interactions with NMDAR currents are necessary

484 for reinforcement, we performed disconnection experiments of NAc D1R and NMDAR

485 function during acquisition of FR1 lever pressing. *Drd1a*^fl/fl^ mice were injected with AAV-

486 GFP-Cre and infused with AP5 (700 ng per infusion site) in the ipsilateral hemisphere

487 (control group) or injected with AAV-Cre and infused with AP5 in the contralateral

488 hemisphere (experimental group) (Fig. 7m). AP5 microinjection on day two of FR1

489 acquisition session decreased FR1 lever pressing (Fig. 7n), consistent with deficits in

490 reward reinforcement. Importantly, decreased lever pressing was not influenced by the

491 number of lever presses during the Day 1 baseline session (Extended Data Fig. 8g).

492 Decreased FR1 lever pressing was not sustained since levels of lever pressing were not

493 significantly difference the day after AP5 microinjection. Collectively, our results reveal

494 key role of NAc D1Rs in the expression of positive and negative action reinforcement.

495 Mechanistically, this process involves, at least in part, amplification of postsynaptic

496 NMDAR-mediated excitatory drive onto NAc D1-MSNs.

497   **Discussion**

498 Here, we have identified distinct roles of NAc D3Rs and D1Rs in regulating different

499 features of D1-MSN physiology that promote complementary features of reward-related

500 behaviors. Activation of presynaptic D3Rs, but not D1Rs, in NAc MSNs inhibits

501 GABAergic transmission from collaterals within local microcircuits to promote effort-based

17

502   motivation. Conversely, NAc D1Rs, but not D3Rs, regulate reinforcement by interacting

503   with NMDARs. These findings indicate that the effects of DA on NAc MSNs are more

504   complex than canonical models of striatal function where D1Rs and D2Rs are largely

505   segregated, and provide a new model wherein DA receptor signaling at distinct receptors

506   (D1R and D3R) within a single cell type can differentially mediate motivation and

507   reinforcement.

508   Our integrative approach of genetic and pharmacological manipulations of D3R

509   expression and function enabled us to isolate the roles of NAc D3R signaling in reward

510   function, surmounting challenges associated with earlier approaches that primarily relied

511   on pharmacology (*i.e.*, lack of cellular or receptor specificity) and constitutive knockouts

512   (*i.e.*, lack of regional/cellular specificity and possible developmental compensations). We

513   employed two different paradigms that permit assessment of motivation, instrumental and

514   running behaviors. We showed that NAc D3R cKO disrupts motivation as assessed by

515   decreased break points in PR schedules in operant settings, a standard measure of

516   motivation. Further, NAc D3R cKO biased choice for low-effort rewards versus high-effort

517   rewards, consistent with a loss in motivation. Since food-seeking driven by hunger was

518   intact in NAc D3R cKO mice, but effort-based motivation was decreased, this suggest

519   that NAc D3Rs regulate properties of motivation that rely on efforts but not homeostatic

520   drive. Importantly, in other striatal compartments, such as the dorsal striatum, D3Rs are

521   not as enriched and the role this region plays in motivation is less established[31]. Here, we

522   also utilized running, a multi-dimensional behavior, to further demonstrate that NAc D3Rs

523   regulate the motivational component of a non-food based rewarding stimulus. We found

524   that NAc D3R signaling was necessary for promoting running on a novel wheel during

525   their inactive cycle and in a choice task during the active cycle, but not general locomotor

526   activity or wheel running under the control of circadian cycle. Indeed, DA signaling in the

527   NAc has been recently shown to underlie motivation to exercise[86]. Together, results from

528   operant and running procedures are consistent with the hypothesis that D3Rs regulate

529   the activational components of motivation, which include effort, persistence, and/or

530   vigor[3,8,11,12, 87]. This is of particular importance since physical activity and effort, or lack

531   thereof, has been linked to fluctuations in motivation in various neuropsychiatric

532   diseases[88].

533   Our study suggests that DA acting presynaptically on D3Rs inhibits GABAergic

534   inhibitory transmission arising from local MSN collaterals to drive motivated behavior.

535   D3R suppression of local inhibitory connections might disinhibit MSNs and concomitantly

536   activate downstream targets of the NAc to promote motivation. Consequently, this work

537   advances our previous understanding of the behavioral relevance of NAc collateral

538   connections, which have been posited to regulate striatal-dependent behavior[71, 75].

539   Furthermore, NAc D1-MSNs also corelease neuropeptides, such as dynorphin and

540   substance P[9], which mediate reward and avoidance behaviors when acting in the

541   dorsomedial or ventromedial NAc shell[89]. Thus, D3Rs may orchestrate multimodal

542   signaling from MSNs by regulating local collateral outputs. Additionally, D3Rs may

543   regulate different aspects of D1-MSN physiology, such as intrinsic excitability[37], within the

544   NAc. Nevertheless, whether these physiological actions of D3R signaling are also

545   important for regulating reward function is presently unclear.

546   Coexpression of *Drd3* and *Drd1a* in NAc D1-MSNs might provide these cells with

547   the ability to detect DA in different spatiotemporal domains. Striatal MSNs, and NAc

548   MSNs by extension, have been classically defined by the expression of a single DA

549   receptor subtype[23, 24], and this is thought to underlie differential effects on reward function.

550   In this study, we have shown that the majority of NAc D1-MSNs highly express *Drd3*, and

551   only a subset of D2-MSNs express *Drd3*. Furthermore, *Drd3* is expressed at higher levels

552   in D1-MSNs than D2-MSNs, suggesting D3R is anatomically poised to complement D1R

553   function in D1-MSNs. We demonstrated that D3Rs and D1Rs are likely providing NAc

554   D1-MSNs with different computational properties via divergent cellular effects in distinct

555   sub-cellular compartments. Electron microscopy studies have shown that D1Rs and

556   NMDARs colocalize in the somatodendritic compartment of NAc MSNs[90]. This is

557   consistent with the present and previous electrophysiological findings showing that D1Rs

558   potentiate NMDA receptor currents or D1R-NMDA receptor interactions are critical for

559   plasticity[26,27,85, 91-93]. Further, we found that D3R signaling inhibits GABA release from

560   MSN collaterals, providing evidence that D3Rs are functionally localized to MSN axon

561   terminals. This dissociation suggests that functional D1R and D3R may be localized to

562   distinct sub-cellular compartments. D1Rs and D3Rs may also both regulate common

563   aspects of MSN physiology not explored in the present study. Even under those

19

564 circumstances, D3Rs and D1Rs are coupled to inhibitory G_i and stimulatory G_s proteins,

565 respectively[35], and these differences in coupling to downstream G protein effectors could

566 also promote the differential effects on MSN physiology in domains where the two

567 receptors may overlap. Further, D3Rs have 100-fold greater affinity for DA than D1Rs[18,

568 35], which is likely to influence how these receptors are engaged by complex DA dynamics.

569 As lower affinity receptors, D1Rs may only be occupied by large increases DA

570 concentrations associated with phasic DA release. This provides a mechanism to

571 potentiate NMDAR activity at excitatory synapses that were coincidentally active during

572 phasic DA release and subsequently promote long-lasting plasticity, such as long-term

573 potentiation mediated by structural changes and increased AMPAR currents[26,27]. In

574 contrast, D3Rs may be occupied by "tonic" DA signaling generated by spontaneous DA

575 transients or be useful for detecting dips in DA transmission. Further, in contrast to D1Rs,

576 D3Rs would not only be occupied during the peak of phasic DA release but also during

577 the decay phase of the phasic DA response. Together, unique co-expression of D1R and

578 D3R provides NAc D1-MSNs with the molecular machinery to orchestrate dissociable

579 features of reward-related behavior via differential translation of distinct modes of DA

580 transmission into physiological changes.

581   To our knowledge, this is the first demonstration that separate DA receptors

582 provide co-expressing NAc MSNs exert distinct physiological effects to regulate separate

583 features of reward-related behavior. Since D3Rs and D1Rs are present within the same

584 D1-MSN population and exert different cellular effects and have different affinities for DA,

585 this work resolves long-standing questions concerning what behaviors DA signals control

586 at different local concentrations and timescales. Within this framework, we predict that

587 D3Rs would detect slower changes in DA (*i.e.*, changes in tonic DA driven by internal

588 state), and regulate motivation through inhibition of NAc collateral transmission.

589 Conversely, we found that D1Rs acting on postsynaptic NMDAR-mediated currents are

590 critical for reinforcement of reward-seeking behavior. NAc D1R may be necessary for the

591 early stages of learning when reward- and punishment-evoked transients are largest and

592 cue evoked-transients are emerging. Thus, phasic DA acting through NAc D1Rs would

593 permit D1 MSNs to integrate specific representations carried by coincidentally-active

594 excitatory afferent inputs via NMDA-dependent plasticity and changes in excitability[94].

20

595   This mechanism would provide D1 MSNs the capacity to strengthen representations

596   conveyed by upstream excitatory neuronal ensembles converging on individual D1-MSNs

597   to support execution of reinforced behaviors. Motivation and reinforcement are

598   dissociable reward features with complementary roles in establishing and maintaining

599   goal-directed behavior, and coordinated D3R and D1R signaling may help integrate these

600   functions. For example, as DA unbinds D1Rs (lower affinity DA receptor) during the decay

601   phase of phasic DA release triggered by reinforced behavior, D3Rs (which binds DA with

602   higher affinity) may remain bound and activated and increase motivation in response to

603   feedback from a positively reinforced outcome. This is an important consideration given

604   that DA kinetics in the ventral striatum are longer-lasting relative to the dorsal striatum[95].

605   Our model therefore provides a receptor-based mechanism by which motivational states

606   can be adjusted by on-going behavior depending on outcomes. Lastly, DA release can

607   be regulated locally in the NAc independently of VTA DA neuron firing, including via

608   cholinergic and opioid receptors that directly excite and inhibit DA terminals,

609   respectively[96-101]. This is of relevance since DA release controlled at the level of the VTA

610   or locally may differentially contribute to DA dynamics and influence how D1Rs and D3Rs

611   in D1-MSNs are activated.

612   In conclusion, our work refines our circuit-level understanding on how DA release

613   in the NAc is translated into dissociable aspects of reward function via D3Rs and D1Rs

614   co-expressed in NAc MSNs. This provides a novel description of separable control of

615   reward and physiological features by DA within the same cell type. A plethora of

616   psychiatric and neurological disorders are characterized by dysfunctional or amplified

617   reinforcement and/or motivation. The present study provides insight into how dysfunction

618   in DA release and/or signaling in brain disorders may impact specific reward domains via

619   NAc D1Rs and D3Rs, and provides potential therapeutic targets to treat specific

620   alterations in distinct reward features.

621   **Methods**

622   **Mice**

623   Adult female and male mice (aged 8-20 weeks at the start of experiments) were used

624   throughout the study. No significant differences were found between both sexes, and data

21

625 were therefore pooled to complete final group sizes. DA D3 receptor-IRES-Cre (*Drd3*-

626 Cre) (Tg(Drd3-cre)KI196Gsat/Mmucd, GENSAT, KI196, a gift from Charles Gerfen) and

627 *Drd3*-Cre crossed with Ai14-tdTomato reporter mice (*Drd3*-Cre/Ai14) were made

628 congenic with a C57BL/6J background and were used for anatomical characterization

629 and electrophysiological experiments. *Drd3*$^{fl/fl}$ mice (kindly provided by Z. Freyberg) were

630 also bred on a C57/BL6J background and were used for behavioral experiments.

631 Generation of *Drd3*$^{fl/fl}$ mice: To develop this strain, LoxP elements were inserted

632 flanking the transcriptional start site in exon 1 of *Drd3* (Extended Data Fig. 1a).

633 Specifically, a targeting vector was designed via recombineering as described previously

634 [102, 103]. We first retrieved approximately 12.2 kb of *Drd3* genomic sequence encompassing

635 8.3 kb of the 5'-upstream region preceding exon 1 through 3.5 kb of the intron 1 sequence

636 from the BAC, RP24-135K7. This genomic sequence was inserted into a pDTA vector

637 containing the PGK-DTA negative selectable marker by gap repair. We then inserted the

638 5' LoxP site approximately 4 kb upstream of the *Drd3* transcriptional start site in exon 1

639 followed by insertion of Frt-PGFneo-Frt-LoxP approximately 500 bp 3' downstream of

640 exon 1. The final vector contains 5' and 3' arms of 4.2 kb and 3.2 kb, respectively. The

641 vector was then linearized by NotI digestion, purified and electroporated into mouse ES

642 cells derived from an F1(129Sv/C57BL/6J) blastocyst. Electroporated cells were cultured

643 in the presence of G418 48-hrs post-electroporation to select for cells with successful

644 genomic integration of our construct. G418-resistant colonies were subsequently picked

645 and screened by long range PCR using primers corresponding to sequences outside the

646 arms and specific to the 5' and 3' LoxP sites to identify targeted ES clones. Targeted ES

647 clones were then expanded and further analyzed by long-range PCR for confirmation

648 prior to using them for ES-morula aggregation to generate chimeric animals. The resulting

649 chimeric mice were then bred with ROSA26-FlpoER mice to remove the PGKneo

650 cassette to generate the final *Drd3*$^{fl/fl}$ mice. These *Drd3*$^{fl/fl}$ mice were then made congenic

651 with the C57BL/6J genetic background via backcrossing for 10 generations (N10). For

652 PCR genotyping, the following primers were used: *Drd3* Lox gtF 5′-

653 TGAGACTAAGCAGCGTCCAC-3′, *Drd3* Lox gtR 5′- CTCTGAGTTAGATCTCCCCAGC-

654 3′ for WT 372bps/Floxed 468 bp and *Drd3* Frt gtF 5′- GCTGGCTCTCCATAGATTCTGC-

655 3′, *Drd3* Frt gtR 5′- CTTGAACAGATGTAGGCACCCTG -3′ for WT 254 bp/Floxed 347 bp.

22

656   *Drd1a*^{fl/fl} mice were acquired from The Jackson Laboratory (JAX, 025700) and
657   were used for behavioral and electrophysiological experiments. *Drd1a*-tdTomato (B6.Cg-
658   Tg(*Drd1a*-tdTomato)6Calak/J, JAX, 016204) and *Drd1a*-tdTomato/*Drd3*-Cre mice were
659   used for electrophysiological experiments. Wild-type (WT; C57BL/6J, JAX#000664) mice
660   were also used in all experiments and were bred at NIMH or obtained from Jackson
661   Laboratories. *Drd3*-Cre mice used for anatomical and electrophysiology experiments
662   were heterozygous.

663   Mice were group housed (2–5 mice per cage) in temperature- (21-24 ºC) and
664   humidity- (40-65%) controlled facilities and maintained on a reverse 12-h light/12-h dark
665   cycle with lights off at 8 am. All mice were maintained in filter-topped cages and provided
666   food and water *ad libitum*, except for animals undergoing testing in operant procedures.
667   Single housing was necessary for experiments requiring food restriction (operant
668   conditioning) or acclimation to behavioral tasks (wheel running experiments) and is
669   explicitly denoted in those cases. All purchased mice were kept in the local animal facility
670   for at least one week following delivery before initiating experimental procedures. Mice
671   were monitored for health status daily and before experimentation for the entirety of the
672   study. All efforts were made to minimize pain and distress and the number of mice used.
673   All procedures were performed in accordance with the National Institutes of Health (NIH)
674   Guide for the Care and Use of Laboratory Animals and approved by the Animal Care and
675   Use Committee of the National Institute of Mental Health Intramural Research Program.

676   **Viral constructs**

677   Recombinant adeno-associated viruses (AAVs) and type 2 canine adenoviruses (CAV2)
678   were implemented to allow expression of transgenes of interest. AAVs were purchased
679   from Addgene, the NIDA Genetic Engineering and Viral Vector Core, Boston Children's
680   Viral Vector Core and UNC Viral Vector Core. CAV2 was acquired from the Institut de
681   Génétique Moléculaire de Montpellier. All constructs were aliquoted and stored at -80 °C.
682   Titers ranged from 10^{12} to 10^{14} genomic copies per mL. Specific details on each viral
683   construct can be found in Extended Data Table 2.

684   **Stereotaxic surgeries and optical fiber / guide cannula implantation**

685 All surgeries were conducted under aseptic conditions and body temperature was
686 maintained at approximately 36 ºC with a heating pad. Mice, 8-16 weeks of age, were
687 anaesthetized with a mixture of ketamine (100 mg/kg body weight; intraperitoneal
688 injection) and xylazine (10 mg/kg body weight; intraperitoneal injection) as confirmed by
689 complete absence of flinching response to pinch. The animal's head was shaved, and
690 ophthalmic ointment (GenTeal) was applied to the eyes to prevent drying. Mice were
691 subsequently placed in a stereotaxic apparatus (David Kopf Instruments Model 1900,
692 Tujunga, CA, USA) and the surgical site was exposed using a sterile scalpel after cleaning
693 with povidone–iodine and 70% ethanol. The mouse's head was leveled by ensuring the
694 difference in dorsoventral distance between bregma and lambda was within 50 µm. A
695 small craniotomy window was then made above the injection site with a stereotax-
696 mounted drill. The following injection coordinates (in mm) and volumes were used:
697 [anterior-posterior (AP) and medial-lateral (ML) relative to bregma; dorsal-ventral (DV)
698 relative to dura mater at target coordinate]: NAc (AP: +1.40; ML: ±1.65; DV -4.50, 12º
699 angle towards midline; 300 nL), VP (AP: +0.40; ML: ±1.35; DV -5.35; 300 nL), LH (AP: -
700 1.35; ML: ±1.10; DV -5.25; 300 nL), VTA (AP: -3.30; ML: ±1.85; DV -4.60, 14º angle; 300
701 nL). Infusions were made at a rate of 100 nL/min utilizing 29 Ga microinjection needles
702 connected to FEP tubing secured to a 2 µl Hamilton syringe and a microinjection pump
703 (UMP3, World Precision Instruments, Sarasota, FL). The infusion system was filled with
704 distilled water and separated from the infused virus or drug by a small air bubble. The
705 injector tip was first lowered 100 µm deeper than the target DV coordinate and then raised
706 to the planned coordinate before infusion to facilitate viral diffusion at the site of injection,
707 instead of along the needle track. After infusion, the injector was kept for 8 min at the
708 injection site to allow for diffusion and was then slowly withdrawn.

709 For cKO of *Drd1a* or *Drd3* in the NAc, homozygous *Drd1a*fl/fl or *Drd3*fl/fl mice
710 received bilateral injections of AAV8-hSyn-GFP-Cre (4.50E+12 GC/mL) or AAV1-EF1α-
711 eGFP in the NAc; WT mice were used as controls.

712 For anatomical tracing experiments, *Drd3*-Cre mice were injected with AAV2/9-
713 phSyn1(S)-FLEX-tdTomato-T2A-SynaptophysinEGFP or AAV1-Syn-FLEX-Chrimsom-

714   tdTomato (4.10E+12 genome copies (GC)/mL) into the NAc to characterize downstream

715   projections and terminals of NAc *Drd3*-containing neurons.

716   For pathway-specific deletion of NAc *Drd3*, CAV-Flp-GFP (1.05e13 GC/mL) was

717   delivered to the VP, LH or VTA and a mixture of AAV5-EF1α-fDIO-Cre (5.00E+12 GC/mL)

718   and AAV1-CAG-FLEX-tdTomato (5.90E+12 GC/mL) was delivered to the NAc at a ratio

719   of 9 to 1, respectively.

720   For electrophysiological studies examining D3-MSN connectivity and D3R

721   modulation of synaptic transmission, *Drd1a*-tdTomato/*Drd3*-Cre mice received bilateral

722   injections of AAV5-EF1α-DIO-ChR2(H134R)-eYFP (4.00E+12 GC/mL) or AAV1-EF1α-

723   DO-hChR2(H134R)-eYFP (5.88E+12 GC/mL) targeting the NAc.

724   For drug microinjection experiments, mice were bilaterally implanted with stainless

725   steel guide cannulas (26-gauge, 3.5 mm in length, P1 Technologies) 1 mm above the

726   NAc (AP: +1.40; ML: ±1.65; DV -3.50 from dura, 12º angle towards midline). Guide

727   cannulas were then secured to the skull using MetaBond cement and dummy cannulas

728   were used to maintain cannula patency and removed only during the injection period.

729   For disconnection procedures, *Drd3*$^{fl/fl}$ or *Drd1a*$^{fl/fl}$ mice were injected with AAV8-

730   Syn-GFP-Cre and implanted with a guide cannula above the NAc in the same hemisphere

731   (ipsilateral group) or injected with virus and implanted with the guide cannula in the

732   contralateral hemisphere (contralateral group).

733   For validation of the *Drd1a*$^{fl/fl}$ line, *Drd1a*$^{fl/fl}$ mice received bilateral injections of

734   Alexa Fluor 594-conjugated Cholera Toxin Subunit B in PBS (CTB-594, 1.0 mg mL^{-1}, no.

735   C-34776, Thermo Fisher) in either LH or VTA brain regions.

736   For chemogenetic inhibition experiments, *Drd3*-Cre mice received bilateral

737   injections of AAV1-EF1α-DIO-hM4D(Gi)-mCherry in the NAc to inhibit D3R-expressing

738   NAc MSNs. AAV5-hSyn-DIO-mCherry (1.2E+13 GC/mL) was used for control groups.

739   Following all surgical procedures, incisions were closed using VetBond (3M,

740   Maplewood, MN) or surgical staples. Mice were allowed to recover from anesthesia in

741   heating pads until they showed regular breathing and locomotion, at which point they

742   were transferred back to the vivarium. Animals received subcutaneous injections of

743   ketoprofen (5 mg/kg body weight) for three consecutive days for post-operative analgesia

744   and anti-inflammatory purposes. Experiments involving the use of AAVs were initiated 3-

745   4 weeks after injection, 3 weeks for CAV2-Flp-GFP and 7 days for retrobead and CTB

746   injection procedures.

747   **Anatomical characterization of *Drd3*-expressing MSNs**

748   <u>RNAscope fluorescent *in situ* hybridization</u>: Multiplex fluorescence *in situ* hybridization

749   (RNAscope, Advanced Cell Diagnostics, Newark, CA) was used to detect the expression

750   of *Drd1a*, *Drd2*, *Drd3*, and *Cre* mRNAs in the NAc of adult WT and *Drd3*^{fl/fl} mice. For all

751   RNAscope procedures, tools, slides, and equipment were cleaned with 70% ethanol and

752   RNAse inhibitors (RNAZap, Invitrogen) prior to use. Mice were euthanized by cervical

753   dislocation, brains were rapidly dissected, and flash-frozen for 20 seconds in 50 mL of 2-

754   methylbutane chilled on dry ice. Subsequently, brains were stored at -80°C until

755   sectioning. 16-µm slices containing the NAc were obtained using a cryostat (CM3050 S;

756   Leica Biosystems; Deer Park, IL, USA) at -20 °C and thaw-mounted onto Superfrost

757   microscope slides (Fischer Scientific) in a series of four slides. Slides containing sections

758   were stored at -80°C until *in situ* hybridization processing. *Drd1a*, *Drd2*, *Drd3* or *Cre*

759   mRNA signal was detected using the RNAscope fluorescent kit following ACDBio manual

760   [104]. Briefly, slides containing the NAc were removed from -80°C, fixed with prechilled 4%

761   paraformaldehyde for 20 min at 4°C, and subsequently washed twice for 1 min with PBS,

762   before gradual dehydration with 50% ethanol (1 x 5 min), 70% ethanol (1 x 5 min), and

763   100% ethanol (2 x 5 min). Next, slides were air-dried at room temperature for 10 min and

764   a hydrophobic barrier was drawn around the slides using a hydrophobic pen (Vector

765   Laboratories, Newark, CA). Sections were then incubated with Protease Pretreat-IV

766   solution for 20 min at room temperature. Slides were washed with ddH2O (2 x 1 min),

767   before being incubated with the appropriate probes for 2 hr at 40°C in the HybEZ oven

768   (Advanced Cell Diagnostics) and undergoing hybridization. Probes used were purchased

769   from Advanced Cell Diagnostics as follows: Mm-*Drd1a*-C1 (nucleotide target region 444-

770   1358; Accession number NM_010076.3), Mm-*Drd2*-C2 (nucleotide target region 69-1175;

771   Accession number NM_010077.2), Mm-*Drd3*-C3 (nucleotide target region 23-1253;

772   Accession number NM_007877.1), *Cre* recombinase (nucleotide target region 2-972;

773   Accession number N/A). Probes were warmed-up to 40°C in a water bath until use.

774   Slides were washed in wash buffer twice for 2 min, prior to being incubated with

775   three drops of amplification 1 buffer, Amplification 2 buffer, Amplification 3 buffer and

776   Amplification 4-Alt A/C buffer at 40°C in the HybEZ oven for 30, 15, 30, 15 minutes

777   respectively. Slides were washed in wash buffer twice for 2 min. DAPI solution was

778   applied to sections at RT for 20 sec to label nuclei. Finally, slides were coverslipped using

779   Vectashield Hard Set mounting medium (Vector Laboratories). Slides were stored at 4°C

780   until imaging. Z-stacked images including the NAc were acquired using an A1R confocal

781   microscope (Nikon, Tokyo, Japan) with a 20X objective. This produced a tiled image

782   containing the entirety of the NAc which was used for quantification. The following

783   combinations of laser excitation and emission filters were used for various fluorophores:

784   DAPI (405 nm excitation; 450/30 nm emission), eGFP (491 nm laser excitation; 528/38

785   nm emission), tdTomato (561 nm laser excitation; 586/15 nm emission), Cy5 (647 nm

786   laser excitation; 665/35 nm emission). All samples were imaged with the same settings

787   to allow comparison between samples. Background subtraction and thresholds were set

788   uniformly for all images.

789   Quantification of *in-situ* hybridization: Image analysis and cell quantification were

790   performed using ImageJ software (Fiji, version 2017) and CellProfiler software (version

791   3.1.9.; Broad Institute; Cambridge, MA) [105,106]. To analyze the images, each image was

792   opened in ImageJ and converted to a maximum intensity projection. Images were

793   overlapped onto the Allen Mouse Bran atlas to set boundaries for the total NAc area to

794   be analyzed. Two to three serial sections (between approximately AP +1.42 and +1.21)

795   were analyzed on the total NAc area for each mouse. For quantification, images were

796   imported to an automated CellProfiler pipeline that was kept identical across samples

797   from the same experiment. Here, only cells with a clear DAPI+ nucleus were counted,

798   which were then registered and used as markers for individual cells. ROIs for analysis

799   were defined as the 3 μm area surrounding the DAPI signal. A blinded experimenter set

800   thresholds for each channel which determines the minimum intensity of fluorescence for

801   a probe to be counted. These thresholds were validated by visual spot check throughout

802　the image to ensure cells and probes were being appropriately counted. CellProfiler

803　software provided CSV files with the total counts of cells and levels of overlap, which are

804　reported in the data. For co-expression of *Drd1a*, *Drd2* and *Drd3*, cells considered as

805　positive consisted of an area within the radius of a DAPI nuclear staining that measured

806　at least 10 positive pixels for receptor probes. For the percentage of retrobead-positive

807　cells expressing *Drd3* mRNA, retrobead-positive cells contained at least 6 for retrobead

808　labeling.

809　*Anterograde tracing of D3R-expressing NAc MSNs:* To examine the projection pattern of

810　*Drd3*-expressing NAc neurons, 300 nL of AAV1-hSyn1-FLEX-Chrimsom-tdTomato or

811　AAV2/9-phSyn1(S)-FLEX-tdTomato-T2A-SynaptophysinEGFP-WPRE were bilaterally

812　injected into the NAc of *Drd3*-Cre mice as described above. Mice were perfused three

813　weeks following viral injection and 50-µm-thick coronal brain slices were prepared.

814　Images were taken at approximately 300-µm intervals from brain regions expressing

815　tdTomato and/or GFP using a Nikon A1R confocal microscope with a 20X objective.

816　Regions of interest were labeled relative to bregma based on the "Paxinos and Franklin's

817　The Mouse Brain in Stereotaxic Coordinates" (Franklin, K. B. J. & Paxinos; Academic

818　Press, an imprint of Elsevier, 2013). Total integrated fluorescence intensity tdTomato and

819　GFP from each downstream target was quantified using ImageJ with identical pinhole,

820　gain, and laser settings. For each brain region, four images were acquired at the same

821　focal point from each animal. No additional post-processing was performed for any of the

822　images analyzed here.

823　*Retrobead retrograde tracing of D3R-expressing NAc MSNs:* C57BL/6J WT mice were

824　injected bilaterally with 200 nL of Red and Green Retrobeads IX (Lumafluor, Durham,

825　NC) into the VP, LH or VTA/SNc as described above. Per the manufacture's protocol, red

826　Retrobeads were injected at a 1:4 dilution and green Retrobeads were left undiluted.

827　Seven days after injection, brains were collected and processed for RNAscope

828　procedures as described above.

829　**Quantitative real-time PCR**

830　WT and *Drd3*$^{fl/fl}$ mice expressing Cre-recombinase in the NAc were euthanized by cervical

831　dislocation. Brains were rapidly dissected, and 1 mm coronal brain slices containing the

28

832 ventral striatum were obtained by slicing the brain placed in an iron matrix (Kent Scientific,

833 Corp., Torrington, CT). The NAc was microdissected bilaterally and immediately

834 transferred to microcentrifuge tubes on dry ice; samples were stored at -80°C for RNA

835 isolation and processing. Total RNA was extracted from dissected NAc samples using

836 the NZY RNA Total Isolation kit (ref. MB13402, Nzytech, Lisboa, Portugal), and purified

837 mRNA samples were reverse transcribed using the SuperScript IV First-strand cDNA

838 synthesis kit (Thermo Fisher Scientific). Target sequences were amplified from the cDNA

839 using the TaqMan Gene Expression Assay Kit (Thermo Fisher Scientific) and the SYBER

840 Green system (Power SYBR Green PCR Master Mix, Applied Biosystems). All Taqman

841 probes were purchased from Applied Biosystems and were as follows: *Drd1a*

842 (Mm02620146_s1), *Drd2* (Mm00438545_m1), *Drd3* (Mm00432887_m1), GAPDH

843 (Mm99999915_g1). Quantitative PCR (qPCR) was performed using TaqMan Fast

844 Polymerase (Applied Biosystems, Waltham, MA) in an ABI PRISM 7900HT SDS Real-

845 Time PCR system ((Applied Biosystems). Cycling conditions were as follows: initial hold

846 at 95°C for 20 s; 40 cycles of step 1 (95°C for 1 s); and step 2 (60°C for 20 s). Samples

847 were run in triplicates, and negative controls were run in parallel. The relative mRNA

848 expression level for each sample was calculated using the ΔΔCt method, where Ct was

849 the cycle threshold for each reaction and GAPDH was used as internal control (DCt = Ct

850 (gene of interest) – Ct (GAPDH)[107]. Gene expression fold change was calculated by

851 normalizing the value of each sample to the mean of the control samples.

852 **Histology**

853 Upon completion of all experiments, mice were deeply anaesthetized with euthanasia

854 solution (VedCo Inc., St. Joseph, MO), and then transcardially perfused with 40 mL of

855 cold phosphate-buffered saline (PBS 1X, pH 7.4), followed by 40 mL of cold 4% w/v

856 paraformaldehyde (PFA) in PBS. Brains were extracted and post-fixed in 4% PFA at 4 °C

857 overnight and then cryoprotected in 20% sucrose-PBS for 24 hours, followed by 30%

858 sucrose-PBS for 24-hrs, at which point they were stored in PBS or prepared for sectioning

859 on a cryostat. To this end, brains were embedded on the mounting disk with Tissue-Tek

860 Optimum Cutting Temperature Compound (Sakura Finetek USA, Torrance, CA) for

861 freezing over dry ice. Brains were subsequently placed in the cryostat at −20 °C, and

862   consequently sectioned into 50- or 100-μm slices. Slices were mounted on slide glasses

863   with DAPI Fluoromount-G mounting medium (0100-20, Southern Biotech, Homewood,

864   AL) for visualization on a Nikon A1R confocal microscope (10X objective, NA 0.45, lasers:

865   405 nm, 488 nm, 561 nm). Injection sites and optical fiber placements were routinely

866   confirmed in all animals by preparing coronal sections containing the region of interest.

867   After histological verification, animals with insufficient transgene expression, off-target

868   transgene expression outside the region of interest by visual inspection, and/or inaccurate

869   implant placement were excluded from data analyses. A representative scheme of the

870   viral spread for NAc-D3RcKO mice included in this study is included in Extended Data

871   Fig. 1k.

872   ***Ex-vivo* electrophysiology**

873   Slice electrophysiology recordings were performed as previously described[54,75]. Briefly, 3

874   to 8 weeks after surgery, mice were deeply anaesthetized with euthanasia (200mg/kg ip;

875   VedCo, Inc.) and subsequently decapitated after confirmation of absent toe and tail pain

876   reflexes. Brains were rapidly removed and chilled for 2 min in ice-cold NMDG-based

877   slicing solution containing (in mM): 92 NMDG, 20 HEPES, 25 glucose, 30 $NaHCO_3$, 2.5

878   KCl, 1.2 NaH_2PO_4, 5 sodium ascorbate, 3 sodium pyruvate, 2 thiourea, 10 $MgSO_4$, and

879   0.5 $CaCl_2$ (pH 7.35, 303-306 mOsm) and saturated with 95% O_2/5% CO_2. Brains were

880   rapidly blocked, dried on filter paper, and glued to a platform containing ice-cold NMDG

881   slicing solution within a vibratome (VT1200, Leica). Coronal sections (300 μm) containing

882   the NAc, VP, LH and VTA were cut at a speed of 0.07 mm/s while the brain was

883   submerged in ice-cold NMDG-based slicing solution. Following slicing, sections were kept

884   in a custom-built chamber containing NMDG slicing solution for 7 min at 34°C. Slices

885   were subsequently transferred to a chamber filled with modified holding aCSF saturated

886   with 95% O_2/5% CO_2 containing (in mM): 92 NaCl, 20 HEPES, 25 glucose, 30 $NaHCO_3$,

887   2.5 KCl, 1.2 $NaPO_4$, 5 sodium ascorbate, 3 sodium pyruvate, 2 thiourea, 10 $MgSO_4$, and

888   0.5 $CaCl_2$ (pH 7.35, 303-306 mOsm) at room temperature for at least 1 hr. Slices

889   remained in this solution for recovery until transfer to the recording chamber. For

890   recordings, the recording chamber was kept at 31°C and perfused with a pump (World

891   Precision Instruments) at a flow rate of 1.5-2.0 mL per minute with aCSF containing (in

892   mM): 126 NaCl, 2.5 KCl, 1.4 NaH_2PO_4, 1.2 $MgCl_2$, 2.4 $CaCl_2$, 25 $NaHCO_3$, and 11 glucose

893   (303-305 mOsm) at 31°C. Cells were visualized with a 40X water-immersion objective on

894   an Olympus BX5iWI inverted microscope equipped with infrared-differential interference

895   contrast (IR-DIC) optics and epifluorescence (Olympus Corp, Tokyo, Japan). 4IPatch

896   pipettes (2-4 MΩ) were pulled from borosilicate glass (G150TF-4; Warner Instruments,

897   Hamden, CT) and filled with a freshly filtered (0.22 μm syringe filter) cesium-based

898   internal solution (in mM: 117 cesium methanesulfonate, 20 HEPES, 0.4 EGTA, 2.8 NaCl,

899   5 TEA-Cl, 4 Mg-ATP, 0.4 Na-GTP and 5 QX-314 (pH 7.35; 280-285 mOsm). Whole cell

900   access was obtained from individual neurons after acquisition of a giga-ohm seal

901   recording. All recordings were made utilizing a Multiclamp 7400B amplifier (Molecular

902   Devices) and data were digitized at 10 kHz and filtered at 1-2 kHz using a 1440A Digidata

903   Digitizer (Molecular Devices). Series and input resistances (10-20 MΩ) were monitored

904   online using a -5 mV, 70-ms voltage pulse through the recording electrode. Cells with

905   >20% change in access resistance were discarded from further analysis. Liquid junction

906   potentials were ≈ -7 mV and were left uncorrected. Data were analyzed offline using

907   Clampfit 10.6 (Molecular Devices, San Jose, CA).

908   To isolate $GABA_A$ responses evoked by optogenetic stimulation of D3R-

909   expressing MSNs, the AMPA receptor antagonist DNQX (10 μM) and NMDAR antagonist

910   D-AP5 (50 μM) were included in the aCSF, and neurons were voltage-clamped at 0 mV.

911   Optogenetic-evoked inhibitory postsynaptic currents (oIPSCs) were elicited every 10 s by

912   photostimulating ChR2 using two 1-ms pulses of 473-nm LED light (pE-300[ultra], CoolLED,

913   Andover, United Kingdom) separated by a 50-ms interstimulus interval. ChR2-negative

914   cells were identified by the lack of ChR2 currents evoked by blue light stimulation. ChR2

915   currents were characterized by sustained, steady state currents in response to 1-s blue

916   light stimulation with an onset immediately at the start of the laser pulse. Synaptic

917   GABAergic currents in ChR2-negative cells were outward-currents that were not

918   sustained for the duration of a 100-1000 ms blue light pulse and had a delayed onset

919   beyond the 1 ms optical pulse. Cells that did not show a peak that exceeded baseline

920   noise in this window were counted as non-responders. Connectivity was calculated as

921   the percentage of cells receiving oIPSCs from NAc D3R-expressing MSNs. Paired pulse

922   ratios were calculated as the amplitude of the second peak divided by the amplitude of

923   the first peak. IPSCs were recorded until their amplitudes were stable for at least 5

924   minutes, at which point PD-128907 (1 µM), ML417 (1 µM) or SKF 81297 (10 µM) were

925   added to the bath for 10 min. After bath application, drugs were washed out for 5

926   additional min. Timecourse graphs of the effects of drug application were generated by

927   averaging raw oIPSCs measurements in 1-min bins and expressing each point as a

928   percentage of the average of the 5-min baseline. The averaged baseline and 5-min after

929   drug application were used for quantification of modulation of synaptic transmission. To

930   differentiate between D1- and D2-MSNs, slices were obtained from *Drd1a*-tdTomato mice

931   and recording were made from tdTomato positive (i.e. D1-MSNs) or tdTomato-negative

932   (putative D2-MSNs) cells. Because the electrophysiological results from the two MSN

933   populations were similar, data were grouped. Recordings in the VP, LH and VTA were

934   made irrespective of the identity of the cell. Spontaneous IPSCs (sIPSCs) were collected

935   in the presence of DNQX (10 µM) and D-AP5 (50 µM) and the last 5-min of baseline and

936   the last 5-min of drug application were used for quantification. Events were filtered online

937   at 1 kHz and counted manually utilizing Minianalysis software (Synaptosoft, Leonia, NJ).

938   At least 100 events per cell were acquired in 6 s blocks and detected using a threshold of

939   7 pA.

940   For the modulation of NMDAR currents, recordings were made at a +40 mV

941   holding potential with DNQX (10 µM), the GABA$_A$ antagonist picrotoxin (PTX, 50 µM) and

942   TTX (1 µM) in the bath to isolate glutamate uncaging-evoked NMDAR currents and

943   eliminate circuit effects evoked by glutamate uncaging. Glutamate uncaging was

944   achieved by applying a single 150-ms pulse of UV light (356 nm) through the microscope

945   objective every 20 s to a bath containing MNI-glutamate (50 µM, Tocris, Bioscience,

946   Bristol, United Kingdom). NMDA components were measured as currents 20 ms after the

947   peak. LED intensity was chosen to evoke responses at approximately half of maximal

948   amplitude. Evoked NMDAR currents were recorded until their amplitudes were stable for

949   at least 5 min, at which point PD-128907 (1 µM) or SKF-81297 (10 µM) was added to the

950   bath for 10 min. SCH-39166 (1 µM) was already present in the bath to pharmacologically

951   antagonize D1R signaling. Timecourse graphs were generated by averaging raw NMDAR

952   measurements in 1-min bins and expressing each point as a percentage of the average

953   of the 5-min baseline. The averaged baseline and last 5-min of drug application were

32

954 used for quantification. Bath application of AP5 at the end of the experiment abolished

955 glutamate uncaging-evoked currents, confirming that evoked currents were mediated by

956 NMDARs. For validation of *Drd1a* KO, AAV8-Syn-GFP-Cre was injected into the NAc to

957 genetically ablate *Drd1a* and CTB594 was delivered in the LH or VTA to visualize putative

958 NAc D1R-expressing MSNs. Whole-cell recordings of NMDAR currents were performed

959 on GFP-positive and CTB594-positive neurons as detailed above.

960 After recordings, images of the recording pipette were acquired for post hoc

961 estimation of recording location within using the same camera as above and using a 4x

962 Nikon objective. For all pharmacological experiments, one neuron per slice was analyzed.

963 In some cases, the slice was transferred to 4% paraformaldehyde overnight for post-hoc

964 imaging on a confocal microscope. The Clampfit suite v11.0.3.03 (Molecular Devices)

965 was used for data display, acquisition and storage.

966 **Behavior**

967 Behavioral experiments were conducted during the dark cycle (between 10 am and 6 pm)

968 unless otherwise specified. Mice were allowed to recover from surgery for at least 3 weeks

969 before behavioral testing was conducted. Animals were matched according to age, sex

970 and date of birth and single-housed at least one day before the start of testing. To

971 minimize the effect of stress on behavioral outcome, mice were acclimated to the red lit

972 and sound-proofed testing room for at least 30-min before the start of each assay.

973 Animals undergoing running behavioral testing were subjected to the following assays

974 in this order: wheel running, running disks choice test, open field test, sucrose preference

975 test, social interaction, light-dark box, and novel object recognition test (Extended Data

976 Fig. 1b). Separate cohorts of mice were used for operant conditioning experiments. For

977 pathway-specific D3R cKO, mice underwent testing in running wheel, running disk choice

978 behavior, and operant procedures.

979 <u>Wheel running</u>

980 Voluntary running was performed in mice with free access to a running wheel in their

981 cage. At least 24-h before the start of the experiment, mice were singly housed in clean,

982 standard cages to habituate them with social isolation in activity recording chambers. At

983   the start of the light cycle (*i.e.*, 8 pm), mice were transferred into cages that contained a

984   running wheel connected to an infrared sensor that recorded beam breaks on the wheel

985   to calculate distance traveled (ACT-551-FIL-MS-SS, Coulbourn Instruments, Holliston,

986   MA). Animals were provided with provided with ad libitum access to food and water, and

987   running activity was monitored for 60 consecutive hours. Data was collected every 5-min

988   from each mouse using Clocklab (Actimetrics, Wilmette, IL).

989   Running disks test

990   We designed an effort-related choice-behavior task to disentangle motivational running

991   behavior. Mice had to choose between two disks, one that was fixed, where animals could

992   not run on it, and another one that was freely moving, where animals experienced reward

993   by running on it. Disk were angled at approximately 30° relative to the floor. Each session

994   consisted of baseline and test phases. During baseline, the animal was placed in the

995   empty open-field arena and allowed to explore the environment for 10 min. After baseline,

996   the fixed and freely moving disks were inserted into the arena and disk-running activity

997   and general locomotion were recorded for 3 hrs. There was no interruption between

998   baseline and test phases. Visual (circles or stripes) and odor cues (ddH2O or 5% acetic

999   acid) were attached adjacent to each disk to further facilitate the recognition of each area

1000   of the arena. Tracking data was analyzed offline using TopScan software (CleverSys,

1001   Inc., Reston, VA). The position of the mouse was defined as the zone in which both front

1002   paws and center were located.

1003   Open-field test

1004   Mice were placed singly in an open field arena (43.8 cm x 43.8 cm x 39.4 cm) to assess

1005   general locomotor activity and anxiety-like behavior. For the former, the total distance

1006   traveled was measured for 30 min. For the latter, the arena was divided into 'center' (23

1007   x 23 cm) and 'edges' zones and the percentage of time spent in the center of the arena

1008   was measured. For both analyses, TopScan (CleversSys, Inc.) video tracking software

1009   was used to score the movement and location of the animals.

1010   Sucrose preference test

1011   Hedonic reward-seeking was measured using the sucrose preference test. Single-housed

1012   mice were first habituated by being placed a standard cage (45 × 27 × 15cm) that

34

1013   contained two bottles of tap water. Water intake was measured by weighing the bottles

1014   four hours after the start of the habituation period. The following day, one of the bottles

1015   was replaced with a 1% sucrose solution (wt/vol), and animals were again given a free

1016   choice between the two bottles. The total amount of tap water and sucrose consumed

1017   was recorded by again weighing the bottles after four hours. Sucrose preference was

1018   calculated as the amount of sucrose solution consumed relative to the total amount of

1019   liquid consumed and multiplied by 100 (sucrose solution intake/total intake) *100). To

1020   control for side preferences the location of the sucrose and water bottles was

1021   counterbalanced between cages. Sucrose preference testing occurred approximately 2

1022   hrs after the start of the animal's active cycle.

1023   Light-dark box

1024   The light-dark box test was performed to assess anxiety-like behavior. Mice were place

1025   in an open-field arena (43.8 cm x 43.8 cm x 39.4 cm) divided into two compartments

1026   connected by a small circular aperture (4 W x 5 H cm). One side was exposed to light in

1027   the room and the other was enclosed and dark. During testing, mice were placed in the

1028   lit side of the box, facing the wall farthest from the entrance to the dark side. Animals were

1029   allowed to explore the two compartments for 5 min. Videos were recorded with a camera

1030   positioned above the chamber. The latency to enter the dark compartment and the time

1031   spent in each side were quantified offline with TopScan software. Room lighting was

1032   measured with the aid of a lux meter during testing (~100 Lux).

1033   Novel object recognition test

1034   The novel object recognition task assessed novelty-seeking behavior, capitalizing on

1035   rodents' natural inclination to spend more time with a novel object than over a familiar

1036   one[108]. Object recognition testing was carried out in a plexiglass open-field box (43.8 cm

1037   x 43.8 cm x 39.4 cm) and comprised in two sessions: habituation and recognition. During

1038   the habituation session, animals were allowed to freely explore the environment, which

1039   contained two identical Lego® constructs in opposite corners of the box, for 10 minutes.

1040   Items were placed on a metal base to ensure they could not be moved or knocked over

1041   by the animals. Subsequently, mice were taken back to their home cages for an ITI of 1

1042   hour and were reintroduced in the apparatus for the recognition test lasting ten minutes.

1043   In this 10-min session, one of the two objects used in the habituation phase was replaced

1044   with a novel object that was differently colored and shaped compared to the original,

1045   familiar object. The identity and position of the novel and familiar objects were

1046   counterbalanced across groups. Objects were thoroughly cleaned with water between

1047   phases to remove odor traces. Total spent time exploring each of the objects during both

1048   phases was quantified offline using TopScan software. The discrimination ratio was

1049   calculated as the time spent interacting with the novel object area divided by the time

1050   spent in a novel object area plus the time spent in the familiar object area.

1051   <u>Social interaction assay</u>

1052   For social interaction experiments, mice were temporarily moved to a target-free holding

1053   arena (56 × 24 x 24 cm) that contained two empty mesh pencil cups (5× 6.5 × 8 cm) in

1054   opposite corners of the arena. Animals were first allowed to freely explore the chamber

1055   for 2.5 min before a novel juvenile mouse (3-6 weeks) of the same sex and strain (to avoid

1056   mutual aggression) was placed into one of the holders. The test mouse was allowed to

1057   freely interact for 7.5 min, and video was recorded with a camera suspended above the

1058   arena. The 'interaction zone' encompassed a circular area projecting 6.5 cm around the

1059   pencil cup. The 'corner zones' encompassed a 9 cm × 9 cm area projecting from both

1060   corner joints opposing the wire-mesh enclosure. Social interaction was automatically

1061   scored with AnyMaze software (Stoelting, Kiel, WI) and defined as the ratio of time spent

1062   in the interaction zone with a juvenile mouse (*i.e.* in active contact with the intruder's

1063   snout, flank, or anogenital area, grooming, 6.5 cm from the enclosure of the pencil cup)

1064   over time spent with the target absent.

1065   <u>Operant conditioning</u>

1066   Prior to initiating operant procedures, mice were weighed to the nearest 0.1 g to determine

1067   a baseline for free-feeding body weight. Mice were singly housed and maintained under

1068   food restriction to achieve 85-90% of their free-feeding body weights for 3 days before

1069   and throughout the experiments, which motivated them to perform the behavioral task.

1070   Mice were weighed daily and fed 1-hour after their daily behavioral sessions with 2 g of

1071   standard laboratory chow. Animals had free access to water throughout. Operant

1072   procedures were conducted 7 days per week over a 4-wk period.

1073   Chocolate pellet self-administration was used to examine reward-related behaviors and
1074   took place in sound-attenuated mouse operant chambers (ENV307A-CT, Med-
1075   Associates, Fairfax, VT, PC 5 software). Chambers were equipped with two retractable
1076   levers and a reward pellet dispenser. One lever was designated as 'active' and was paired
1077   with the delivery of chocolate pellets (20 mg, Bio-Serv, Flemington, NJ), while the other
1078   lever was designated 'inactive' awhere lever-pressing had no consequence on reward
1079   delivery. The assignment of active and inactive levers was counter-balanced between
1080   mice. There was a 5-s time-out after every pellet delivery during which lever pressing did
1081   not trigger any delivery. The location of active and inactive levers was counterbalanced
1082   across animals and chambers were kept dark (house light off) during all sessions. A
1083   house light was positioned above the levers and a fan was present to maintain ventilation
1084   throughout testing. Before the start of the conditioning experiments, animals first
1085   underwent two pretraining sessions in which chocolate pellets were delivered at a random
1086   interval schedule (mean of 45 s, range 4–132 s), where pressing in either lever had no
1087   consequence on reward delivery. Days 1-6 of operant training were conducted on a fixed-
1088   ratio 1 (FR1) schedule, and days 7-12 were conducted on an FR5 schedule, where mice
1089   had to press the active lever 1 and 5 times, respectively, to earn a reward. Mice underwent
1090   testing in one session each day. All FR sessions lasted 45 min.

1091   *Operant Choice task*: Our operant choice task was modified from previous reports[46,47].
1092   After 6 days of testing on FR5 schedule, mice underwent testing on the operant choice
1093   task. First, mice experienced a session where they were presented with a food receptacle
1094   containing freely-available regular laboratory chow or chocolate pellets in the corner of
1095   the operant chamber opposite of the wall containing the active lever and operant reward
1096   receptacle. This was done to expose the animals to freely-available food in the operant
1097   chambers. During this session, active and inactive levers were retracted. Freely-available
1098   reward exposure sessions with regular laboratory chow or chocolate pellets were
1099   conducted on different days prior to choice testing. Mice were subsequently tested in a
1100   choice task, where they could either lever-press on an FR5 schedule to obtain a highly
1101   palatable food (20 mg chocolate food pellets) or consume the freely available food over
1102   the grid located on the opposite side of the operant chamber in a food receptacle. Choice
1103   sessions with regular lab chow or chocolate pellets were conducted on different days.

37

1104   After a choice session, a retrain session where only chocolate pellets delivered on the
1105   FR5 schedule were available was presented to the mice. The number of lever-presses,
1106   quantity of freely-available food (standard chow or chocolate pellet) consumed, total
1107   amount of food consumed (pellets plus chow) and the amount of chocolate pellets
1108   obtained by lever pressing were recorded.

1109   *Progressive ratio operant tasks*: After FR schedule sessions, a progressive ratio (PR)
1110   schedule of reinforcement for chocolate pellets was used to assess the motivation to work
1111   for chocolate pellets. To familiarize animals with a schedule requiring more effort, a PR3
1112   schedule was used for 3 days. Under this schedule, response increments linearly
1113   increase by three lever presses (3, 6, 9, 12, 15, etc.) for delivery of each subsequent food
1114   pellet. Animals subsequently underwent 4 days of training on a PR7 schedule to assess
1115   motivation under a schedule with higher demands. During PR testing, sessions continued
1116   until 5 min had elapsed without the animal responding in the active lever. In each PR
1117   session the break point (the final number of responses an animal completes where a
1118   reward is delivered), was recorded. All PR sessions ended after 3 hours or until 5 mins
1119   elapsed without a response in the active lever.

1120   Platform-mediated avoidance task

1121   This modified tone-shock conditioning experiment tested for reinforcement of avoidance
1122   behavior. Experiments were conducted in sound-attenuated fear conditioning chambers
1123   (30 cm length × 25 cm width × 25 cm height, Med Associates) that were illuminated with
1124   red light. The floor of the chamber was composed of a metal grid that delivered an electric
1125   foot shock. All tests began with a 2-min baseline habituation. Following the baseline
1126   period, 20 pairings of a conditioned stimulus (CS, 30 sec, 80-dB, 4 kHz noise) co-
1127   terminating with an unconditioned footshock stimulus (US, 0.4 mA, 2 sec). The ITI
1128   between trials was 40-60 sec. Animals could avoid the shock by jumping onto a square
1129   Plexiglas platform (8 x 8 x 0.33 cm) located on a corner of the chamber that was fixed to
1130   the shock floors. Each experiment lasted for two days with one 30-min session conducted
1131   each day. Day 2 consisted of identical stimuli presentations as day one. Between
1132   experiments, shock grids and floor trays were cleaned with soap and water, and chamber
1133   walls were cleaned with wet paper towels. Tracking data was acquired and analyzed

1134 using AnyMaze software (Wood Dale, IL). This task was modified from previous reports
1135 to adapt it to mice[77,78].

D3R pharmacological inactivation

1137 Microinjection of the D3R antagonist SB-277011A (Tocris) was used to pharmacologically
1138 inhibit D3R signaling in the NAc. Animals were allowed to recover for 4 weeks after
1139 surgery before habituation to the microinjection procedure. For 2 days prior the start of
1140 the experiments, mice were habituated to handling and cannula manipulation. On the
1141 experimental day, 350 nL of 10 µM SB-277011A (1.79 ng, dissolved in 1% DMSO) or
1142 vehicle (1% DMSO) were bilaterally infused into the NAc. This was accomplished using
1143 33-gauge injector cannulas connected to a syringe pump (UMP3, World Precision
1144 Instruments) with PE20 tubing that protruded 1 mm beyond the tip of the 26-gauge guide
1145 cannula All microinjections were delivered over the course of 1 min. After infusion,
1146 injectors were left in place for 2 min to allow for complete drug diffusion. For D3R
1147 functional disconnection procedures, mice were habituated 2 days before the experiment
1148 by receiving an infusion of vehicle (1% DMSO). 5 min after the end of the intra-NAc
1149 injection, animals were placed in the open-field arenas and running disk choice testing
1150 was conducted. Cannula placements were verified by histology after injection of 300 nL
1151 per hemisphere of red fluorescent Retrobeads (Lumafluor).

D1R-NMDAR functional disconnection

1153 For 2 days prior the start of D1R-NMDAR procedures, mice were habituated to handling
1154 and cannula manipulation. On the experiment day, 350 nL per hemisphere of the
1155 competitive NMDAR antagonist AP5 (700 ng per infusion, dissolved in 0.9% saline) were
1156 infused according to the same procedure as D3R pharmacological inactivation. Cannula
1157 placements and spread of infused drug were verified by histology after injection of 300 nL
1158 per hemisphere of red fluorescent Retrobeads (Lumafluor).

Chemogenetic inhibition of D3R-expressing NAc MSNs

1160 *Drd3*-Cre mice undergoing inhibitory DREADD testing were allowed to recover for 4weeks
1161 following viral injection before the start of behavioral testing. On the day prior to testing,
1162 mice received an intraperitoneal injection of saline to habituate them with the injection

1163 procedure. On the day of the experiment, the DREADD agonist clozapine N-oxide
1164 hydrochloride (CNO; Enzo Life Sciences, East Farmingdale, NY) was administered
1165 intraperitoneally 30 min before the running disks test. CNO solutions were
1166 intraperitoneally injected at 0.1 ml solution per 10 g of mouse for a final concentration of
1167 1 mg/kg (in sterile saline).

Drugs

1169 (+)-PD 128907 hydrochloride (PD128907, Tocris), ML417 (Sibley Lab, NINDS) and SKF-
1170 81297 (Tocris) were dissolved in distilled water. SCH-39166 (Tocris) was dissolved in
1171 DMSO. SB-277011A (Tocris Biosciences) was dissolved in 1 % DMSO and administered
1172 at 10 µM. AP5 (Abcam, Cambridge, UK) was diluted in sterile 0.9 % saline. For
1173 electrophysiology experiments, 1 mM PD128907 and 1mM SCH-39166 were diluted to a
1174 final concentration of 1 µM in aCSF and 10 mM SKF-81297 was diluted to a final
1175 concentration of 10 µM in aCSF.

Quantification and Statistical Analysis

1177 Data analysis was performed using GraphPad Prism 9, (GraphPad Software, Inc., La
1178 Jolla, CA). Paired t-tests were used for within-group comparison of two treatments and
1179 an unpaired test was used for comparison between two groups. Differences across more
1180 than two groups were analyzed with either a one-way analysis of variance (ANOVA) with
1181 Tukey's or Dunnet's multiple comparison post-hoc test, a two-way ANOVA for data with
1182 Tukey's or Sidak's multiple comparison post-hoc test for two independent variables, or a
1183 two-way repeated-measures (RM) ANOVA for data with two independent variables and
1184 multiple measurements from the same subject. ANOVAs were followed by post hoc tests
1185 with multiple comparisons correction. In the case of datasets with missing values, we
1186 analyzed the data instead by fitting a (one-way) mixed model as implemented in
1187 GraphPad Prism 9.0. Kolmogorov–Smirnov test was used for cumulative probability plots.
1188 P values for linear regressions were calculated by using Pearson's correlation. For each
1189 experiment, the values and definitions of sample size (n) are explicitly explained in
1190 Extended Data Table 1. Statistical significance was defined as $*P < 0.05$, $**P < 0.01$,
1191 $***P < 0.001$, $****P < 0.0001$. R^2 represents a Pearson's correlation coefficient. Results

40

1192 are shown as mean ± SEM unless stated otherwise. Error bars represent SEM. See Table

1193 S1 for detailed statistics.

1194 **Data and code availability**

1195 Data and analysis code reported in this paper is available from the lead contact upon

1196 reasonable request.

1197 <div align="center">**Acknowledgements**</div>

1219 <div align="center">**Author information**</div>

1220 Conceptualization, J.E.T. and H.A.T.; Methodology, J.E.T., T.B.U., and H.A.T, Software,

1221 J.E.T., R.J.F. and S.R.; Validation, J.E.T.; Formal Analysis, J.E.T. and V.T.; Investigation,

1222 J.E.T., H.E.Y., H.A.T., Z.F., T.W., C.T.L., M.A., H.W. and R.J.F.; Resources, Z.F., A.E.M.,

1223 D.R.S. and H.A.T.; Data Curation, J.E.T.; Writing – Original Draft, J.E.T.; Writing, Revision

1224 and Editing, J.E.T., Z.F. and H.A.T.; Visualization, J.E.T.; Supervision, R.M. and H.A.T.;

1225 Project Administration, J.E.T. and H.A.T.; Funding Acquisition, Z.F. and H.A.T.

1226 **Declaration of interests**

1227 The authors declare no competing interests.

1228 **References**

1229 1.   Gershman, S.J. & Uchida, N. Believing in dopamine. *Nature Reviews*
1230 *Neuroscience* **20**, 703-714 (2019).
1231 2.   Dayan, P. & Balleine, B.W. Reward, Motivation, and Reinforcement Learning.
1232 *Neuron* **36**, 285-298 (2002).
1233 3.   Wise, R.A. Dopamine, learning and motivation. *Nature Reviews Neuroscience* **5**,
1234 483-494 (2004).
1235 4.   Salamone, J.D.*, et al.* Complexities and paradoxes in understanding the role of
1236 dopamine in incentive motivation and instrumental action: Exertion of effort vs.
1237 anhedonia. *Brain Research Bulletin* **182**, 57-66 (2022).
1238 5.   Grace, A.A. Dysregulation of the dopamine system in the pathophysiology of
1239 schizophrenia and depression. *Nature Reviews Neuroscience* **17**, 524-532 (2016).
1240 6.   Volkow, N.D., Wise, R.A. & Baler, R. The dopamine motive system: implications
1241 for drug and food addiction. *Nature Reviews Neuroscience* **18**, 741-752 (2017).
1242 7.   Russo, S.J. & Nestler, E.J. The brain reward circuitry in mood disorders. *Nature*
1243 *Reviews Neuroscience* **14**, 609-625 (2013).
1244 8.   Floresco, S.B. The Nucleus Accumbens: An Interface Between Cognition,
1245 Emotion, and Action. *Annual Review of Psychology* **66**, 25-52 (2015).
1246 9.   Castro, D.C. & Bruchas, M.R. A Motivational and Neuropeptidergic Hub:
1247 Anatomical and Functional Diversity within the Nucleus Accumbens Shell. *Neuron* **102**,
1248 529-552 (2019).
1249 10.   Berke, J.D. What does dopamine mean? *Nature Neuroscience* **21**, 787-793
1250 (2018).
1251 11.   Bromberg-Martin, E.S., Matsumoto, M. & Hikosaka, O. Dopamine in Motivational
1252 Control: Rewarding, Aversive, and Alerting. *Neuron* **68**, 815-834 (2010).
1253 12.   Mohebi, A.*, et al.* Dissociable dopamine dynamics for learning and motivation.
1254 *Nature* **570**, 65-70 (2019).
1255 13.   Jong, J.W.d., Fraser, K.M. & Lammel, S. Mesoaccumbal Dopamine Heterogeneity:
1256 What Do Dopamine Firing and Release Have to Do with It? *Annual Review of*
1257 *Neuroscience* **45**, 109-129 (2022).
1258 14.   Jeong, H.*, et al.* Mesolimbic dopamine release conveys causal associations.
1259 *Science* **378**, eabq6740 (2022).

1260 15.   Schultz, W. Multiple Dopamine Functions at Different Time Courses. *Annual*
1261 *Review of Neuroscience* **30**, 259-288 (2007).
1262 16.   Liu, C., Goel, P. & Kaeser, P.S. Spatial and temporal scales of dopamine
1263 transmission. *Nature Reviews Neuroscience* **22**, 345-358 (2021).
1264 17.   Kim, H.R.*, et al.* A Unified Framework for Dopamine Signals across Timescales.
1265 *Cell* **183**, 1600-1616.e1625 (2020).
1266 18.   Sippy, T. & Tritsch, N.X. Unraveling the dynamics of dopamine release and its
1267 actions on target cells. *Trends in Neurosciences* **46**, 228-239 (2023).
1268 19.   Yang, H.*, et al.* Nucleus Accumbens Subnuclei Regulate Motivated Behavior via
1269 Direct Inhibition and Disinhibition of VTA Dopamine Subpopulations. *Neuron* **97**, 434-
1270 449.e434 (2018).
1271 20.   Schultz, W. Dopamine reward prediction-error signalling: a two-component
1272 response. *Nature Reviews Neuroscience* **17**, 183-195 (2016).
1273 21.   Hamid, A.A.*, et al.* Mesolimbic dopamine signals the value of work. *Nature*
1274 *Neuroscience* **19**, 117-126 (2016).
1275 22.   Steinberg, E.E.*, et al.* A causal link between prediction errors, dopamine neurons
1276 and learning. *Nature Neuroscience* **16**, 966-973 (2013).
1277 23.   Gerfen, C.*, et al.* D1 and D2 dopamine receptor-regulated gene expression of
1278 striatonigral and striatopallidal neurons. *Science* **250**, 1429-1432 (1990).
1279 24.   Gerfen, C.R. & Surmeier, D.J. Modulation of striatal projection systems by
1280 dopamine. *Annual review of neuroscience* **34**, 441-466 (2011).
1281 25.   Lee, S.J.*, et al.* Cell-type-specific asynchronous modulation of PKA by dopamine
1282 in learning. *Nature* (2020).
1283 26.   Yagishita, S.*, et al.* A critical time window for dopamine actions on the structural
1284 plasticity of dendritic spines. *Science* **345**, 1616-1620 (2014).
1285 27.   Shen, W., Flajolet, M., Greengard, P. & Surmeier, D.J. Dichotomous Dopaminergic
1286 Control of Striatal Synaptic Plasticity. *Science* **321**, 848-851 (2008).
1287 28.   Iino, Y.*, et al.* Dopamine D2 receptors in discrimination learning and spine
1288 enlargement. *Nature* **579**, 555-560 (2020).
1289 29.   Calabresi, P., Picconi, B., Tozzi, A. & Di Filippo, M. Dopamine-mediated regulation
1290 of corticostriatal synaptic plasticity. *Trends in Neurosciences* **30**, 211-219 (2007).
1291 30.   Schwartz, J.C.*, et al.* The dopamine D3 receptor in nucleus accumbens: selective
1292 cellular localisation, function and regulation. *European Neuropsychopharmacology* **4**,
1293 190-191 (1994).
1294 31.   Sokoloff, P., Giros, B., Martres, M.-P., Bouthenet, M.-L. & Schwartz, J.-C.
1295 Molecular cloning and characterization of a novel dopamine receptor (D3) as a target for
1296 neuroleptics. *Nature* **347**, 146-151 (1990).
1297 32.   Le Moine, C. & Bloch, B. Expression of the d3 dopamine receptor in peptidergic
1298 neurons of the nucleus accumbens: Comparison with the D1 and D2 dopamine receptors.
1299 *Neuroscience* **73**, 131-143 (1996).
1300 33.   Gangarossa, G.*, et al.* Distribution and compartmental organization of GABAergic
1301 medium-sized spiny neurons in the mouse nucleus accumbens. *Frontiers in Neural*
1302 *Circuits* **7** (2013).
1303 34.   Tritsch, Nicolas X. & Sabatini, Bernardo L. Dopaminergic Modulation of Synaptic
1304 Transmission in Cortex and Striatum. *Neuron* **76**, 33-50 (2012).

1305   35.   Beaulieu, J.-M. & Gainetdinov, R.R. The Physiology, Signaling, and Pharmacology
1306   of Dopamine Receptors. *Pharmacological Reviews* **63**, 182-217 (2011).
1307   36.   Xi, Z.X.*, et al.* Blockade of dopamine D3 receptors in the nucleus accumbens and
1308   central amygdala inhibits incubation of cocaine craving in rats. *Addict Biol* **18**, 665-677
1309   (2013).
1310   37.   Manvich, D.F.*, et al.* Selective D2 and D3 receptor antagonists oppositely
1311   modulate cocaine responses in mice via distinct postsynaptic mechanisms in nucleus
1312   accumbens. *Neuropsychopharmacology*, 439398 (2018).
1313   38.   Song, R.*, et al.* Increased vulnerability to cocaine in mice lacking dopamine D3
1314   receptors. *Proceedings of the National Academy of Sciences* **109**, 17675-17680 (2012).
1315   39.   Simpson, E.H.*, et al.* Selective overexpression of dopamine D3 receptors in the
1316   striatum disrupts motivation but not cognition. *Biol Psychiatry* **76**, 823-831 (2014).
1317   40.   Shin, S.*, et al.* Drd3 Signaling in the Lateral Septum Mediates Early Life Stress-
1318   Induced Social Dysfunction. *Neuron* **97**, 195-208.e196 (2018).
1319   41.   Pribiag, H.*, et al.* Ventral pallidum DRD3 potentiates a pallido-habenular circuit
1320   driving accumbal dopamine release and cocaine seeking. *Neuron* **109**, 2165-2182.e2110
1321   (2021).
1322   42.   Ridray, S.*, et al.* Coexpression of dopamine D1 and D3 receptors in islands of
1323   Calleja and shell of nucleus accumbens of the rat: opposite and synergistic functional
1324   interactions. *European Journal of Neuroscience* **10**, 1676-1686 (1998).
1325   43.   Meijer, J.H. & Robbers, Y. Wheel running in the wild. *Proc Biol Sci* **281** (2014).
1326   44.   Greenwood, B.N.*, et al.* Long-term voluntary wheel running is rewarding and
1327   produces plasticity in the mesolimbic reward pathway. *Behav Brain Res* **217**, 354-362
1328   (2011).
1329   45.   Lett, B.T., Grant, V.L. & Koh, M.T. Naloxone attenuates the conditioned place
1330   preference induced by wheel running in rats. *Physiol Behav* **72**, 355-358 (2001).
1331   46.   Novak, C.M., Burghardt, P.R. & Levine, J.A. The use of a running wheel to
1332   measure activity in rodents: relationship to energy balance, general activity, and reward.
1333   *Neurosci Biobehav Rev* **36**, 1001-1014 (2012).
1334   47.   Sherwin, C.M. Voluntary wheel running: A review and novel interpretation. *Animal
1335   Behaviour* **56**, 11-27 (1998).
1336   48.   Garland, T., Jr*, et al.* The biological control of voluntary exercise, spontaneous
1337   physical activity and daily energy expenditure in relation to obesity: human and rodent
1338   perspectives. *Journal of Experimental Biology* **214**, 206-229 (2011).
1339   49.   Greenwood, B.N. & Fleshner, M. Voluntary Wheel Running: A Useful Rodent
1340   Model for Investigating the Mechanisms of Stress Robustness and Neural Circuits of
1341   Exercise Motivation. *Curr Opin Behav Sci* **28**, 78-84 (2019).
1342   50.   Basso, J.C. & Morrell, J.I. The medial prefrontal cortex and nucleus accumbens
1343   mediate the motivation for voluntary wheel running in the rat. *Behavioral Neuroscience*
1344   **129**, 457-472 (2015).
1345   51.   Salamone, J.D.*, et al.* Haloperidol and nucleus accumbens dopamine depletion
1346   suppress lever pressing for food but increase free food consumption in a novel food
1347   choice procedure. *Psychopharmacology (Berl)* **104**, 515-521 (1991).
1348   52.   Hutchison, M.A.*, et al.* Genetic inhibition of neurotransmission reveals role of
1349   glutamatergic input to dopamine neurons in high-effort behavior. *Molecular Psychiatry* **23**,
1350   1213-1225 (2018).

1351 53.   Baldo, B.A. & Kelley, A.E. Discrete neurochemical coding of distinguishable
1352 motivational processes: insights from nucleus accumbens control of feeding.
1353 *Psychopharmacology* **191**, 439-459 (2007).
1354 54.   Koob, G.F., Riley, S.J., Smith, S.C. & Robbins, T.W. Effects of 6-hydroxydopamine
1355 lesions of the nucleus accumbens septi and olfactory tubercle on feeding, locomotor
1356 activity, and amphetamine anorexia in the rat. *J Comp Physiol Psychol* **92**, 917-927
1357 (1978).
1358 55.   Salamone, J.D. & Correa, M. Motivational views of reinforcement: implications for
1359 understanding the behavioral functions of nucleus accumbens dopamine. *Behavioural*
1360 *Brain Research* **137**, 3-25 (2002).
1361 56.   Correa, M., Pardo, M., Carratalá-Ros, C., Martínez-Verdú, A. & Salamone, J.D.
1362 Preference for vigorous exercise versus sedentary sucrose drinking: an animal model of
1363 anergia induced by dopamine receptor antagonism. *Behavioural Pharmacology* **31**, 553-
1364 564 (2020).
1365 57.   Kupchik, Y.M.*, et al.* Coding the direct/indirect pathways by D1 and D2 receptors
1366 is not valid for accumbens projections. *Nature Neuroscience* **18**, 1230-1232 (2015).
1367 58.   Thoeni, S., Loureiro, M., O'Connor, E.C. & Lüscher, C. Depression of Accumbal to
1368 Lateral Hypothalamic Synapses Gates Overeating. *Neuron* (2020).
1369 59.   O'Connor, Eoin C.*, et al.* Accumbal D1R Neurons Projecting to Lateral
1370 Hypothalamus Authorize Feeding. *Neuron* **88**, 553-564 (2015).
1371 60.   Soares-Cunha, C.*, et al.* Distinct role of nucleus accumbens D2-MSN projections
1372 to ventral pallidum in different phases of motivated behavior. *Cell Reports* **38**, 110380
1373 (2022).
1374 61.   Tejeda, H.A.*, et al.* Pathway- and Cell-Specific Kappa-Opioid Receptor Modulation
1375 of Excitation-Inhibition Balance Differentially Gates D1 and D2 Accumbens Neuron
1376 Activity. *Neuron* **93**, 147-163 (2017).
1377 62.   Baimel, C., McGarry, L.M. & Carter, A.G. The Projection Targets of Medium Spiny
1378 Neurons Govern Cocaine-Evoked Synaptic Plasticity in the Nucleus Accumbens. *Cell*
1379 *Reports* **28**, 2256-2263.e2253 (2019).
1380 63.   Gibson, G.D.*, et al.* Distinct Accumbens Shell Output Pathways Promote versus
1381 Prevent Relapse to Alcohol Seeking. *Neuron* **98**, 512-520.e516 (2018).
1382 64.   Larson, E.B., Wissman, A.M., Loriaux, A.L., Kourrich, S. & Self, D.W. Optogenetic
1383 stimulation of accumbens shell or shell projections to lateral hypothalamus produce
1384 differential effects on the motivation for cocaine. *J Neurosci* **35**, 3537-3543 (2015).
1385 65.   Zhou, K.*, et al.* Reward and aversion processing by input-defined parallel nucleus
1386 accumbens circuits in mice. *Nature Communications* **13**, 6244 (2022).
1387 66.   Bocklisch, C.*, et al.* Cocaine Disinhibits Dopamine Neurons by Potentiation of
1388 GABA Transmission in the Ventral Tegmental Area. *Science* **341**, 1521-1525 (2013).
1389 67.   Edwards, N.J.*, et al.* Circuit specificity in the inhibitory architecture of the VTA
1390 regulates cocaine-induced behavior. *Nature Neuroscience* **20**, 438-448 (2017).
1391 68.   Pignatelli, M.*, et al.* Cooperative synaptic and intrinsic plasticity in a disynaptic
1392 limbic circuit drive stress-induced anhedonia and passive coping in mice. *Molecular*
1393 *Psychiatry* (2020).
1394 69.   Yim, Y.Y., Zurawski, Z. & Hamm, H. GPCR regulation of secretion. *Pharmacol*
1395 *Ther* **192**, 124-140 (2018).

70. Lovinger, D.M.*, et al.* Local modulation by presynaptic receptors controls neuronal communication and behaviour. *Nature Reviews Neuroscience* **23**, 191-203 (2022).

71. Burke, D.A., Rotstein, H.G. & Alvarez, V.A. Striatal Local Circuitry: A New Framework for Lateral Inhibition. *Neuron* **96**, 267-284 (2017).

72. Dobbs, Lauren K.*, et al.* Dopamine Regulation of Lateral Inhibition between Striatal Neurons Gates the Stimulant Actions of Cocaine. *Neuron* **90**, 1100-1113 (2016).

73. Lemos, Julia C.*, et al.* Enhanced GABA Transmission Drives Bradykinesia Following Loss of Dopamine D2 Receptor Signaling. *Neuron* **90**, 824-838 (2016).

74. Banghart, Matthew R., Neufeld, Shay Q., Wong, Nicole C. & Sabatini, Bernardo L. Enkephalin Disinhibits Mu Opioid Receptor-Rich Striatal Patches via Delta Opioid Receptors. *Neuron* **88**, 1227-1239 (2015).

75. Wilson, C.J. GABAergic inhibition in the neostriatum. *Prog Brain Res* **160**, 91-110 (2007).

76. Moritz, A.E.*, et al.* Discovery, Optimization and Characterization of ML417: A Novel and Highly Selective D3 Dopamine Receptor Agonist. *Journal of Medicinal Chemistry* (2020).

77. Carnicella, S.*, et al.* Implication of dopamine D3 receptor activation in the reversion of Parkinson's disease-related motivational deficits. *Translational Psychiatry* **4**, e401-e401 (2014).

78. Khaled, M.A.T.M., Pushparaj, A., Di Ciano, P., Diaz, J. & Le Foll, B. Dopamine D3 Receptors in the Basolateral Amygdala and the Lateral Habenula Modulate Cue-Induced Reinstatement of Nicotine Seeking. *Neuropsychopharmacology* **39**, 3049-3058 (2014).

79. Diaz, J.*, et al.* Dopamine D3 receptors expressed by all mesencephalic dopamine neurons. *J Neurosci* **20**, 8677-8684 (2000).

80. Gao, C.*, et al.* Molecular and spatial profiling of the paraventricular nucleus of the thalamus. *eLife* **12**, e81818 (2023).

81. Clarkson, R.L., Liptak, A.T., Gee, S.M., Sohal, V.S. & Bender, K.J. D3 Receptors Regulate Excitability in a Unique Class of Prefrontal Pyramidal Cells. *The Journal of Neuroscience* **37**, 5846-5860 (2017).

82. Roth, B.L. DREADDs for Neuroscientists. *Neuron* **89**, 683-694 (2016).

83. Bravo-Rivera, C., Roman-Ortiz, C., Brignoni-Perez, E., Sotres-Bayon, F. & Quirk, G.J. Neural Structures Mediating Expression and Extinction of Platform-Mediated Avoidance. *Journal of Neuroscience* **34**, 9736-9742 (2014).

84. Bravo-Rivera, H.*, et al.* Characterizing Different Strategies for Resolving Approach-Avoidance Conflict. *Frontiers in Neuroscience* **15** (2021).

85. Cahill, E.*, et al.* D1R/GluN1 complexes in the striatum integrate dopamine and glutamate signalling to control synaptic plasticity and cocaine-induced responses. *Molecular Psychiatry* **19**, 1295-1304 (2014).

86. Dohnalová, L.*, et al.* A microbiome-dependent gut–brain pathway regulates motivation for exercise. *Nature* (2022).

87. Salamone, J.D., Yohn, S.E., López-Cruz, L., San Miguel, N. & Correa, M. Activational and effort-related aspects of motivation: neural mechanisms and implications for psychopathology. *Brain* **139**, 1325-1347 (2016).

88. Ashdown-Franks, G.*, et al.* Exercise as Medicine for Mental and Substance Use Disorders: A Meta-review of the Benefits for Neuropsychiatric and Cognitive Outcomes. *Sports Med* **50**, 151-170 (2020).

89. Al-Hasani, R.*, et al.* Distinct Subpopulations of Nucleus Accumbens Dynorphin Neurons Drive Aversion and Reward. *Neuron* **87**, 1063-1077 (2015).

90. Hara, Y. & Pickel, V.M. Overlapping intracellular and differential synaptic distributions of dopamine D1 and glutamate N-methyl-D-aspartate receptors in rat nucleus accumbens. *Journal of Comparative Neurology* **492**, 442-455 (2005).

91. Ladepeche, L.*, et al.* Single-molecule imaging of the functional crosstalk between surface NMDA and dopamine D1 receptors. *Proc Natl Acad Sci U S A* **110**, 18005-18010 (2013).

92. Scott, L.*, et al.* Allosteric changes of the NMDA receptor trap diffusible dopamine 1 receptors in spines. *Proceedings of the National Academy of Sciences* **103**, 762-767 (2006).

93. Lee, F.J.*, et al.* Dual regulation of NMDA receptor functions by direct protein-protein interactions with the dopamine D1 receptor. *Cell* **111**, 219-230 (2002).

94. Lahiri, A.K. & Bevan, M.D. Dopaminergic Transmission Rapidly and Persistently Enhances Excitability of D1 Receptor-Expressing Striatal Projection Neurons. *Neuron* (2020).

95. Wei, W., Mohebi, A. & Berke, J.D. A Spectrum of Time Horizons for Dopamine Signals. *bioRxiv*, 2021.2010.2031.466705 (2022).

96. Mohebi, A., Collins, V.L. & Berke, J.D. Accumbens cholinergic interneurons dynamically promote dopamine release and enable motivation. *eLife* **12**, e85011 (2023).

97. Liu, C.*, et al.* An action potential initiation mechanism in distal axons for the control of dopamine release. *Science* **375**, 1378-1385 (2022).

98. Kramer, P.F.*, et al.* Synaptic-like axo-axonal transmission from striatal cholinergic interneurons onto dopaminergic fibers. *Neuron* (2022).

99. Brown, M.T.*, et al.* Ventral tegmental area GABA projections pause accumbal cholinergic interneurons to enhance associative learning. *Nature* **492**, 452-456 (2012).

100. Cachope, R.*, et al.* Selective Activation of Cholinergic Interneurons Enhances Accumbal Phasic Dopamine Release: Setting the Tone for Reward Processing. *Cell Reports* **2**, 33-41 (2012).

101. Spanagel, R., Herz, A. & Shippenberg, T.S. Opposing tonically active endogenous opioid systems modulate the mesolimbic dopaminergic pathway. *Proceedings of the National Academy of Sciences* **89**, 2046-2050 (1992).

102. Lee, E.C.*, et al.* A Highly Efficient Escherichia coli-Based Chromosome Engineering System Adapted for Recombinogenic Targeting and Subcloning of BAC DNA. *Genomics* **73**, 56-65 (2001).

103. Liu, P., Jenkins, N.A. & Copeland, N.G. A highly efficient recombineering-based method for generating conditional knockout mutations. *Genome Res* **13**, 476-484 (2003).

104. Wang, F.*, et al.* RNAscope: a novel in situ RNA analysis platform for formalin-fixed, paraffin-embedded tissues. *J Mol Diagn* **14**, 22-29 (2012).

105. McQuin, C.*, et al.* CellProfiler 3.0: Next-generation image processing for biology. *PLoS Biol* **16**, e2005970 (2018).

106. Erben, L. & Buonanno, A. Detection and Quantification of Multiple RNA Sequences Using Emerging Ultrasensitive Fluorescent In Situ Hybridization Techniques. *Curr Protoc Neurosci* **87**, e63 (2019).

107. Schmittgen, T.D. & Livak, K.J. Analyzing real-time PCR data by the comparative CT method. *Nature Protocols* **3**, 1101-1108 (2008).

1488 108. Bevins, R.A. & Besheer, J. Object recognition in rats and mice: a one-trial non-
1489 matching-to-sample learning task to study 'recognition memory'. *Nature Protocols* **1**,
1490 1306-1311 (2006).

1491
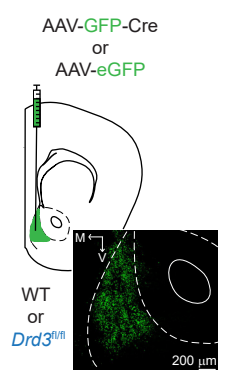
1492

1493
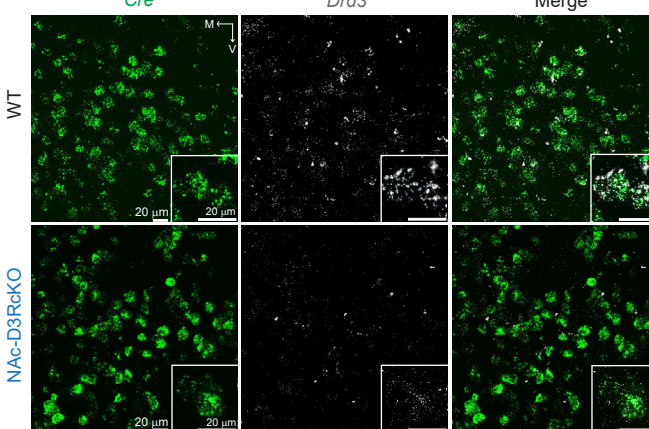
1494

1495
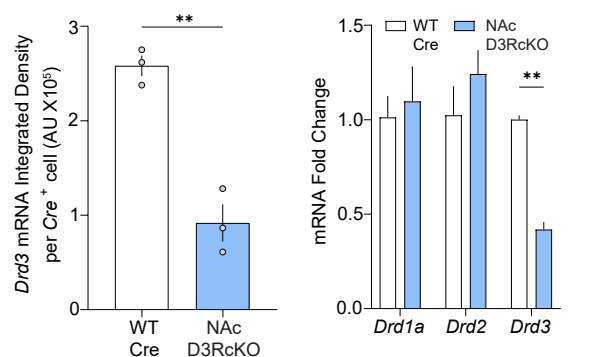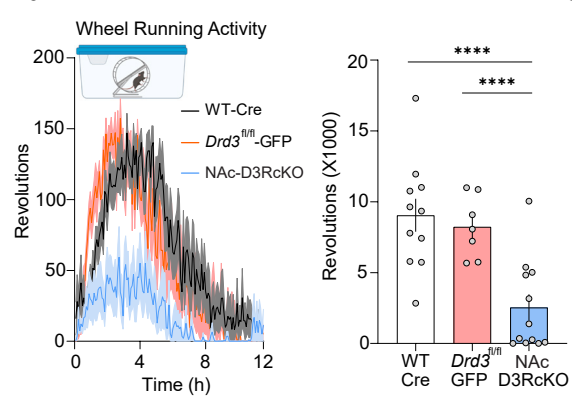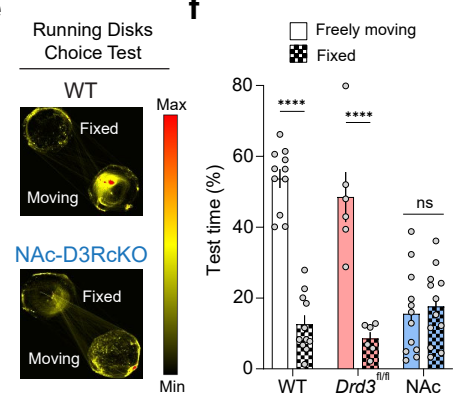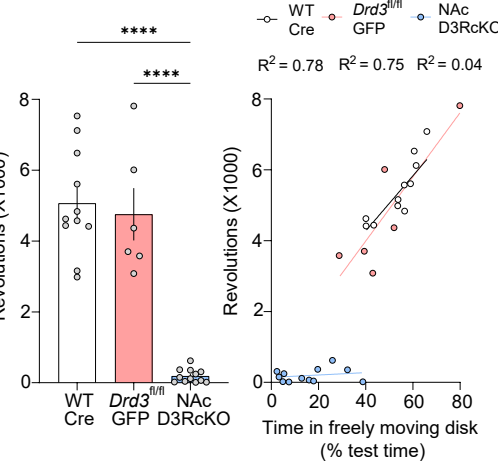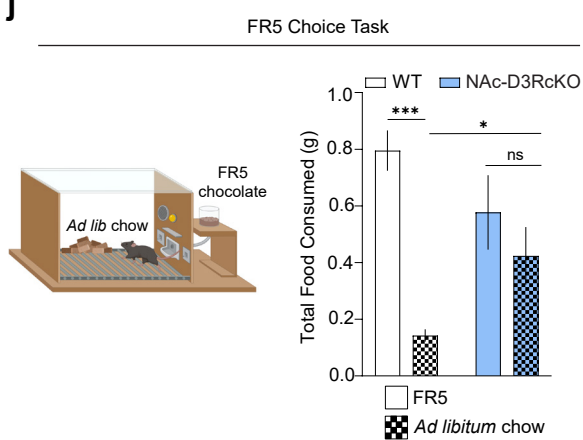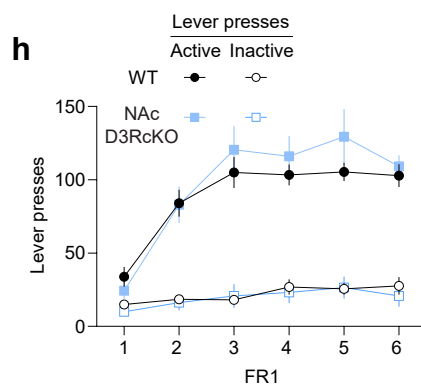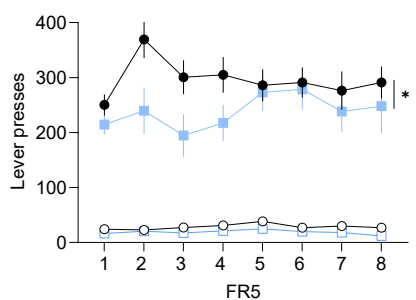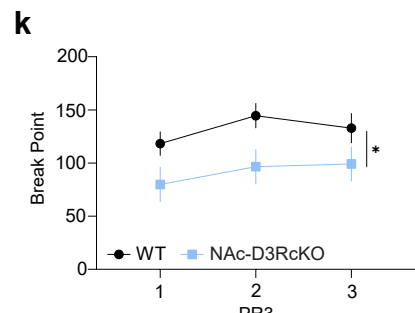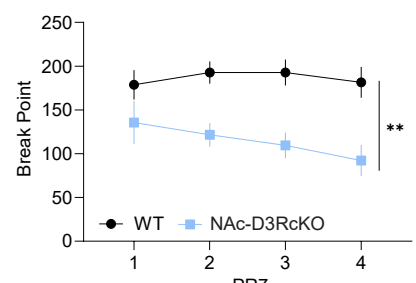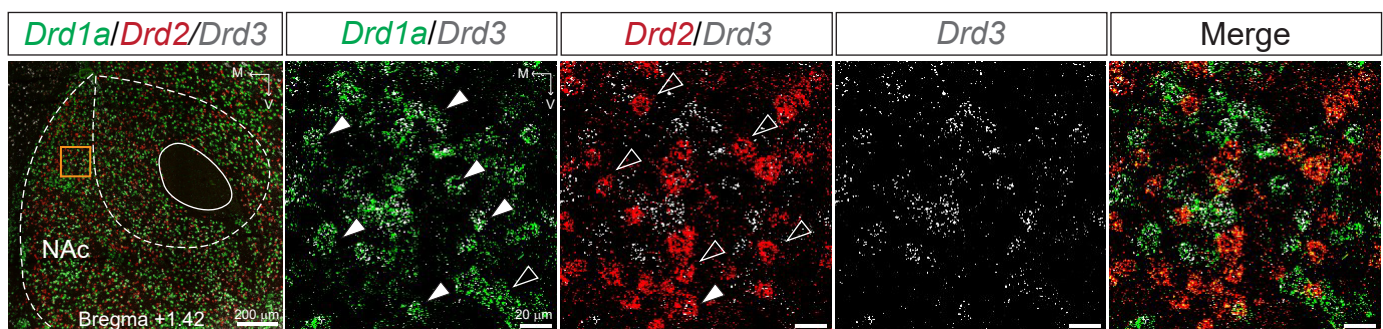
Figure 1

Figure 1. Conditional knockout of NAc D3Rs results in motivational deficits (see also Extended Data Figures Figure 1, 2 and 3)
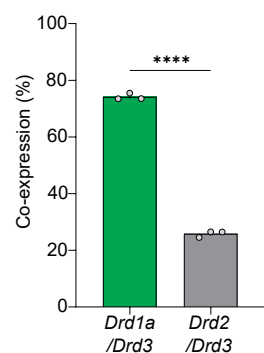
a. Experimental scheme (top) and representative image (bottom) of the NAc targeted with AAV-GFP-Cre or AAV-eGFP.

b. (Left) Representative *in situ* hybridization images showing *Cre* (green) and *Drd*3 (white) mRNA expression in the NAc of WT (top) or NAc-D3RcKO mice (bottom). Insets depict higher-magnification images. (Right) Quantification of *Drd3* mRNA expression in *Cre*-positive neurons in the NAc of WT and NAc-D3RcKO mice.

c. Quantitative real-time PCR analysis of *Drd1a*, *Drd2* and *Drd3* mRNA expression in the NAc of WT (white) and NAc-D3RcKO (blue) mice injected with Cre-expressing virus.

d. (Left) Time-course of wheel-running activity in WT-Cre (black), *Drd3*$^{fl/fl}$-GFP (red) and NAc-D3RcKO (blue) mice during the first 12 hrs of running wheel exposure. (Right) Quantification of revolutions across the 12-hr period.

e. Representative occupancy heatmaps from WT (top) and NAc-D3RcKO (bottom) mice during running disks choice task.

f. (Left) Quantification of time spent on the freely-moving and fixed disk. (Middle) Revolutions registered on the freely-moving disk for WT, *Drd3*$^{fl/fl}$-GFP controls and NAc-D3RcKO mice. (Right) Spearman's correlation between time spent in the freely-moving disk and revolutions.

g. Timeline of operant conditioning experiment.

h. Number of active and inactive lever presses of WT (black) and NAc-D3RcKO (blue) animals during FR1 acquisition sessions.

i. Number of active and inactive lever presses of WT (black) and NAc-D3RcKO (blue) animals during FR5 (right) acquisition sessions.

j. (Left) Scheme of the FR5 choice behavioral setup. Mice had free access to standard lab chow and could also lever press (FR5) for higher-palatable chocolate food pellets. (Right) Amount of food consumed represented as effort-based (FR5; solid) or freely-available lab chow (checkered).

k, l. Break points for WT and NAc-D3RcKO mice during PR3 and PR7 sessions.

Data in this figure and the rest of the manuscript are presented as mean ± SEM. Detailed figure statistics are included in Extended Data Table 1.
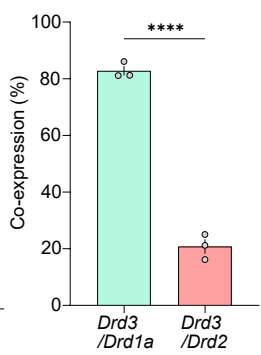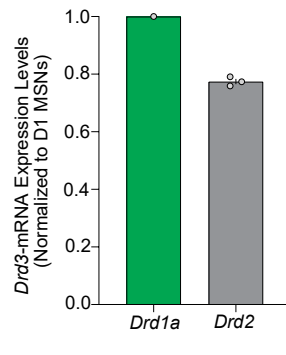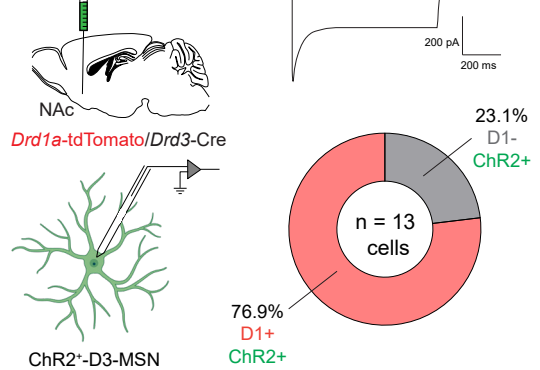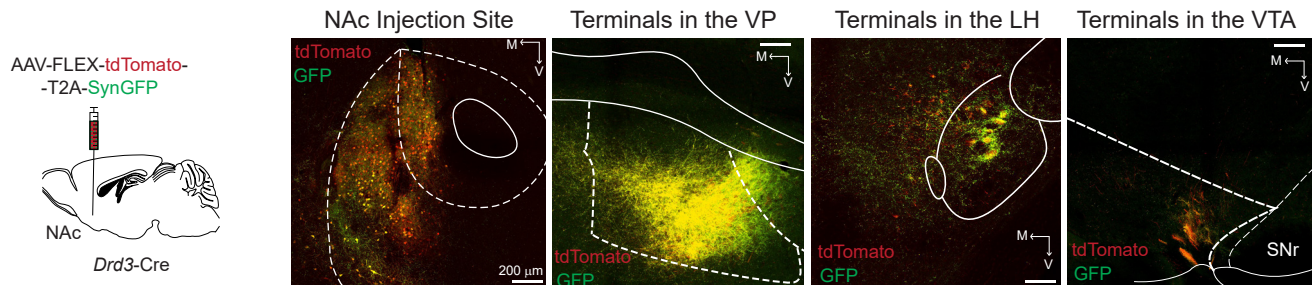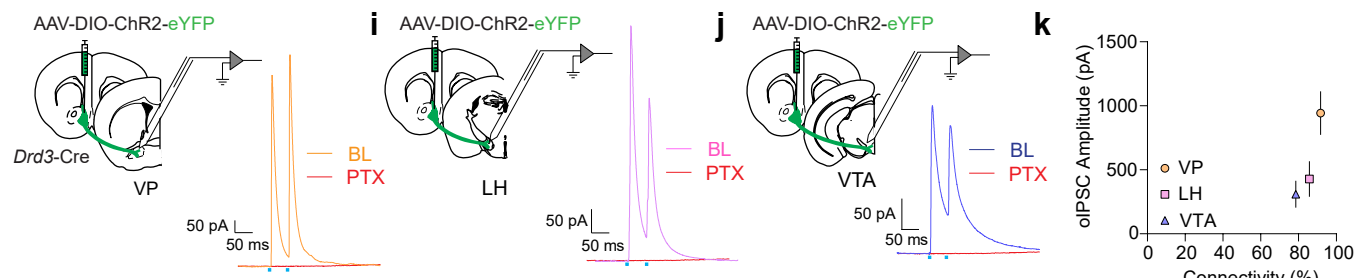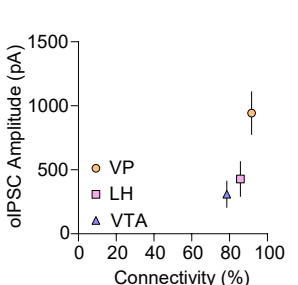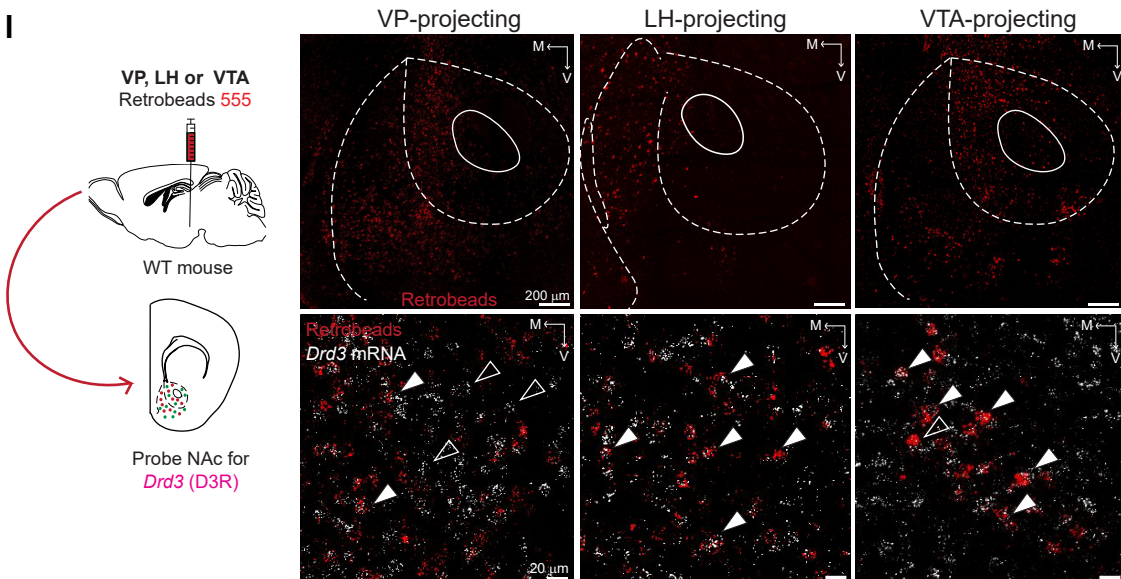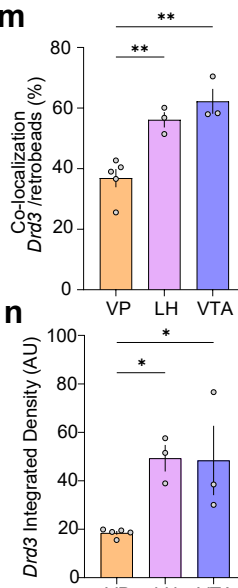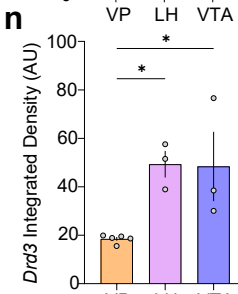
Figure 2

Figure 2. NAc D3Rs are primarily expressed in D1-MSNs and D3-MSNs display D1-MSN projection pattern (see also Extended Data Figure 3)

a. Representative low-magnification confocal image of RNA *in situ* hybridization for *Drd1a* (green), *Drd2* (red), and *Drd3* (white) transcripts in the NAc. Orange inset shows the region targeted for zoomed images in b.

b. Split high-magnification images of *Drd1a*/*Drd3*, *Drd2*/*Drd3*, and *Drd3* RNA expression in the NAc. Right image is an overlay of all channels. Filled arrowheads show co-labeled cells, and empty arrowheads show single-labeled cells.

c. Percentage of *Drd3*$^+$ cells co-expressing *Drd1a* or *Drd2* RNA in the NAc of WT mice.

d. Percentage of *Drd1a*$^+$ or *Drd2*$^+$ cells co-expressing *Drd3* mRNA in the NAc.

e. Mean relative expression levels of *Drd3* mRNA (mean integrated density/area) relative to D1-MSNs in *Drd3*-mRNA-positive D2-MSNs.

f. (Left) Schematic for quantification of *Drd3*$^+$ cells using electrophysiological recordings. (Right) Representative trace showing light-evoked ChR2-mediated inward current in a ChR2-EYFP$^+$ NAc MSN evoked by 1 s stimulation with 470 nm blue light. Pie-chart shows quantification of tdTomato-positive (*i.e.* D1-MSN) vs tdTomato-negative (putative D2-MSNs) in recorded ChR2 positive cells.

g. (Left) Cre-dependent AAV-Syn-FLEX-tdTomato-T2A-SynaptophysinGFP was injected in the NAc of *Drd3*-Cre mice to visualize fibers (red) and synaptic terminals (green) in the outputs from D3-MSNs. (Right) Representative images showing a high density of NAc D3-MSN synaptic terminals in the VP, LH and VTA.

h-k. (Right) Schematic of the electrophysiology experiment to assess functional connectivity from NAc D3-MSNs. A Cre-dependent AAV vector expressing ChR2-eYFP was injected in the NAc of *Drd3*-Cre mice. Acute slices containing the VP, LH or VTA were prepared from brains of *Drd3*-Cre mice 2–3 weeks after viral injection. (Left) Representative trace showing oIPSCs in VP, LH, and VTA cells. Red trace denotes bath-application of picrotoxin (PTX).

k. Mean oIPSC amplitudes evoked by light stimulation of NAc D3-MSN to vs. connectivity of D3-MSNs to neurons VP, LH, and VTA. oIPSCs were detected in the majority of neurons recorded (VP, n= 11 of 12 neurons from 7 mice; LH, (n= 12 of 14 neurons from 8 mice; VTA, n= 11 of 14 neurons from 9 mice)

l. Schematic of the retrograde tracing approach to compare NAc *Drd3*-expressing projection MSNs. Red retrobeads were injected into the VP, LH or VTA of WT mice. NAc sections were probed for *Drd3* mRNA) using *in situ* hybridization. Representative 20X confocal image showing retrobead labeling from VP-, LH- or VTA-projecting NAc MSNs (top). High-magnification images showing red-labeled retrobeads in the NAc co-localized with *Drd3* mRNA indicated by filled arrowheads (bottom).

m. Quantification of the percentage of retrobead+ cells projecting to VP, LH or VTA that express *Drd3* in the NAc.

n. Mean expression levels of *Drd3* mRNA (mean integrated density/area) in neurons projecting to VP, LH or VTA.
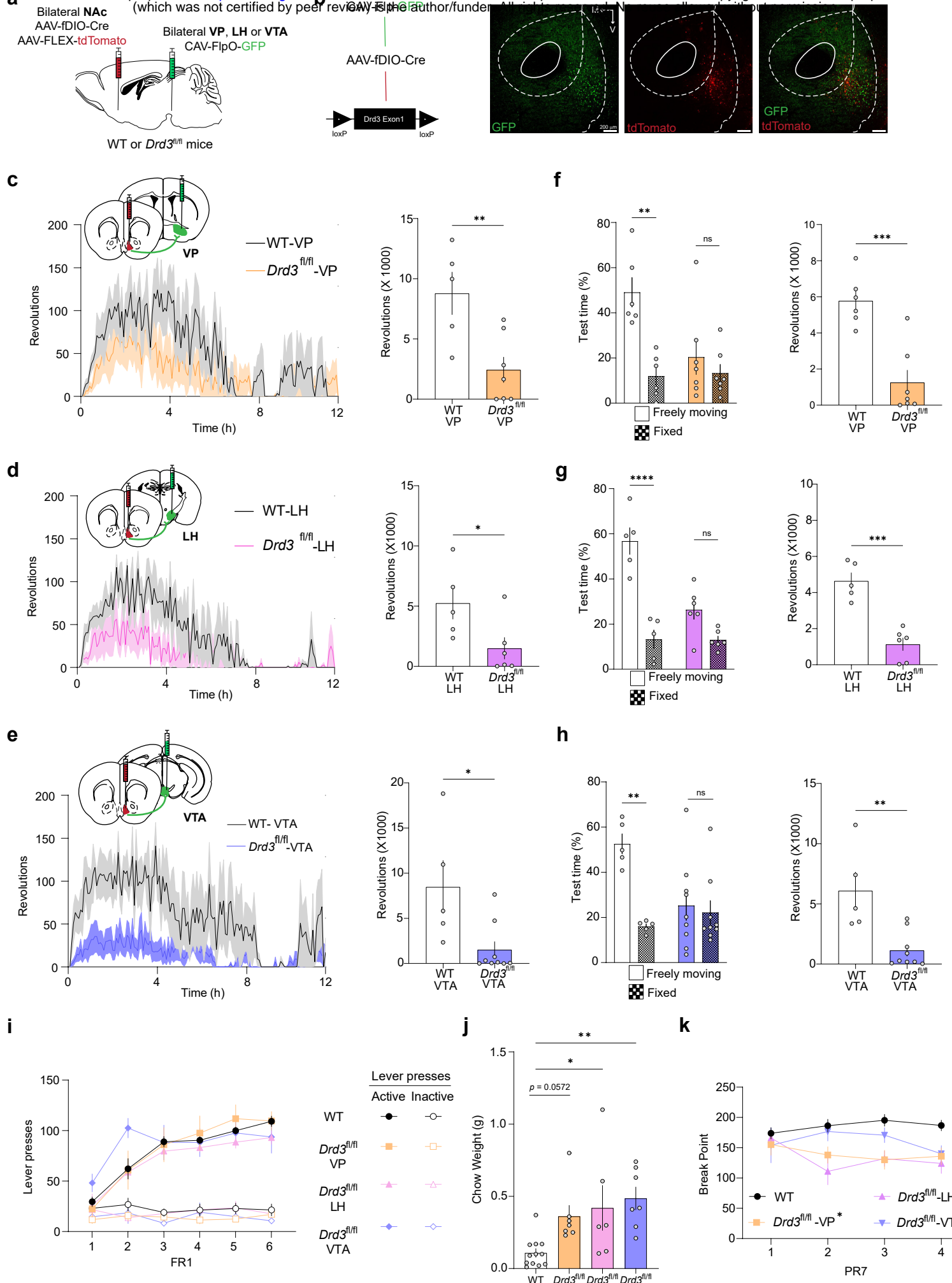
Figure 3

Figure 3. NAc D3R is essential for motivated behavior independent of projection neuron (see also Extended Data Figure 4 and 5)

a. Diagram of viral injections for pathway-specific deletion of NAc *Drd3* from distinct MSN projections. Flp-dependent Cre and Cre-dependent tdTomato were injected bilaterally in the NAc of wild-type (WT) or *Drd3*^{fl/fl}, and CAV-Flp-GFP was injected in the VP, LH or VTA to selectively knockdown *Drd3* expression in VP, LH or VTA-projecting NAc MSNs.

b. (Left) Scheme showing fDIO-dependent Cre expression and recombination resulting in excision of exon 1 of the *Drd3* gene between flanking loxP sites. (Right) Representative images of GFP and tdTomato expression in NAc MSNs. Note: AAV-fDIO-Cre did not cause recombination in Ai14-tdTomato reporter mice injected in the NAc (Extended data Fig. 4).

c-e. Time-course (left) and revolutions (right) of wheel-running activity during the first 12 hrs of running wheel exposure in WT or *Drd3*^{fl/fl} mice with pathway-specific deletion in the VP (Fig. 3c) LH (Fig. 3d) and VTA (Fig. 3e).

f-h. Quantification of both time spent and wheel revolutions on the freely-moving and fixed disk for mice with the following injections: WT-VP and *Drd3*^{fl/fl} -VP (Fig. 3f), WT-LH and *Drd3*^{fl/fl} -LH (Fig. 3g), and WT-VTA and *Drd3*^{fl/fl} -VTA (Fig. 3h).

i. Number of active and inactive lever presses of WT (black), *Drd3*^{fl/fl}-VP (orange), *Drd3*^{fl/fl}-LH (pink) and *Drd3*^{fl/fl}-VTA (purple) animals during FR1 sessions.

j. Amount of freely-available food consumed in the FR5 choice task.

k. Break points for WT and *Drd3*^{fl/fl} mice during PR7 sessions.

Figure 4

Figure 4. D3Rs regulate GABAergic transmission from NAc collaterals and to the VP via a presynaptic site of action (see also Extended Data Figure 6)

a. (Left) Diagram of virus injection of AAV-EF1a-DIO-ChR2-eYFP (Cre-ON) and AAV-EF1a-DO-ChR2-eYFP (Cre-OFF) in the NAc of *Drd1a*-tdTomato/*Drd3*-Cre mice. (Right) ChR2-eYFP–expressing cell bodies of D3R-positive (top) and D3R-negative (bottom) terminals in the NAc. Note the lack of expression in the Islands of Calleja (IC) in mice expressing Cre-OFF ChR2 in the ventral striatum.

b. oIPSCs originating from D3R-positive and D3R-negative collaterals were recorded from NAc D1- or D2- MSNs.

c,g,k,o.   Time-course of oIPSCs in NAc MSNs (Fig. 4c), VP cells (Fig. 4g), LH cells (Fig. 4k), and VTA cells (Fig. 4o) before, during and after bath application of the D3R-selective agonist PD-128907 (1 μM). For NAc MSNs and VP neurons Cre-ON groups are shown in blue (NAc MSN collaterals) or VP neurons (orange) while the Cre-OFF group is shown in black. (Inset) Representative oIPSCs traces recorded in NAc MSNs before and after bath application of PD-128907,

d,h,l,p. Paired-pulse ratio (PPR, % baseline) versus oIPSC (% baseline) for NAc MSNs (Fig. 4d), VP cells (Fig. 4h), LH cells (Fig. 4l), and VTA cells (Fig. 4p).

e,i,m.   Coefficient of variation ($1/CV^2$, % baseline) versus oIPSC (% baseline) for NAc MSNs (Fig. 4e), VP cells (Fig. 4i), and LH cells (Fig. 4m).

f,j,n. (Left) Images of ChR2-eYFP-containing terminals in VP for Cre-ON (top) and Cre-OFF (bottom) conditions (Fig. 4f). Note the larger fiber density in the Cre-OFF condition arising from D3R-lacking D1-MSNs and D2-MSNs. (Right) oIPSCs originating from D3R-positive and D3R-negative MSNs were recorded from VP neurons. Fig. 4j and 4n show images of ChR2-positive fibers in the LH and VTA (left) and schematic depicting evoked GABA release from D3-MSNs onto LH and VTA cells, respectively (right).

q. Summary graph of the inhibition of oIPSCs by PD-128907 from NAc, VP, LH or VTA neurons in Cre-ON condition.
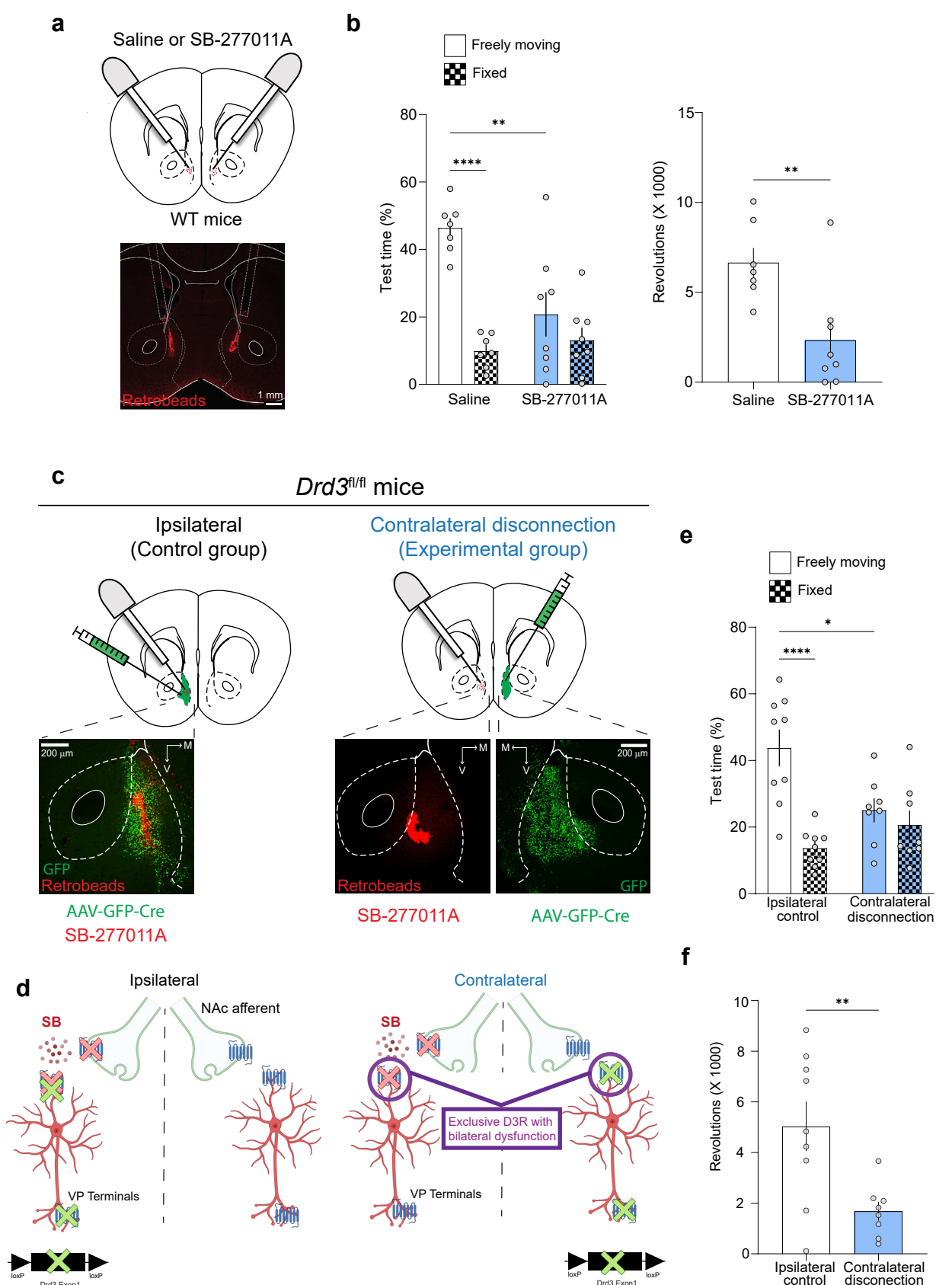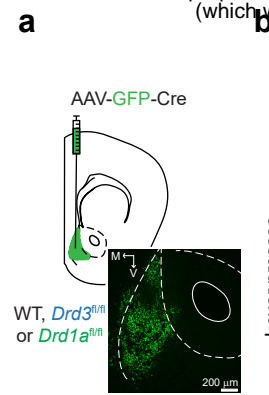
Figure 5
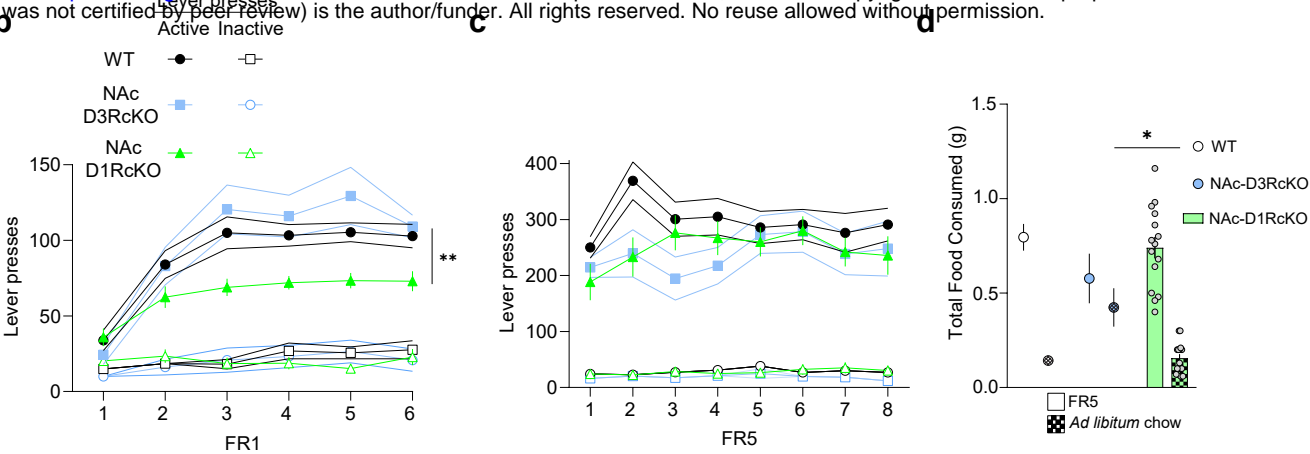
Figure 5. Motivated behavior requires local D3R signaling within the NAc (see also Extended Data Figure 7)

a. Diagram (top) and representative image (bottom) of bilateral microinjection of the D3R antagonist SB-277011A (1.79 ng per hemisphere) into the NAc of WT mice. Red retrobeads were infused after the experiment to confirm accuracy of cannula placement.

b. (Left) Percentage of time spent on the freely-moving and fixed disk for saline (white) and D3R antagonist (blue) groups during the running-disk choice task. (Right) Number of revolutions recorded in the freely moving disk.

c. Diagram (top) and representative images (bottom) of selective inactivation of local NAc D3R function using functional disconnection experiments. Mice were injected unilaterally with AAV8-Syn-GFP-Cre into the NAc of *Drd3*^{fl/fl} mice. Ipsilateral (control) and contralateral disconnection (experimental) groups were infused with SB-277011A into the ipsilateral or contralateral NAc, respectively.

d. Diagram describing rationale for disconnection procedures. In the ipsilateral group (left), one hemisphere was targeted with SB-277011A and AAV-GFP-Cre to suppress D3R signaling within the NAc and at terminals in the VP, while the other hemisphere had intact D3R signaling. For the contralateral group, the only common D3R dysfunction in both hemispheres was local D3R signaling within the NAc (purple circles), which was targeted by antagonist infusion and contralateral injection of AAV-GFP-Cre.

e. Percentage of time spent on the freely-moving (solid) and fixed disk (checkered) for ipsilateral control (white) and contralateral disconnection (blue) groups.

f. Number of revolutions registered in the freely moving disk.
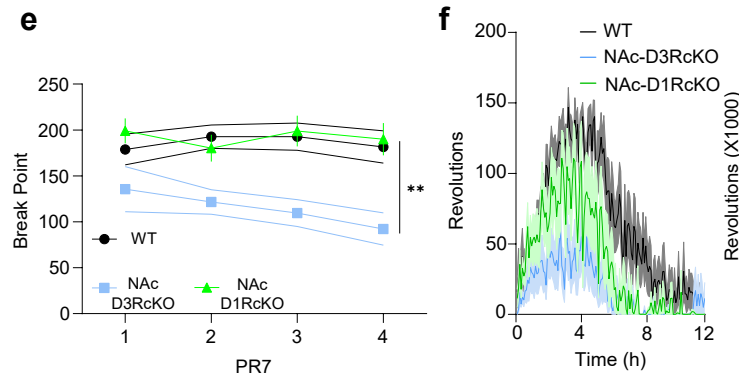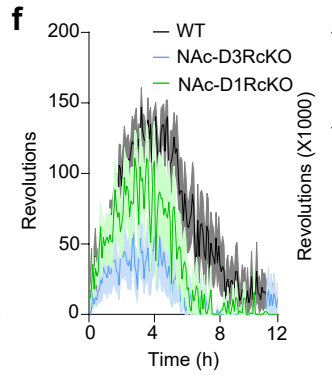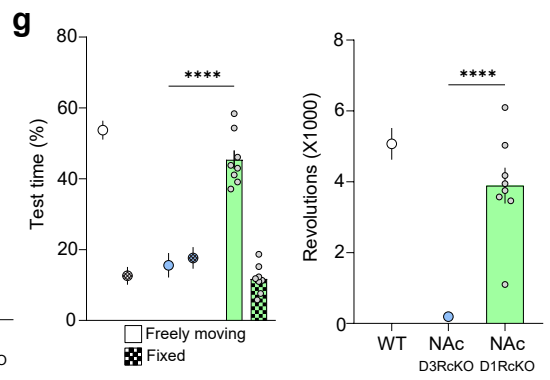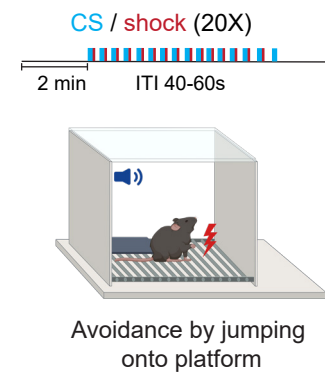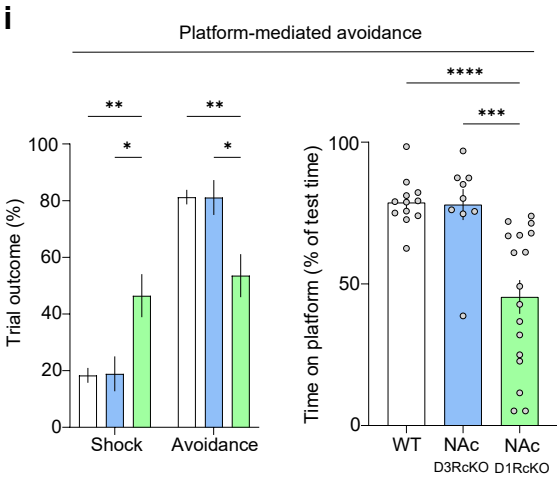
Figure 6

Figure 6: NAc D1Rs mediate reinforcement but not motivation (see also Extended Data Figure 8)

a. Scheme (top) and representative image (bottom) depicting the NAc area targeted with AAV-GFP-Cre (green) for experiments shown in b-i.

b-c. Number of active (filled) and inactive (unfilled) lever presses of WT (black), NAc-D3RcKO (blue) and NAc-D3RcKO (green) animals during sessions with FR1 and FR5 schedules of reinforcement.

d. Amount of food consumed during the effort-related choice task represented as FR5 effort-based (solid) or freely-available lab chow (checkered).

e. Break points for WT, NAc-D3RcKO and NAc-D1RcKO mice during PR7 sessions.

f. (Left) Timecourse of wheel-running activity during the initial 12 hr period of wheel exposure (in the animal's inactive cycle) in WT-Cre, NAc-D3RcKO and NAc-D1RcKO mice. (Right) Quantification of revolutions during the 12 hr period.

g. Quantification of time and revolutions for WT, NAc-D3RcKO and NAc-D1RcKO groups during the running disk choice task. (Left) Percentage of test time spent on the freely-moving and fixed disk. (Right) Number of revolutions recorded in the freely moving disk for each group.

h. Scheme of the platform-mediated avoidance task. Mice were placed in an operant box and were presented with 20 pairings of conditioned stimulus (CS) and a footshock as the unconditioned stimulus (US). Animals could step onto the platform to actively avoid a footshock.

i. Quantification of trial outcome (avoidance or shock) as percentage of total trials for day 1.

j. Percent time spent on the platform.

Note: operant and running data from WT and NAc-D3RcKO groups were acquired concomitantly with NAc-D1RcKO mice and were replicated from Fig. 1. Thus, data from WT and NAc-D3RcKO groups are displayed differently (mean and error bars).
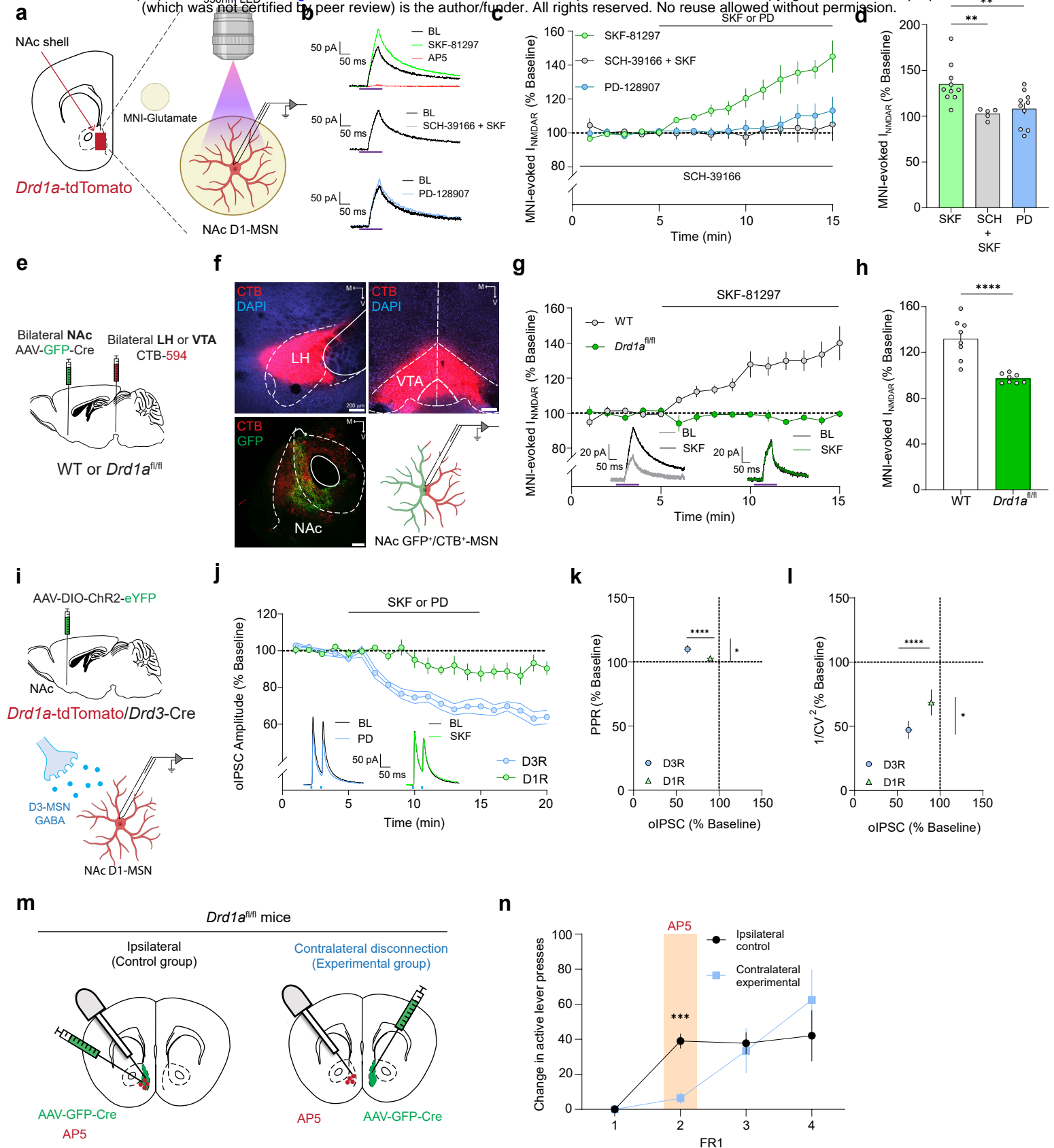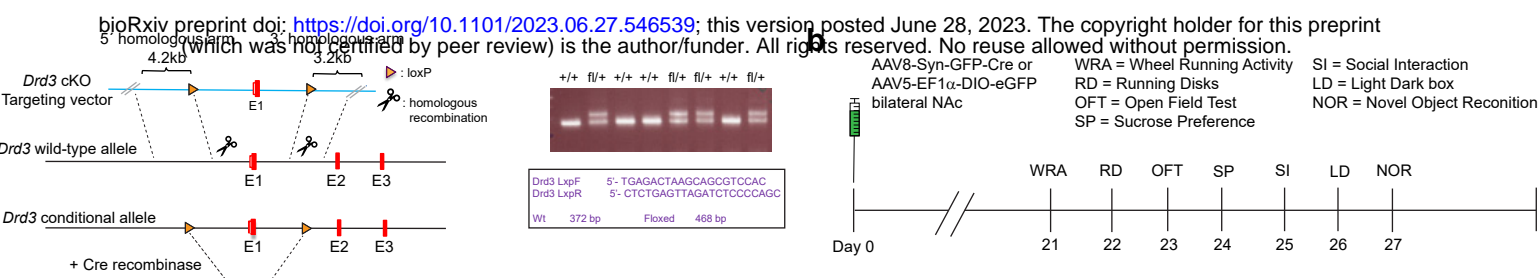
Figure 7
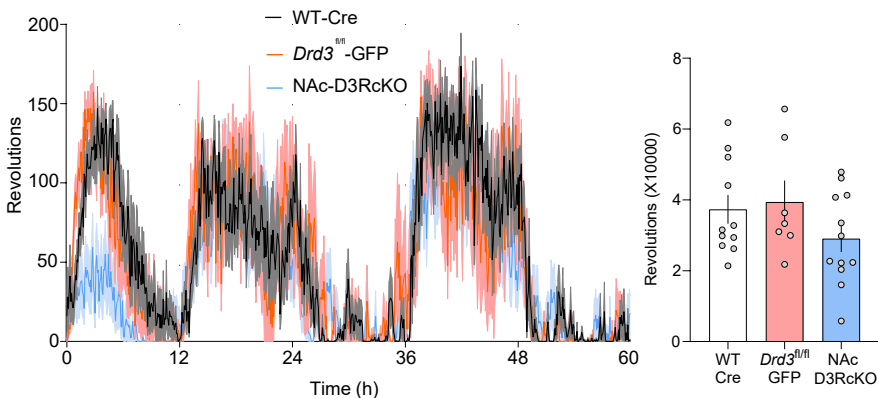
Figure 7: D3R and D1Rs regulate separable synaptic features of NAc D1-MSNs (see also Extended Data Figure 8)

a. Schematic showing location of patch-clamp recordings (left) and glutamate uncaging (right). MNI-Glutamate (50 µM) was uncaged using 365 nm UV light (150 ms pulses) and biophysically-isolated NMDAR-currents were recorded at +40 mV from NAc D1-MSNs using DNQX (10 µM), PTX (50 µM) and tetrodotoxin (TTX; 1 µM).

b. Representative traces of evoked NMDAR currents in NAc D1-MSNs before and after bath-application of the D1R agonist SKF-81297 (green, top), application of SKF-81297 in the presence of the D1R antagonist SCH-39166 (grey, middle) and application of the D3R agonist PD-128907 (blue, bottom). Red trace indicates that evoked NMDAR currents were eliminated with AP5 (50 µM). Purple bars indicate ultraviolet light pulses.

c. Time-course of normalized NMDAR-current amplitude in NAc D1-MSNs before and during bath application of SKF-81297 (10 µM, green), preincubation with SCH-39166 (1 µM) and application of SKF-81297 (black) or application of PD-128907 (1 µM, blue).

d. Evoked NMDAR currents after treatment with SKF-81297, preincubation with SCH-39166 and treatment with SKF and application of PD-128907 (% baseline).

e. Schematic of experimental details to demonstrate D1R-NMDAR interactions and validation of *Drd1a* cKO in NAc of *Drd1a*^{fl/fl} mice. AAV8-Syn-GFP-Cre was injected bilaterally in the NAc of WT or *Drd1a*^{fl/fl} mice to genetically ablate *Drd1a*, and the retrograde tracer CTB-594 was injected in the LH or VTA to selectively label NAc D1-MSNs.

f. Representative images of CTB injection sites in LH and VTA, and colabelling of GFP and CTB in the NAc. Recordings were made from colabeled GFP+/CTB+ NAc MSNs.

g. Time-course of normalized NMDAR-current amplitude in NAc D1-MSNs before and during and after bath application of SKF-81297 in WT or *Drd1a*^{fl/fl}
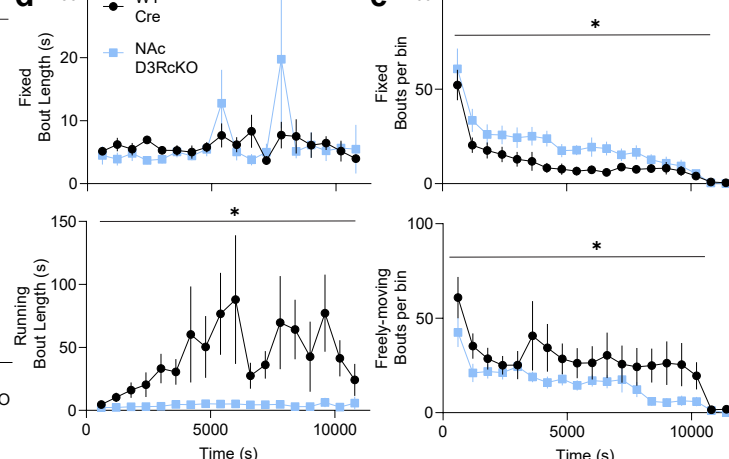
groups. (Inset) Representative NMDAR traces recorded in NAc D1-MSNs for each genotype.

h. I_{NMDAR} (% baseline) change after treatment with SKF-81297 for WT and *Drd1a* groups.

i. Schematics of experiment to determine regulation of NAc collaterals by D1Rs and D3Rs. *Drd1a*-tdTomato/*Drd3*-Cre mice we injected with AAV5-Ef1a-DIO-ChR2-eYFP (Cre-ON) in the NAc (top) and GABA release was evoked from D3R-positive terminals (1ms pulses). Biophysically-isolated oIPSCs were recorded from NAc D1-MSNs (bottom).

j. Time-course of oIPSCs in NAc MSNs from D3R collaterals before, during and after bath application of SKF-12897 or PD-128907. (Inset) Representative traces recorded in NAc MSNs before and after bath application of PD-128907 (blue) or SKF-81297 (green). Note: data using PD-12897 were replicated from Fig. 4 and was therefore displayed with different error bars.

k. Paired-pulse ratio (PPR, % baseline) versus oIPSC (% baseline).

l. Coefficient of variation ($1/CV^2$, % baseline) versus oIPSC (% baseline).

m. Diagram of disconnection procedures of D1R and NMDAR function in the NAc. Mice were injected unilaterally with AAV-Syn-GFP-Cre into the NAc of *Drd1a*$^{fl/fl}$ mice. Ipsilateral control (left) and contralateral disconnection (right) groups were infused with AP5 into the ipsilateral or contralateral NAc, respectively.

n. Change in active lever presses lever presses under an FR1 schedule of reinforcement relative to Day 1 in ipsilateral (black) and contralateral (blue) groups. AP5 was microinjected on Day 2 of FR1 sessions.
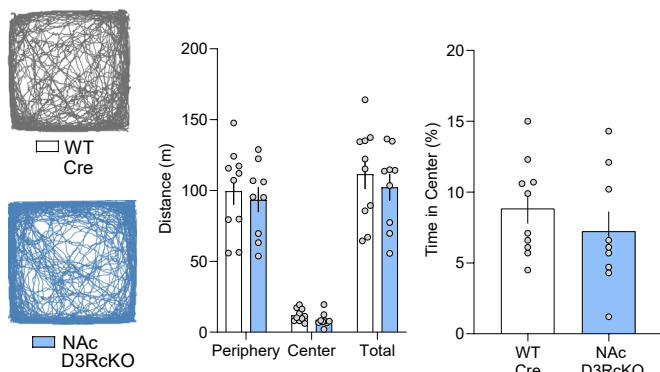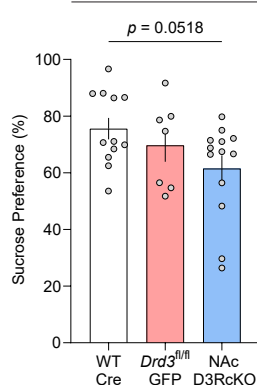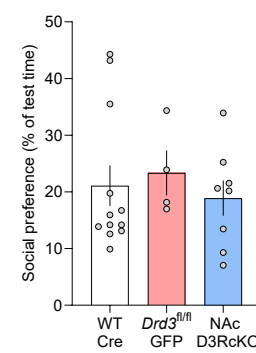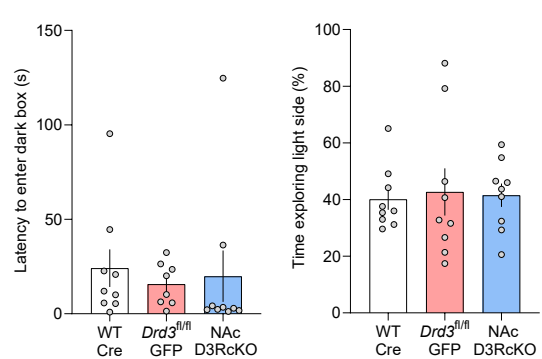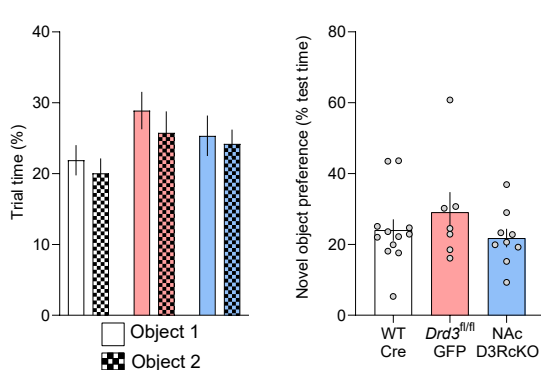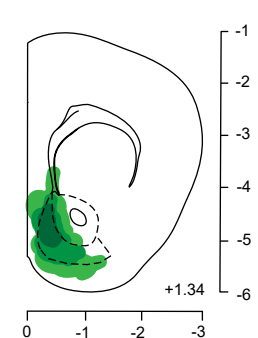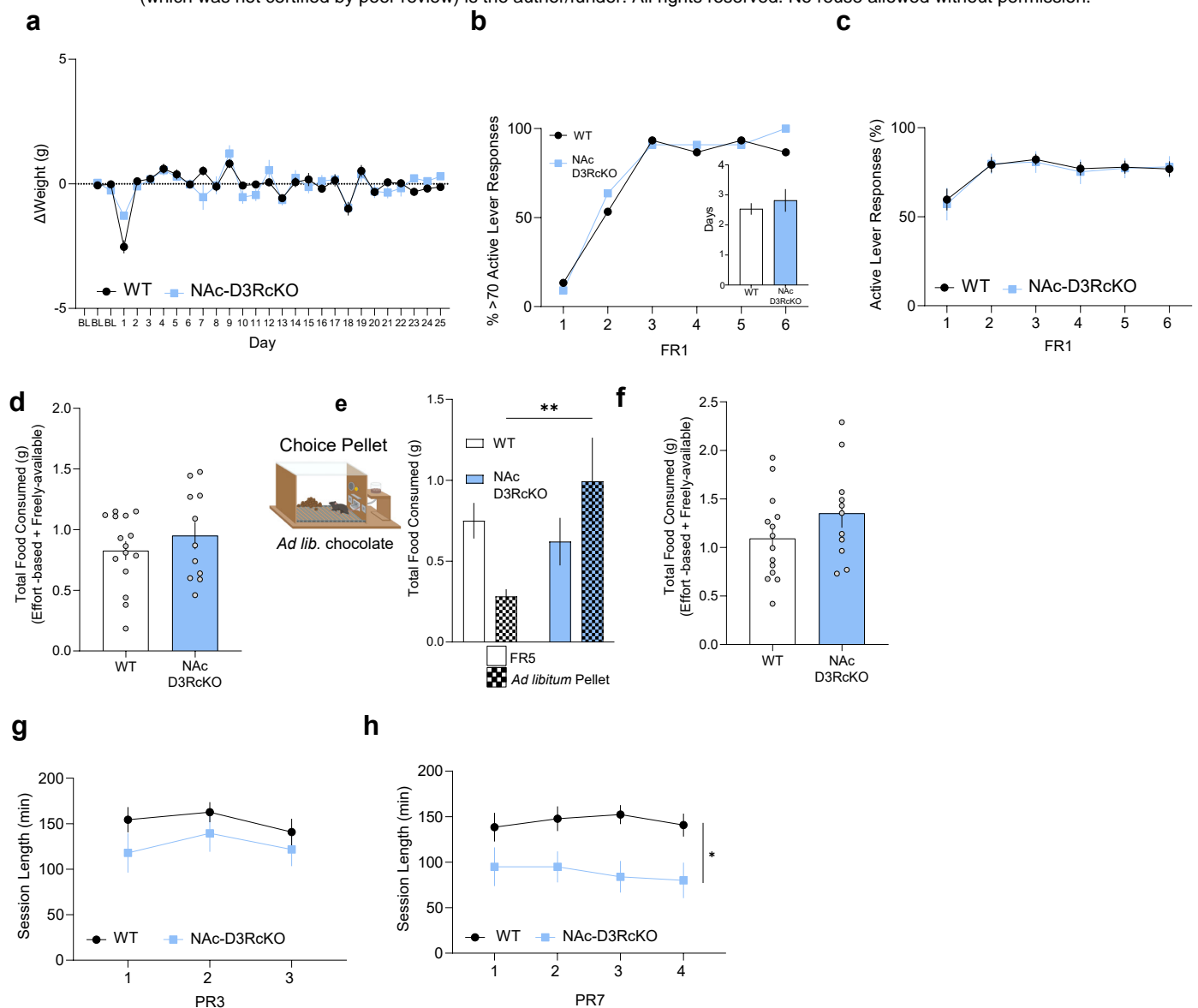
Extended Data Figure 1

Extended Data Figure 1. NAc D3Rs does not affect locomotion, anhedonia, social reward, anxiety or novel object-recognition, Related to Figure 1.

a. (Left) Schematic depicting the strategy used to generate the *Drd3*^{fl/fl} conditional-knockout (cKO) mouse strain. LoxP cassettes flanking the exon 1 were inserted in the coding region of the *Drd3* gene that encodes the D3R protein using homologous recombination approaches. (Right) Confirmation of the inserted LoxP sites within the chimeric animals by using PCR strategies (see primers in purple). The successful insertion of the LoxP elements was confirmed by the presence of two PCR bands (fl/+ lanes) versus a single band in the wildtype littermates (+/+ lanes).

b. Experimental timeline of behavioral experiments in mice involving running behavior.

c. (Left) Timecourse of wheel-running activity for the entire duration of the experiment (60 hrs) (Right) Quantification of total revolutions per group during the entire 60 hr period.

d. Length of visit (bout) to the fixed disk (top) or freely-moving disk (bottom, putative running bout) across the running disks session.

e. Number of entries into the fixed (top) or freely-moving disk (bottom) across the running disks session.

f. (Left) Representative cumulative locomotion traces of open field activity in WT-Cre and NAc-D3RcKO groups. (Middle) Quantification of cumulative distance traveled. (Right) Percentage of time spent in the center during the open field test.

g. (Left) Percentage of sucrose preference. (Right) Overall intake in the sucrose preference test.

h. Social preference as reflected by the % time (test-habituation) spent interacting with a novel, juvenile mouse.

i. Anxiety-like behavior as represented by the latency to enter dark chamber in the light–dark box (left) or time spent in the light side of the light-dark box (right).
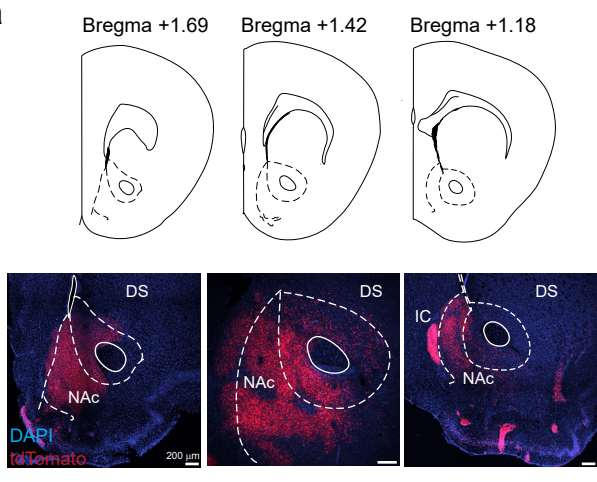
j. (Left) Time spent interacting with each of the objects during the baseline period. (Right) Preference for the novel object over a familiar one during the discrimination test.

k. Schematic of combined viral spread map of local *Drd3* cKO. Dark green indicates animal with most restricted expression and lighter green indicates animals with broader pattern of viral spread.

Extended Data Figure 2
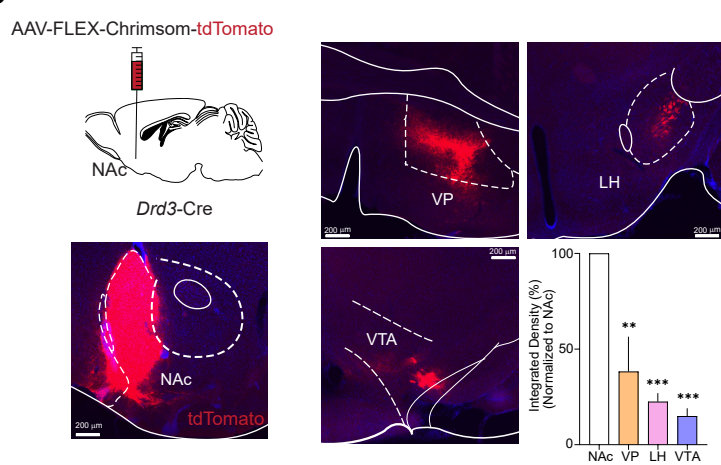
Extended Data Figure 2. NAc D3R regulates motivation towards working for rewards, but does not affect weight, or FR acquisition schedules of reinforcement, Related to Figure 1.

a. Body weight changes at baseline before food deprivation or across the overall duration of operant conditioning procedures in Figures 1 and S1.

b. FR1 acquisition, as measured by the percentage of animals reaching the criteria of 70 active lever responses per session. (Inset) Days required to acquire FR1 (criteria for acquisition was 70 responses in a 45 min session).

c. Percentage of active lever responses during FR1 schedules.

d. Total food consumed in choice chow session.

e. (Left) Diagram of the FR5 choice pellet session. (Right) Amount of food consumed, which is represented as FR5 effort-based or freely-available chocolate pellets.

f. Total food consumed in FR5 choice pellet session.

g. PR3 session length.

h. PR7 session length.

a

Bregma +1.69   Bregma +1.42   Bregma +1.18

Drd3-Cre/Ai14

b

AAV-FLEX-Chrimsom-tdTomato
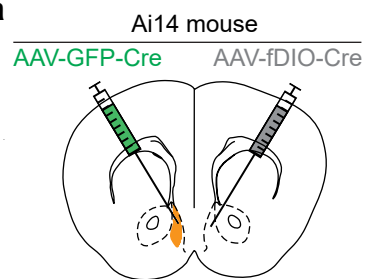
Drd3-Cre

Extended Data Figure 3
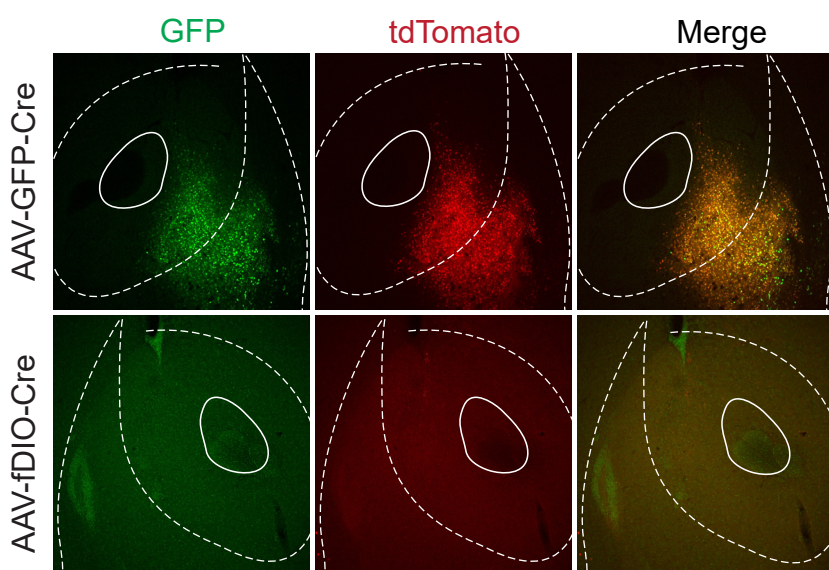
Extended Data Figure 3. ***Drd3*-Cre lines provide genetic access to *Drd3* expression in the NAc and outputs of D3-MSNs, Related to Figure 2**

a. *Drd3* expression in the NAc of *Drd3*-Cre/Ai14 mice. Coronal diagrams depicting the region analyzed and confocal images showing the *Drd3* expression pattern in the NAc along the dorsal-ventral and rostral-caudal axis (bottom). DS = dorsal striatum; IC = islands of Calleja

b. (Left) A virus encoding the anterograde tracer (AAV1-Syn-FLEX-Chrimsom-tdTomato) was targeted to the NAc in *Drd3*-Cre mice that express tdTomato in a Cre-dependent manner. (Right) Representative images and quantification of tdTomato[+] fibers in NAc, VP, LH and VTA regions.

Extended Data Figure 4
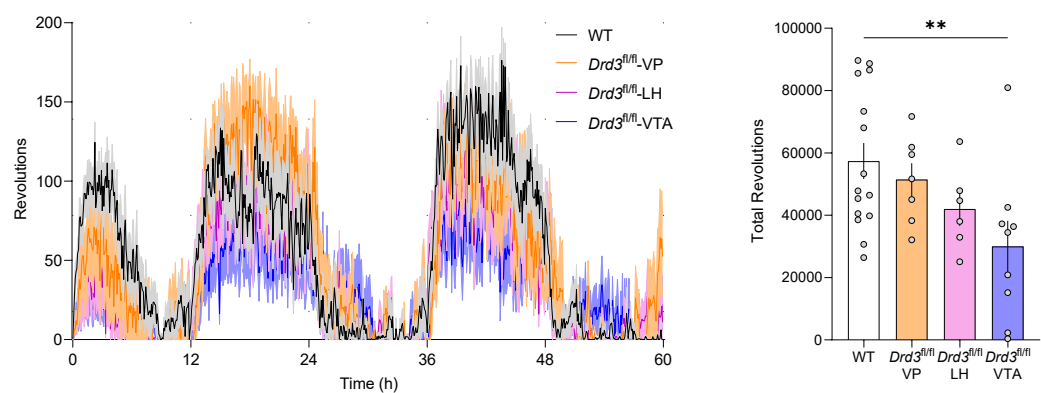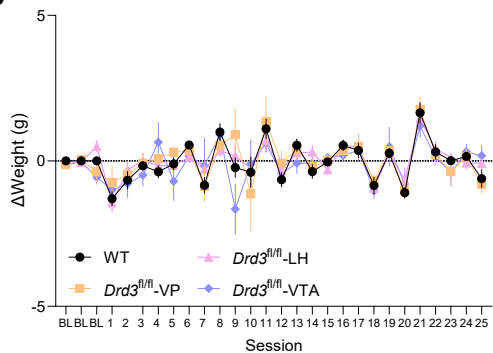
Extended Data Figure 4. Validation of lack of Cre leakage in our intersectional approach for pathway-specific NAc *Drd3* cKO, Related to Figure 3.

a. Scheme of the experimental design to validate the pathway-specific strategy for the pathway-specific cKO of NAc *Drd3*. AAV8-Syn-GFP-Cre and AAV9-EF1a-fDIO-Cre were injected in contralateral hemispheres of Ai14-tdTomato reporter mouse.

b. Representative images showing colabeling of GFP and tdTomato in hemisphere injected with AAV-GFP-Cre (top) and lack of tdTomato expression in hemisphere injected with AAV-fDIO-Cre (bottom).
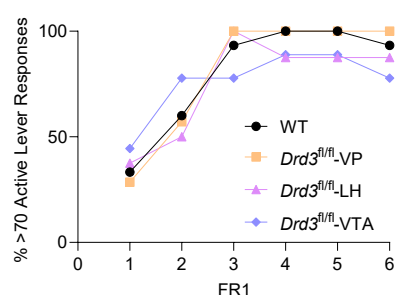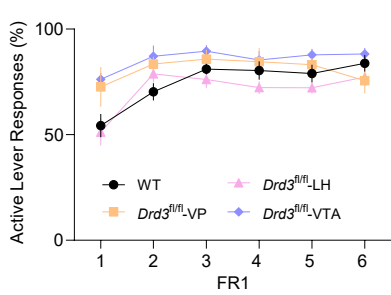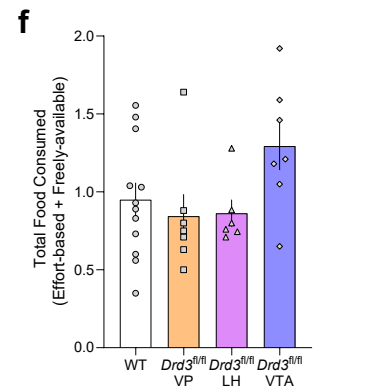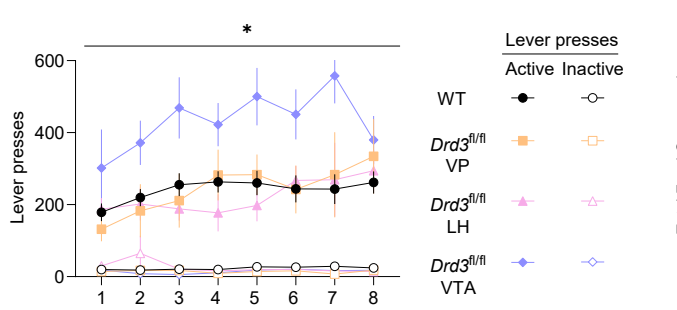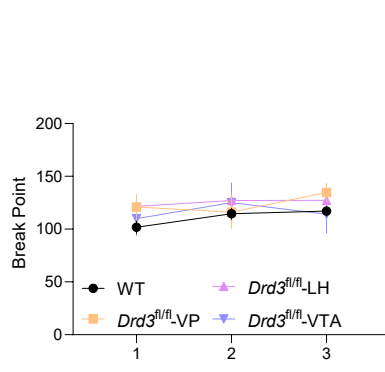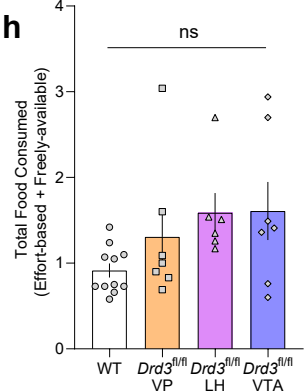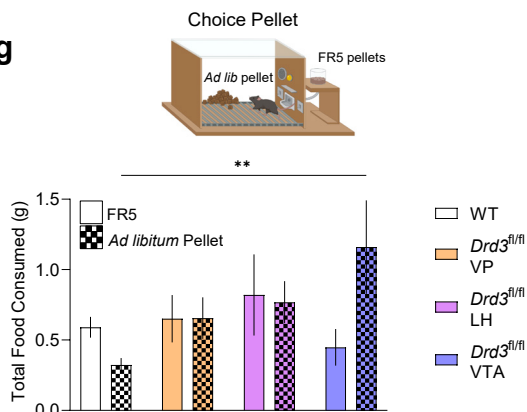
Extended Data Figure 5
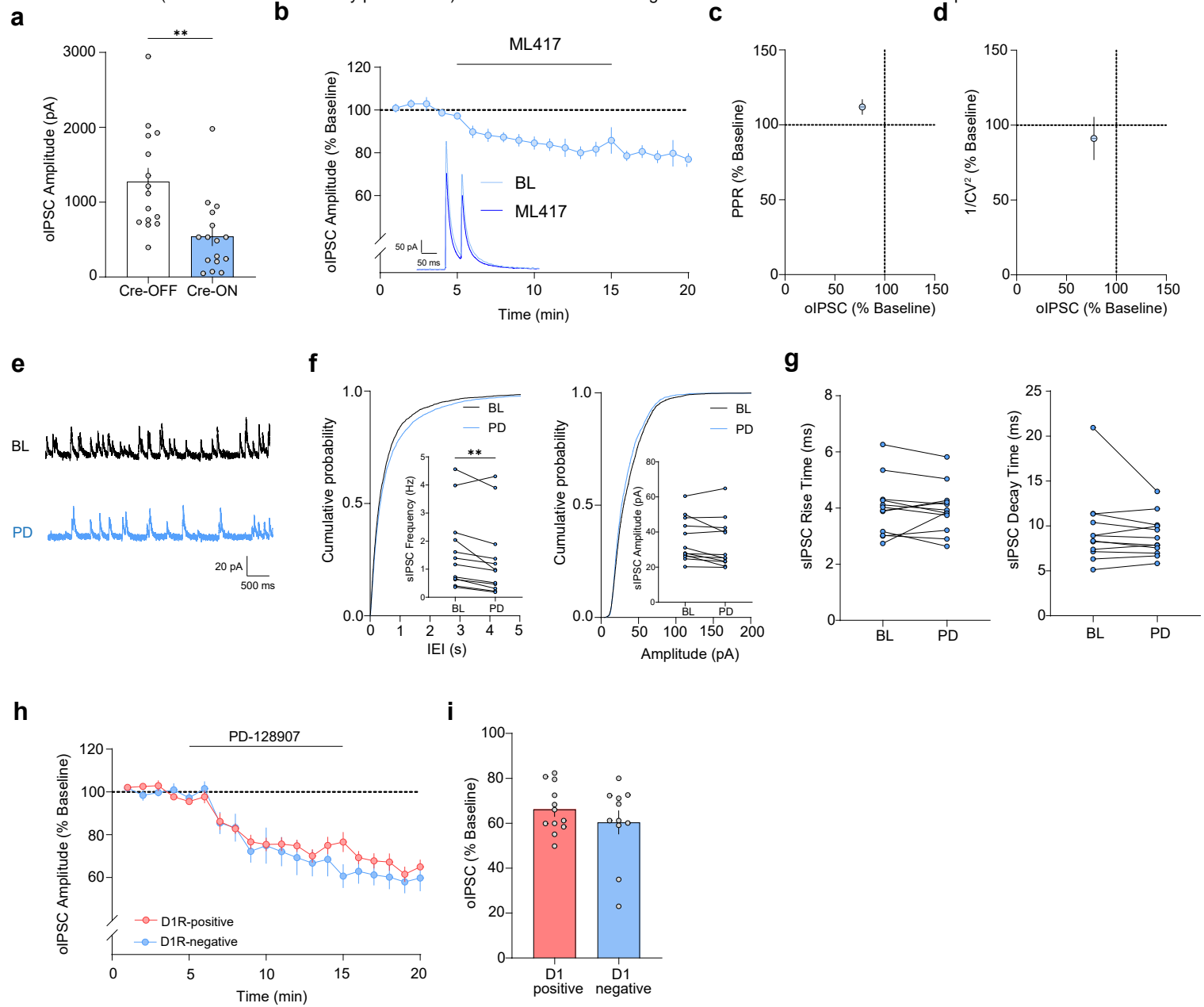
Extended Data Figure 5. NAc D3Rs provide value to running and working for reward, but does not regulate acquisition of reinforcement, Related to Figure 3.

a. Wheel running activity for pathway-specific deletion of NAc D3Rs. (Left) Timecourse of running activity during the complete 60-hr experiment. (Right) Quantification of total revolutions during the 60-hr period.

b. Body weight changes at baseline before food deprivation (p= 0.86) or across the overall duration of operant conditioning procedures in Figure 3.

c. FR1 acquisition, as measured by the percentage of animals reaching the criteria of 70 active lever responses per session.

d. Percentage of active lever responses during FR1 schedules

e. Lever presses during FR5 acquisition sessions.

f. Total food consumed in choice chow session.

g. (Top) Diagram of the FR5 choice pellet session. (Bottom) Amount of food consumed which is represented as either FR5 effort-based (solid) or freely-available chocolate pellets (checkered).

h. Effects of region-specific D3R cKO on total consumption of chocolate pellets in a FR5 choice pellet session.

i. Break points during the PR3 reinforcement schedule for VP-, LH-, and VTA-specific D3R cKO versus WT controls.

Extended Data Figure 6

Extended Data Figure 6. NAc D3R decreases GABA release probability presynaptically onto both D1- and D2-MSNs, Related to Figure 4

a. Mean baseline oIPSC amplitude (pA) for Cre-OFF (white bar) and Cre-ON (blue bar) evoked in NAc MSNs.

b. Timecourse of oIPSCs in NAc MSNs before, during and after bath application of the D3R-selective agonist ML417 (1 µM) in *Drd3*-Cre mice expressing Cre-dependent ChR2 (blue). (Inset) Representative oIPSC traces recorded in NAc MSNs before and after bath application of ML417.

c. Paired-pulse ratio (PPR, % baseline) versus oIPSC (% baseline) after ML417 application.

d. Coefficient of variation ($1/CV^2$, % baseline) versus oIPSC (% baseline) after ML417 application.

e. Representative traces of sIPSCs during baseline (BL, black) and after bath-application of the D3R-selective agonist PD-128907 (PD, blue).

f. Cumulative probability of sIPSC inter-event interval (left) and amplitude (right) recorded from NAc MSNs. (Inset) Quantification of frequency and amplitude of sIPSCs events during baseline and after PD-128907 application

g. Rise (left panel) and decay time (right panel) of sIPSC events during baseline and after PD-128907 application

h. Time-course of oIPSCs before, during and after bath application of PD-128907 in NAc D1R-positive and D1R-negative NAc neurons (putative D2-MSNs) in the Cre-ON condition. (Inset) Representative oIPSCs traces recorded in NAc D1- and D2-MSNs before and after bath application of PD-128907.

i. Bar-graph quantification of oIPSC inhibition after PD-128907 application in D1R-positive and D1-negative NAc MSNs.
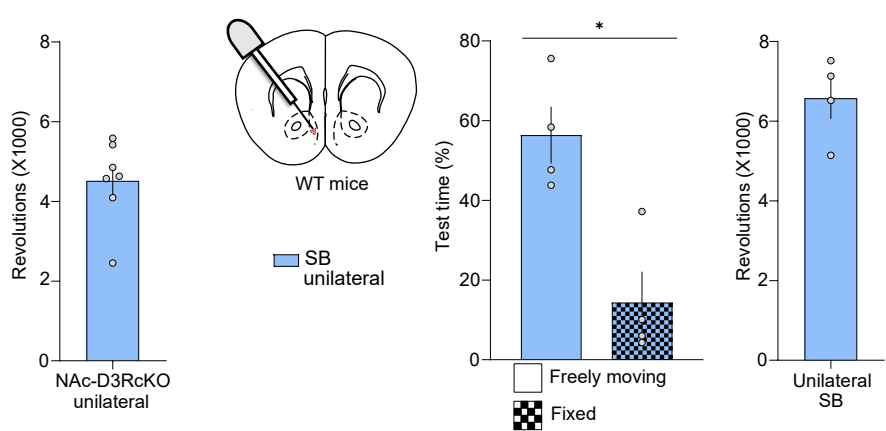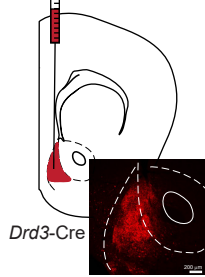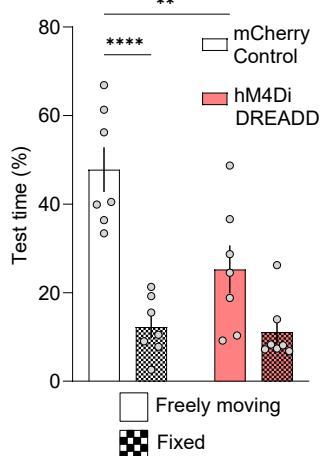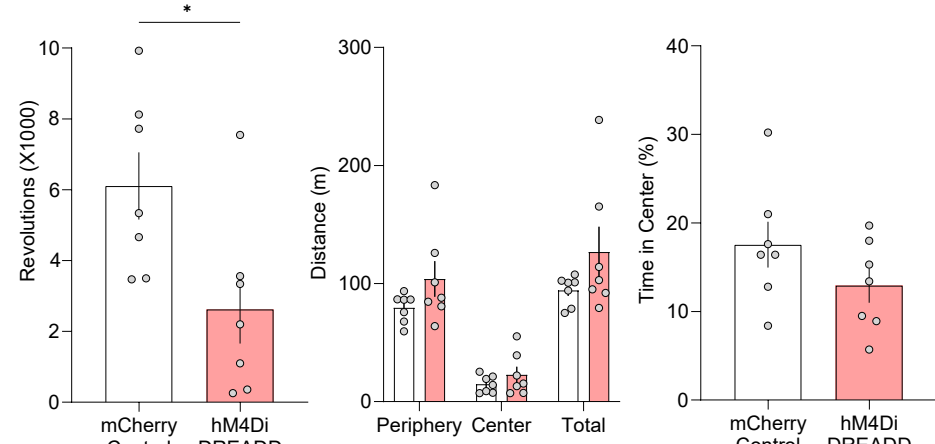
Extended Data Figure 7
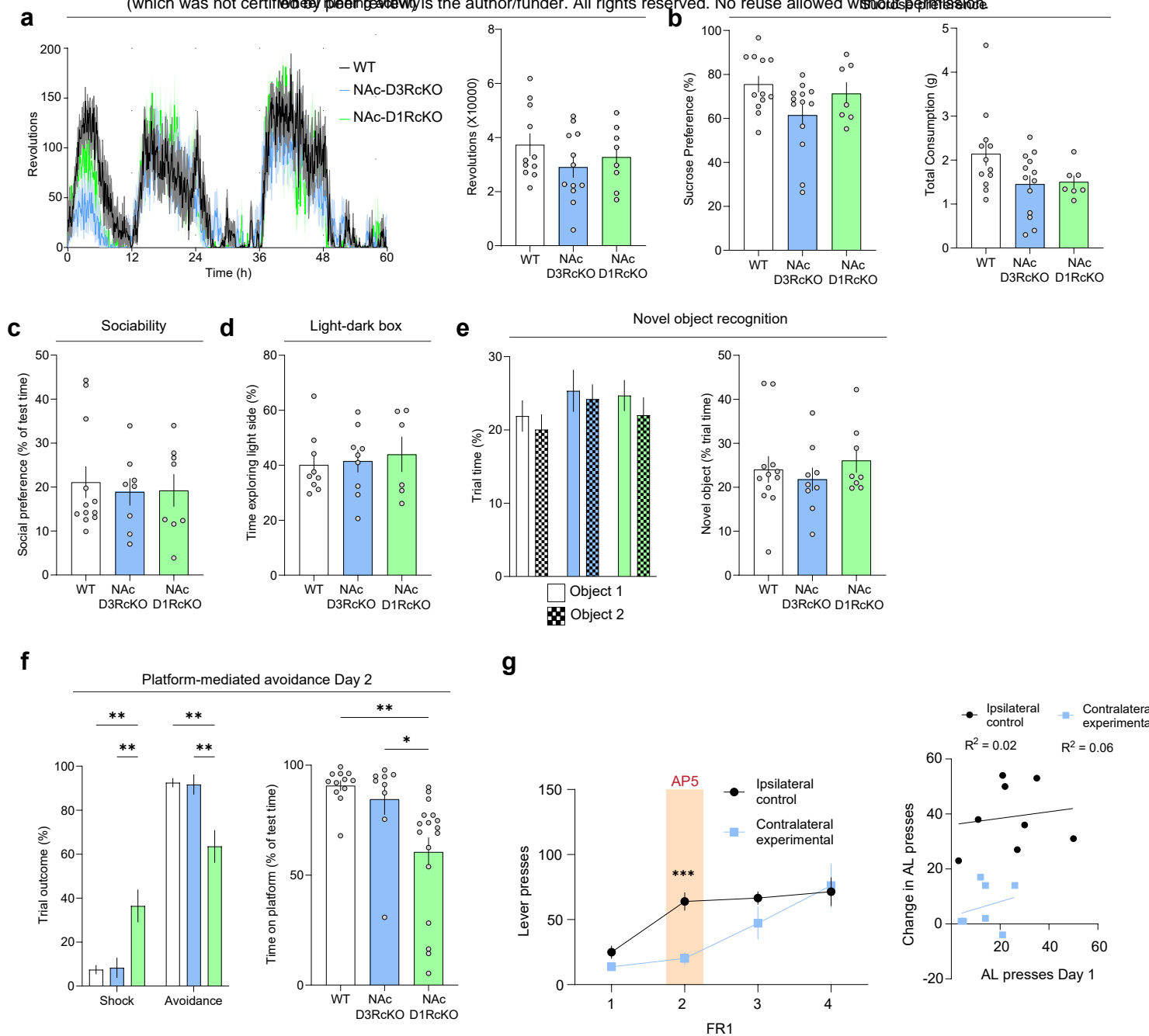
**Extended Data Figure 7: Unilateral suppression of D3R signaling does not disrupt motivated running behavior, Related to Figure 5**

a. Quantification of time spent in the freely-moving and fixed disk and revolutions for *Drd3*^{fl/fl} mice expressing unilateral Cre recombinase.

b. Same as in (a) but for WT control mice unilaterally infused with SB-277011A into the NAc.

c. Schematic (top) and representative image (bottom) of viral expression of AAV5-hSyn-DIO-mCherry in the NAc of *Drd3*-Cre mice

d. (Left) Percentage of time spent on fixed or freely-moving disk during the running disk task for mCherry and HM4Di groups. (Right) Running behavior as represented by the number of revolutions registered in the freely moving disk.

e. (Left) Quantification of cumulative distance traveled in each zone during the open-field test. (Right) Percentage of time spent in center.

Extended Data Figure 8

Extended Data Figure 8: NAc D1Rs do not mediate motivated, anxiety-like or social reward or sucrose preference, Related to Figure 6 and Figure 7

a. (Left) Time course of wheel-running activity across the entire duration of the experiment (60-hrs) for WT, NAc-D3RcKO and NAc-D1RcKO groups in 5 min bins. (Right) Quantification of total revolutions across the 60 hr period..

b. (Left) Percentage of sucrose preference for WT, NAc-D3RcKO and NAc-D1RcKO groups. (Right) Overall water and sucrose intake.

c. Social preference as reflected by the % time (test-habituation) spent interacting with a novel, juvenile mouse.

d. Anxiety-like behavior as represented by the time spent in the light side of the box.

e. Preference for the novel object over a familiar one during the discrimination test.

f. (Left) Quantification of trial outcome (avoidance or shock responses) upon re-exposure to the platform-mediated avoidance task on day 2. (Right) Overall time spent on platform (Day 2) as percentage of test time.

g. (Left) Absolute number of active lever responses in FR1 sessions for D1R-NMDAR disconnection experiments. AP5 infusion was performed on Day 2 of FR1. (Right) Correlation between number of AL presses on Day 1 and change in active lever presses on Day 2 (AP5 challenge).